DETERMINATION OF SENSORS CHARACTERISTICS OF CURB

AND DEVELOPMENT OF SURROGATE CURB FOR THE

EVALUATION OF VEHICLE ACTIVE SAFETY SYSTEMS

A Thesis

Submitted to the Faculty

of

Purdue University

by

Seeta Ram Pandey

In Partial Fulfillment of the

Requirements for the Degree

of

Master of Science in Electrical and Computer Engineering

May 2020

Purdue University

Indianapolis, Indiana

THE PURDUE UNIVERSITY GRADUATE SCHOOL

STATEMENT OF THESIS APPROVAL

Dr. Stanley Yung-Ping Chien, Chair

    Department of Electrical and Computer Engineering

Dr. Yaobin Chen

    Department of Electrical and Computer Engineering

Dr. Brian King

    Department of Electrical and Computer Engineering

Approved by:

    Dr. Brian King

      Head of the Graduate Program

ACKNOWLEDGMENTS

Completing a Master of Science in Electrical and Computer Engineering program from a country like the USA is an achievement on which one should always be proud. It was challenging for a person like me who was in the corporate industry for the last thirteen years. The education industry has evolved drastically from the days of my undergraduate completion year 2005 and I was totally unaware of the nitty-gritty of advanced education courses and systems. I am thankful to IUPUI for embracing me in their coveted program and encouraging me to explore and triumph the unseen.

I would like to use this platform to express my sincere appreciation to my supervisor, Professor Stanley Chien. He absorbed my weaknesses and persistently steered and inspired me to be professional and raise the standards. He is an epitome of patience and I am sincerely thankful to him for trusting me to pull off the work. Without his expertise and help, the objective of this project was not realizable.

I am thankful to Professor Yaobin Chen, whose in time suggestions and encouragement helped me to achieve the deadlines. I am also thankful to Dr. Brian King for motivating me to learn and implement new things. They were always available to me whenever I needed. I am thankful to both for generously agreeing to be in my supervising committee.

Many thanks to Dr. Lin Li, Dr. Lingxi Li and Dr. Renran Tian for their valuable technical contribution and guidance.

This study has useful contributions from students like Dan Shen, Wensen Niu, Jun Li and Yuto Shishikura who helped me in testing, model preparation and equipment handling in severest of weather, both day and night. I would also like to thank TASI and everyone associated with it from time to time.

I also wish to thank Electrical and Computer Engineering department officials such as Ms. Sherrie Tucker whose implicit support was a great help.

TABLE OF CONTENTS

LIST OF TABLES

LIST OF FIGURES

ABBREVIATIONS

AEB	Autonomous Emergency Braking
BRDF	Bidirectional Reflectance Factor
CW	Continuous Wave
DIL	Driver-in-the-Loop
FMCW	Frequency Modulated Continuous Wave
FOV	Field of View
FSK	Frequency Shift Keying
LDW	Lane Departure Warning System
LKA	Lane Keeping Assistant System
RCS	Radar Cross Section
RDAT	Road Departure Assisting Techniques
RDMS	Road Departure Mitigation System
RDWS	Roadway Departure Warning System
SDR	Software Defined Radar
SNR	Signal to Noise Ratio

ABSTRACT

Pandey, Seeta Ram. M.S.E.C.E., Purdue University, May 2020. Determination and Application of Sensors Characteristics to Develop Surrogate Curb for The Evaluation of Vehicle Active Safety Systems. Major Professor: Stanley Y.P. Chien.

Over the years, car driving experience has evolved drastically. Many new and useful technologies have emerged, which have enhanced safety and reliability measures. The Automotive world is now trying to build capabilities for driverless or vehicle assisted driving. One of the critical aspects of building capabilities for driverless cars is to have a test environment that is capable of testing these capabilities and is safe and consistent. One such critical model is the model adopting the Road Departure Assisting Techniques (RDAT). These techniques are primarily the standards for alleviating the risk of roadside fatalities. The different models developed or proposed for RDAT falls under "The Road Departure Mitigation System" (RDMS). But, almost every RDMS to date, in the absence of lane markings or of proper lane markings, these RDMS are unreliable. Therefore, RDMS requires new references such as roadside objects and road edges for detecting road departures. This new system should propose and establish a standard for RDMS testing with roadside objects. As the foremost task, this new system requires the creation of a testing environment consisting of soft, robust, and reusable surrogates. Critically, these surrogates must have comparable sensors characteristics to those of real roadside objects from various commonly used object detection sensors on the vehicles such as camera, radar, and LiDAR. One of such everyday roadside objects is the curbs. This thesis first demonstrates and proposes the methods for extracting the color, Radar reflectivity, and the LiDAR reflectance properties of real roadside curbs. That is, the study deals with what all color combinations and patterns represent the US roadside curbs, what should be the range of Radar reflectivity values, and LiDAR reflectance bounds that a surrogate curb should

satisfy. The later part of the thesis illustrates methods and steps on how to mimic the extracted properties, design a surrogate curb as per federal standards, and then develop a surrogate curb.

1. INTRODUCTION

1.1 Motivation

Over the years, the automobile industry has progressed considerably in the development of Vehicle Active Safety System features. The active safety features are always active and help to prevent an accident. These active features include features such as traction control, electronic stability control, braking systems and driver-assist systems. The driver-assist systems like forward collision warning and lane departure warning helps to mitigate or prevent roadside crashes. There are passive systems also like the airbags and seat belts, which helps to reduce the post-collision impact, whereas the active systems help to avoid collisions by way of early warning system by detecting the potentially dangerous situations. But why is it so rush for active systems? Before answering the questions, lets first define the road departure crash.

A roadside departure crash is defined as a crash that occurred after a vehicle crosses a road edge or a centerline, or otherwise leaves the traveled way. Road departure means that the vehicle begins to move out of its trafficway when a turn signal is not on. According to ANSI D16.1 Seventh Edition, a traffic way is described as any land way which is as a matter of right or as a custom, open to the public for transportation of persons or property from one place to another [1, 3]. Figure 1.1 (from https:// crashstats.nhtsa.dot.gov) shows the typical trafficway.
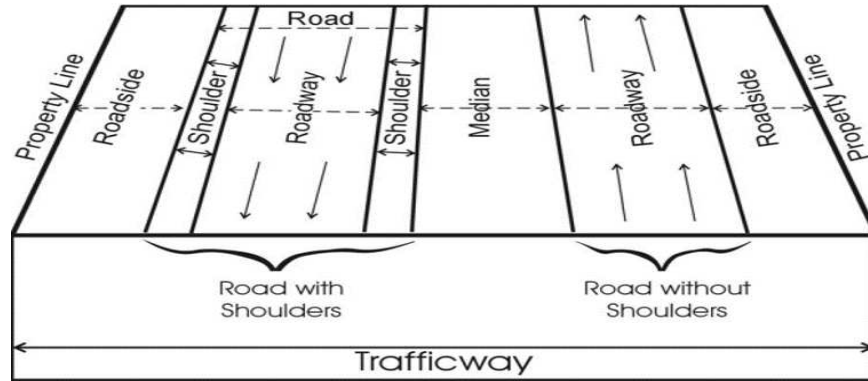
Fig. 1.1. Typical Traffic Way Layout of the US Roads.

According to the US Department of Transportation "Roadway Safety Data Dashboard [2, 3], from the year 2015 to 2017, an average of 19,223 fatalities have resulted from roadway departures (Figure 1.2). The fatalities numbers due to vehicle road departure account for nearly 52 percent of all the traffic fatalities in the United States (https://safety.fhwa.dot.gov). Therefore, owing to such a high percentage of casualties taking place because of road departures, the development of systems that could prevent roadside departures are now an essential objective of automobile industries. Development of the curb surrogates that could mimic the real curbs with respect to properties related to sensors such as radar, LiDAR, and the camera is considered to be is one of those objectives.
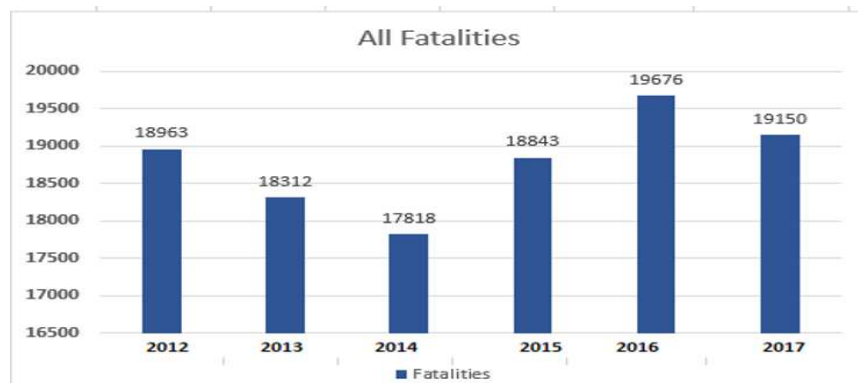
Fig. 1.2. Roadside Fatalities Due to Roadway Departure

1.2 Background

For subsiding the fatalities due to road departures, automotive makers incorporated safety features such as Lane Departure Warning (LDW) and Lane Keeping Assist (LKA) [3]. These features, as the word "Lane" suggests, require clear lane markings for proper functioning (Figure 1.3). As many US roads either do not have proper lane markings or are devoid of lane markings, these features are only partially compatible with the requirements. Hence, there is a need for new technology that can not only use the earlier lane detecting feature but also detect the road edge reference objects such as curbs, metal guardrails, concrete dividers, and grass for early warning signals. The new technology being developed is called the "Road Departure Mitigation System (RDMS)." The RDMS can use lane markings, roadside objects, and roadside edges as road edge references (Figure 1.4, referenced from https://www.autoevolution.com).

Fig. 1.3. LKA and LDW Illustration
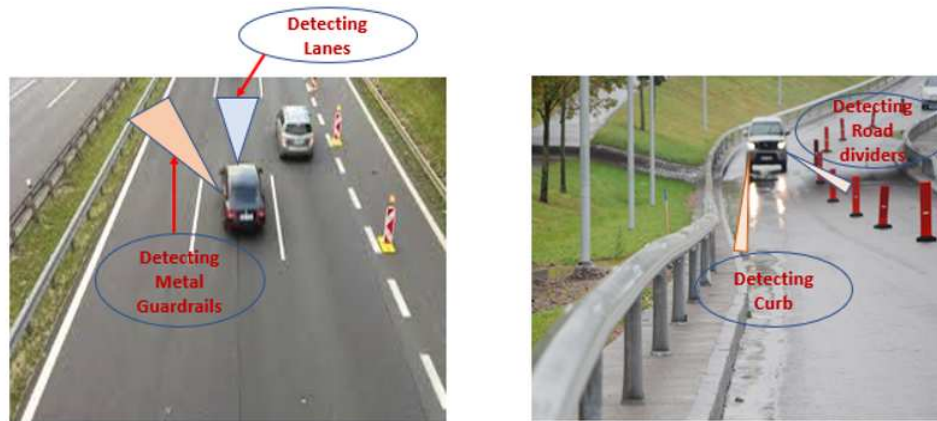
Fig. 1.4. RDMS Illustration

Nowadays, almost every car boasts of many different safety technologies [4, 5, 6], such as lane departure warning and forward collision warning, which aims to reduce fatalities by ways such as auto-steering and warning, and shield drivers, and other road and roadside commuters. But, unfortunately, there is no standard testing procedure in place for evaluating the performances of these features. Every automaker has its propriety RDMS technology, and in the absence of any standard testing procedures, it is difficult to trust these newer technologies.

1.3   Problem Description

As discussed, there is a need to test RDMS. There are generally two approaches for testing; using human factors DIL (Driver-in-the-loop) simulators and direct testing of a vehicle on real roads. DIL simulators allow monitoring, measuring and recording of the reactions of drivers to interventions by a vehicle's active safety systems in a safe, consistent lab environment. Though DIL simulators expose the driver and vehicle to zero real-world collision hazards but have few potential shortcomings, it fails to engage expectations of skilled drivers appropriately; that is, it is not able to properly engage expectations of how a car should feel on a real road. DIS simulator is suitable for recording human behaviors, but it is not good for vehicle engineering

dynamics. Therefore, some potential problems that could have been discovered during direct road testing may remain unknown. Direct testing of vehicles on the actual road, though it seems to be reliable, the scenarios may not be repeatable. The direct test on roads creates potential safety hazards for both vehicles under test and the driver. Therefore, creating a safe, consistent and controllable testing environment is undeniably essential wherein vehicles will no longer be evaluated in isolation, but in a real-world environment with respect to other vehicles, pedestrians, roadside objects, and other unexpected interactions. The Euro New Car Assessment Program (Euro NCAP) has worked on Car safety performance assessment since 1997 [4] but, since the RDMS technology is new, there is not a standard testing environment and methodology defined anywhere in the world yet.

With aid and collaboration with Toyota Collaborative Safety Research Center (CSRC), Transportation Active Safety Institute (TASI) at Indiana University-Purdue University Indianapolis (IUPUI) has developed procedures, scenarios, and equipment for testing the new RDMS technologies. It has developed surrogates of roadside objects that are able to mimic the real ones with respect to properties related to automotive sensors such as radar, LiDAR, and camera. The surrogates help to build a testing environment that is safe and consistent. That is, the testing of vehicles in the new environment does not damage the objects used for the test and also do not harm the vehicle under test and the driver. According to the study by TASI [42], the top five roadside objects are grass (54.65%), curb (16.02%), metal guardrail (8.7%), a concrete divider (4.17%) and traffic cone (0.28%) (Figure 1.5). Therefore, as curbs are present in abundance on US roadsides, the development of its surrogate is selected as the primary goal of this thesis study. The sensor characteristics of developed curb surrogates must match that of the real concrete curbs. Reflectance or reflectivity is the fundamental characteristic of roadside objects used for object detection. The surrogates should be visually a replica of the real objects and ought to reflect automotive

radar and LiDAR the same as the real objects. They should also be soft and reusable so that they can be crashed multiple times without causing damage to the test track, the vehicles being tested, and the surrogate objects themselves.

This project deals with the ways to extract standard colors and patterns for the curb and, then, develop a skin that could be used on a durable curb foam model. In Particular, concrete curb development requires two significant tasks. The first task is to generate the requirements for the curb shape, color, infrared, and radar characteristics. The second task is the development of a surrogate curb that satisfies the requirements.
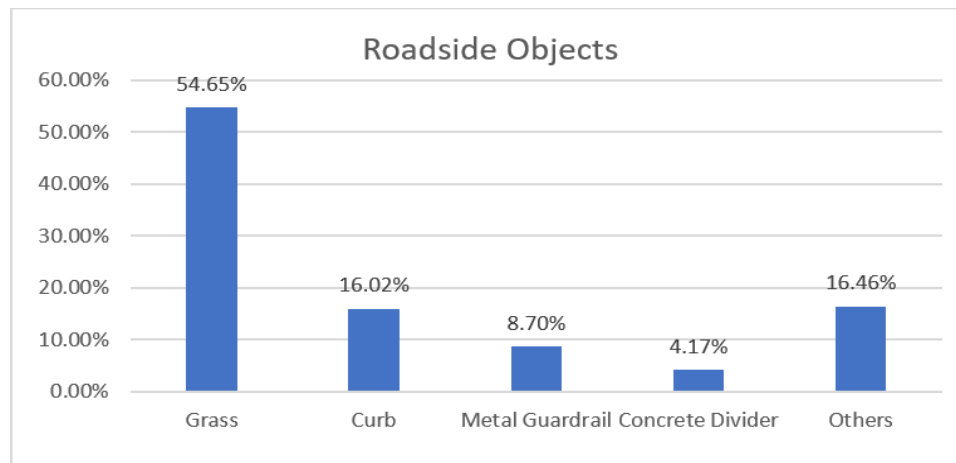
Fig. 1.5.   US Roadside Objects Distribution Percentage

1.4   Previous and Related Works

Some work for the development of the surrogate curb has been partially done before. The requirement for curb shape, color, infrared, and radar characteristics were initially determined, and a surrogate curb was also developed that satisfy the requirement. However, the color of the previously developed surrogate curb was too uniform like a new curb. A significant percentage of the curb seen on the road are old with some damages. Hence, the study focused on building a realistic curb that could mimic the real roadside curb in shape and properties when perceived from sensors

like radar, LiDRAS, and Camera. The project aims at developing all different kinds of common curb patterns, which could cover at least 90% of US roads. Figure 1.6 shows one such curb on US roads.

Fig. 1.6.   A Curb on US Roads

The automotive world uses a combination of three primary sensors, such as radar, LiDAR, and camera for vehicle active safety systems. Working together, they provide visuals of car surroundings, distance, and speed of nearby objects along with their 3-D shape. Cameras placed on every side (front, rear, left, and right) of the vehicle stitches together a 360-degree view of their environment. Though they can provide accurate visuals, cameras cannot detect the speed and the distance of the objects. More so, it is difficult for camera-based sensors to detect objects in low visibility conditions, like fog, rain, or nighttime. The radar sensors surround the car to detect objects at every angle and are capable of detecting objects even in low visibility. They can determine the speed and distance of the target, but they can not distinguish between different types of vehicles. LiDAR provides a 3D view of their environment. They are particularly useful where the shape of surrounding objects like cars, pedestrians, and road geography is required.

Hence, owing to such widespread use of these sensors, this study develops surrogate curbs with properties related to these sensors. The study utilizes properties such as radar reflectivity, infrared reflectance, and color for developing a surrogate curb that could effectively mimic the real curbs. The requirement of surrogates curb is that it could mimic the real curb in properties related to the mentioned sensors. However, for having a better understanding of the properties of the sensors, how these properties are measured, and what factors affect the measurement need to be investigated from various previous works. These works include material properties, color properties, sensors working principle, and measurement data interpretation.

For the LiDAR system, the related property is the reflectance. Reflectance is defined as a ratio of radiance over irradiance of the surface. Two types of reflectance measurements are most popular: directional hemispherical reflectance and bidirectional reflectance [5]. Directional hemispherical reflectance is usually measured in a laboratory where the source is a collimated directional beam, and light is captured from all possible view angles using an integrating sphere. On the other hand, bidirectional reflectance is determined by measuring the incident energy and reflected energy from a set of incident and view angles [6]. For the measurement of bidirectional reflectance across a range of wavelengths both indoors and outdoors, spectrometers are used. Herold et al. [7], Kerekes [8] and Akamatsu [9] studied the bidirectional reflectance of different urban objects such as roof tiles, asphalt, and concrete under the sun within two hours of solar noon. For all these pieces of literature, the reflectance measurement was done from one view angle (from perpendicular position) and a limited range of light incident angles (during solar noon). Honkavaara et al. [10] studied the effect of different incidence and viewing angles on the reflectance of concrete for visible green wavelengths. However, for accurately specifying the required reflectance range for roadside curb objects, RDMS requires properties related to more than one viewing angle, and in the near-infrared wavelength. This study provides IR values from 0 to 70 degrees viewing angles.

For the radar system, work has been done in developing in High-resolution Radar for automobile applications, which aims to work efficiently on millimeter waves [11]. Work by Dong-Su Lee; Seokwon Yeom; Jung-Young Son; Shin-Hwan Kim on Image segmentation of concealed objects detected by passive millimeter-wave imaging [12] was one of pioneer works in Radar sensing and imaging of roadside objects. Further work done by the department of mechanical engineering of the University of California at Berkeley illustrated the use of Frequency Modulated Continuous Wave (FMCW) radars for roadside imaging and detection [13]. Daisaku Ono, Kobe's work on Stationary object detection method for use with scanning radar [14], relates to modern-day radar imaging and detection techniques. The study focused on the detection method of a stationary object by a radar. It uses peaks generated based on radar signals, which are reflected from a target. The peaks with the same frequency are grouped, and then a decision is made to ascertain that the frequency of the grouped peaks is equal to or higher than a predetermined value. This study uses FMCW radars for the measurement of radar reflectivity values of the curbs.

Not much previous works have been done to study the color composition and patterns of the roadside curb. The previous work done did not represent all kind of curbs on US roads. The color composition of the previous work looked like a very new curb, whereas the maximum percentage of curbs on the US roads are old. Different color models like RGB and CIELAB, and clustering techniques such a K-means and Silhouette indexing are used in this study. There are many pieces of literature available regarding the color models, their advantages, disadvantages, and usage [14-19]. One can also find various literature for image processing and clustering techniques [20-25]. This study provides different representative colors, color combinations, and representative patterns for making a surrogate curb.

1.5   Sensor Technology Overview

Before moving further, it is imperative to have an overview of sensor technologies that are used for this study. The automated vehicles nowadays use sensors, which the automobile world broadly classifies into active and passive sensors. The active sensors such as radar and LiDAR works on wave theory and Doppler effects. These sensors transmit the wave (Electromagnetic or Lightwaves) and rely on the information received back from the target object. The passive sensors, such as the camera, capture the environmental information like the colors without emitting waves. The cameras are the most common sensors on cars, and it is mandatory in the US that every vehicle has a back-viewing camera. The vehicles equipped with lane assist technology have front-facing cameras generally fitted at the windshield of the car. Any sensor used on vehicles must have high visibility capabilities both in the day and at night. Apart from visibility, the processing related to data must be smooth and effective. The improved camera radar and LiDAR technologies provide excellent visibility and efficient data processing. The critical difference between Radar and LiDAR is that the radar uses radio or electromagnetic waves, and LiDAR uses a laser or infrared waves. The LiDAR emits rapid rotating laser signals, which bounce back from the obstacles. The radar emits radio waves, which bounce back from the obstacles. The sensor positioned on both the instruments measures the amount of time it takes for each pulse to bounce back. Thus, both these instruments can calculate the distance between themselves and the object with accuracy. Radars are mostly used if the exact shape of the object is not of paramount interest. For exact shapes, LiDAR is often the better choice.

1.6   Structure of the Thesis

Chapter 2 deals with related ideas with regards to radar for developing the surrogate curbs. It presents the related radar theories and the radar instruments used in this study for radar measurements and lists the property requirements for making

surrogate curbs. Chapter 3 provides the required theories and concepts related to the measurements of property related to LiDAR, i.e. The IR reflectance. The chapter illustrates the instruments used in this study for reflectance measurement and gives the characteristics requirement which a surrogate curb should satisfy with regards to LiDAR. As not much work has been done for exploring the color composition of different kinds of curbs on US roads, chapter 4 carries out an in-depth study of the color composition of the curbs for developing the patterns that could be emulated for making surrogate curbs. The chapter explains the different color models and clustering techniques used in the study for developing the different color compositions of curbs. The developed color compositions were used for developing the patterns. Chapter 2, 3, and 4 provides the requirements for making surrogate curbs and chapter 5 uses these requirements for making such surrogates. The chapter describes methods for making the surrogate curb and verifies that the radar and IR requirements are met. Once the sensor requirements were met, the developed surrogates was crash tested. Chapter 6 gives details of the crash test.

2. RADAR CHARACTERISTICS OF CURBS

As stated earlier, the surrogate curb should mimic the real curb in characteristics representative to the sensors such as camera, radar, and the LiDAR. The current chapters discuss the characteristics related to radar sensors, which are used to mimic the real roadside objects successfully. The chapter begins by giving basic concepts related to radar operations. Then it discusses a few types of radar, and the frequency used by automotive radars. Finally, the chapter ends with explaining the instruments used by this study and providing the property that a surrogate should satisfy.

The basic principle of Radar is straightforward [26]. Radar generates electromagnetic (EM) waves [27], which travels forward at the speed of light until they hit an object. Depending on the property of the object (such as shape, material), some of the radar waves travel through the target, and the rest of the waves are reflected back. Based on the difference (frequency, phase) between the transmitted waves and the reflected waves, a Radar can determine the distance between the Radar and the object, the moving speed of the object, and the other properties of the object, such as the reflectivity. There are several different types of Radar [20].

- Based on the applications, there are Tracking Radar, Weather Radar, Automotive Radar. This research focuses on Automotive Radar [21].

- Based on the signal frequency, there are L-band Radar, S-band Radar, C-band Radar, X-band Radar

- Based on the waveform modulation, there are Frequency Shift Key (FSK) Radar, Continuous Wave (CW) Radar, Frequency Modulated Continuous Wave (FMCW) Radar.

In this study, we are interested in automotive applications that use FMCW band radar. Typically, the automotive Radar usually uses two frequency bands, one is 24GHz, and the other is 77GHz. 24GHz Automotive Radar is a Short-Range Radar (SRR), it is mostly used for side looking applications. Its measurement range is less than 20m [29]. 77GHz Automotive Radar is a Long-Range Radar, so it is mainly used as a forward-looking Radar. Its measurement range could reach 150m [28]. We explore more about a few of these radars in the below sections.

2.1 Frequency Shift Keying Radar Systems

Frequency Shift Keying (FSK) Radars transmit two discrete frequencies waves, F1 and F2 (or the carrier waves). These waves are switched with a time lag and are transmitted within their TCPI (called the coherent processing interval- TCPI). The principle of FSK modulation is used whereby the two transmitted waves have the same amplitude and phase but have different frequencies. The difference in two frequencies (F1 - F2) is called the frequency shift, F_{shift}. The target velocity induces phase difference between the echo signals of the transmitted signals. The F_{shift} is kept small; therefore, the moving target is detected at almost the same Doppler frequency position in the adjacent CPIs but with different phases. Due to small F_{shift} , F_{d1} $\approx F_{d2}$. And both the Doppler frequencies are called the beat frequency FB, which determines the velocity. Below equation shows the beat frequency.

$$FB = F_{d1} \approx F_{d2} = -(\tfrac{2*V_r}{\lambda})$$

Where $\lambda = \frac{C}{F_1}$ or $\frac{C}{F_2}$ and V_r is the velocity of the object.

The range of the object, "Range," is determined using phase information of the two received radar echo signals carrying ϕ_1 , ϕ_2.

$$Range = \tfrac{C*(\phi_1-\phi_2)}{4\pi*F_{shift}}$$

Where C is the speed of light, ϕ_1 is the phase of 1st echo wave, ϕ_2 is the phase of 2nd echo wave and difference of ϕ_1 and ϕ_2 is the phase difference between the two echo waves. The equation suggests that for frequency shifts, there should be a non-zero speed of targets. Hence, they are not good for stationary objects.

2.2 Continuous Wave Radar

These Radar operates with continuous-wave and uses the Doppler principle for detecting moving targets. These Radars operate with continuous-wave for detecting moving targets. They have two antennas, of which one antenna transmits the signal, and the other antenna receives the signal. It can measure only the speed of the target but not the object's distance from the Radar. It is a single frequency operated device and works only if the object is moving because a stationary object won't produce any Doppler shift. As there is no phase difference (as an only single wave is used) hence the distance to the target is not measurable. The velocity of the object is measured by formula

$$F_d = -\left(\frac{2V*F_t}{C}\right)$$

Where F_d is the Doppler frequency (F_t - F_r), C =speed of light. F_t is the frequency of the transmitted signal, F_r is the frequency of the received signal.

2.3 Frequency Modulated Continuous Wave Radar

If CW Doppler Radar is coupled with Frequency Modulation capability, then that Radar is called the Frequency Modulated Continuous Wave Radar, FMCW [31]. CW Radar [24] can easily measure the target's moving speed but cannot tell the distance between Radar and object. FSK Radar [30] is good at measuring moving objects but does not work well for stationary objects. FMCW radar can measure both the

speed and the distance of the target. Hence, Automotive Radar chooses Frequency Modulated Continuous Wave (FMCW) as the waveform. It can measure both moving and stationary objects.

Moreover, FMCW Radar has a very high range resolution. For FMCW Radar [26], the frequency of the transmitted signal changes periodically over time. In other words, time is marked by frequency. By knowing the frequency change of the received echo signals, the system can calculate the time difference between transmitted and received signals. The formula for R is given by:

$$R = \frac{C * \Delta t}{2}$$

The above formula calculates the distance, R, between the Radar and object according to the time change. It also calculates the distance between the radar and object according to the frequency change.

Where R is the distance between Radar and object. C is light speed (3∗108m/s). Δt is the delay time between transmitting and receiving. Since Δt equals to Δf/ (df/dt), the following formula can also be used to calculate the distance.

$$R = \frac{C * \Delta f}{2 * (df/dt)}$$

Where f is a measured frequency difference between transmitting and receiving signals, and df/dt is the frequency shift per unit of time.

2.4   Radar Frequency of Automotive World

The automotive Radars generally operates in 24 GHz (K-band) and 77 GHz (mm-wave) bands. The 24 GHz band has two sub-bands called the Narrowband (NB) and Ultra-Wideband (UWB). But, the automotive operations in the 24 GHz band are mostly limited to NB because the UWB is used for other applications. Hence, due to low bandwidth (200 MHz) available from 24 GHz band, most automakers are moving towards 77 GHz bands. This band has an advantage of large bandwidths

(4 GHz) and hence better range resolution. Moreover, the high frequency decreases the required antenna size, and hence the size of the 77 GHz Radar is considerably reduced as compared to 24 GHz radars. Figure 2.1 shows the frequency bands used in automotive radars (https://e2e.ti.com/blogs_/b/behind_the_wheel/archive/2017/10/25/why-are-automotive-radar-systems-moving-from-24ghz-to-77ghz).
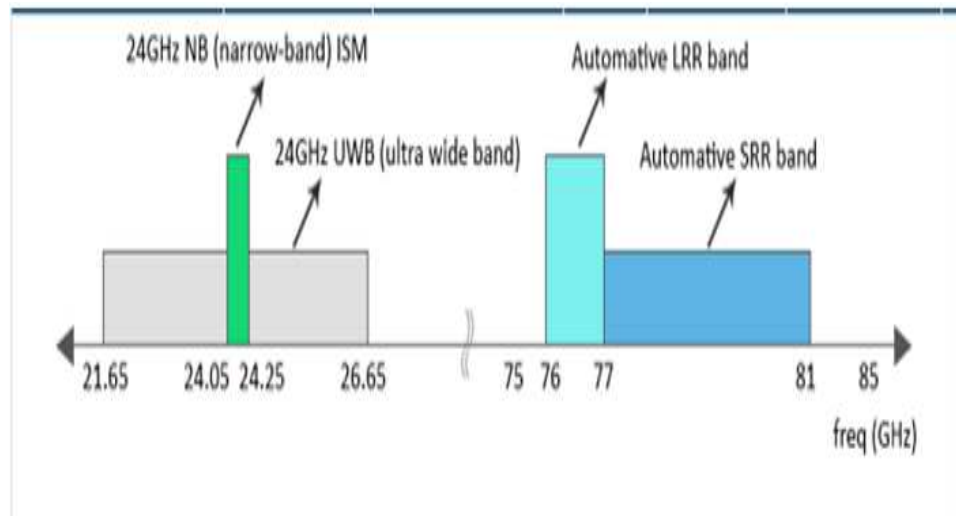
Fig. 2.1.   Automotive Frequency Bands

2.5   Radar Property of Objects

This section explores the property of Radar, which is used for mimicking. In general, there are two measures of Radar response of an object: Radar Reflectivity and Radar Cross Section (RCS). As the curb is mostly flat for and is small in dimensions, for this project, we are more interested in Radar reflectivity.

We define reflectivity as a measure of the fraction of the wave radiated back by the target to the source. Thus, the Radar reflectivity is defined as the fraction of transmitted wave (by radar), which is received back from the goal. Generally, an object having higher electrical conductivity receives stronger Radar reflectivity than

the same shaped object that has lower electrical conductivity. The shape of the object also affects the Radar response. For example, an object with a concave cone shape facing the radar has a higher Radar response than an object that has a flat surface.

Moreover, the Radar response is affected by the smoothness of the object's surface as well. Usually, if the Radar center beam is perpendicular to the surface, then the smoother surface gets higher Radar response than the rough surface; because the rough surface lets some of the waves reflect in other directions and is not received by the antenna. However, if the Radar center beam is not perpendicular to the surface, then the smoother surface gets lower Radar response than the rough surface since most of the waves that shoot on a smooth surface does not reflect back.

Reflectivity is a material property of the object [33]. To be more precise, reflectivity refers to the electrical conductivity of the object. Since the radar signal is electromagnetic (EM) wave, the higher conductive material has higher reflectivity. When resistivity is as low as in metals, the difference between the resistivity of different metals is too small to be detected by both 24GHz and 77GHz automotive radar. Therefore, 24GHz and 77GHz Radar cannot distinguish different metals. In other words, when using radar to measure different metals, the power strengths of responses of different metals are almost identical for the same frequency measurement. The reflectivity of metal is defined as 0dB. The power response that gets from the flat and smooth metal plate is usually used as a reference for reflectivity measurement. The Reflectivity measurement is used when the object has infinite sized flat surface. For example, Ground and wall can be considered having infinite flat-sized surface practically for reflectivity measurements. Moreover, when doing Radar reflectivity measurement, the Radar center beam should be perpendicular to the surface (Figure 2.2). The unit of Radar reflectivity is db. The formula for Radar reflectivity is:

$$\sigma_{target}(dB) = P_r^{target}(dB) - P_r^{reference}(dB) + \sigma_{reference}$$

Where σ_{target} (dB) is the Radar reflectivity of the target, $P_r{}^{target}$ (dB) is the power intensity of the target, $P_r{}^{reference}$ (dB) is power intensity of reference, and $\sigma_{reference}$ (dB) is Radar reflectivity of reference. Additionally, since the metal plate is used as the reference and the reflectivity of metal plate is 0dB, above formula can be written as:

$$\sigma_{target}(dB) = P_r^{target}(dB) - P_r^{reference}(dB)$$
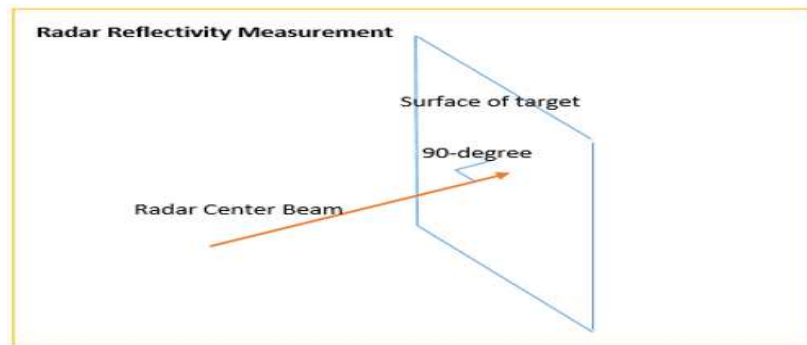
Fig. 2.2. Radar Reflectivity Measurement

2.6 Radar Cross Section (RCS)

Radar Cross Section (RCS) measured in decibel square meter (dBsm) depicts the ability of a target to reflect radar energy [17]. RCS is affected by the Radar frequency, radar-viewing angle, the shape of objects, and the material composition of the objects. For the same material composition and shape, the larger sized object has a higher RCS. For the identically sized objects, the object made of higher conductive material has greater RCS response. Also, if an object is not at the symmetrical shape, or does not have uniform curvature, measuring the object from different angles receives different RCS values. The theoretical formula to calculate RCS is:

$$P_r = \frac{P_t G_t G_r \lambda^2 \sigma}{(4\pi)^3 R^4}$$

Where Pr (watts) is the power received by Radar, Pt (watts) is transmitted power, Gt (dimensionless) is the gain of transmitting antenna, Gr (dimensionless) is gain of receiving antenna, R (meters) is the distance between Radar and the surface of object that is aimed by Radar, (meters) is Radars wavelength, and (meters squared) is RCS. RCS is affected by Radar wavelength. However, most Automotive Radar uses the FMCW waveform, whose frequency (wavelength) is periodically changed. In this case, center frequency (wavelength) is used to calculate the RCS. For instance, if the frequency of FMCW is changed between 24GHz and 26GHz (2GHz bandwidth), then 25GHz is used to calculate the RCS.

For practical RCS measurement, we first measure RCS of a reference object and then of the target. A reference object is generally an object with known reflectivity; therefore, by comparing the known value and the measured value of a reference object, it is ensured that the Radar is working correctly. Then measuring the Pr of the target and Pr of the reference object under the same condition, RCS of the target object is obtained using the following formula.

$$\sigma_{target} = \frac{P_r^{target} * \sigma_{reference}}{P_r^{reference}}$$

RCS relates to the distance between Radar and the target object. Based on the distance, RCS measurement is divided into two types. One is near field measurement; the other one is far-field measurement [27]. The field distribution in near field region changes far more rapidly than the far-field region. The near field consists of two regions, reactive and radiative field. In the reactive field, the electric (E) and magnetic (B) field are 90º out of phase, and hence no propagation of EM waves is feasible; for the propagation of EM waves, the E and B field should be in phase. The radiation field is between the reactive field and the far-field. In this field, the transition is happening from reactive to radiating filed. But, as the transition is not complete, the propagation does not happen in this field also.

Generally, near field region is defined as a region near to antenna as $< 2D^2/ \lambda$ [34]. Where D is called the maximum linear dimension of the antenna, and λ is called the wavelength of the EM wave. In the far-field range, the field distribution is almost

consistent. The RCS measurement result changes as distance changes in near field range, whereas RCS remains the same with distance changes in the far-field range. Therefore, if the target is in far-filed, RCS of the object under test is a property of the test object alone and is not a function of the radar system or the distance between the radar and the target.

$$R = \frac{2D^2}{\lambda}$$

2.7 Radar Used in this Study

This section describes the radar instruments that are used in this study, their parameter settings, and the procedure of using them.

The 24GHz radar we used is a Software-Defined Radar (SDR) [43, 44], SDR-RF 2400AD (shown in Figure 2.3). This radar has the advantage of low power consumption and high performance. The bandwidth of this radar is 2 GHz and supports three operating modes: FMCW (Frequency Modulated Continuous Wave), FSK (Frequency Shift Keying), and CW (Continuous Wave). The radar has two high gain antennas, one act as the transmitter, and the other functions as the receiver. The model of these two horn antennas is VT220SGAH20 + K2.92K. The antenna gain is 22 dB 24-26 GHz. [45].

Fig. 2.3. 24 GHz Radar

When the 24 GHz radar is coupled with an Up/down converter using the jumper cables, we can do 77GHz radar measurements using the same module as used for 24 GHz measurements (Figure 2.4). The 24GHz radar kit generates a 24-26 GHz radar signal and sends the signal to the up/down converter. The up/down converter then converts that signal to a 76-78 GHz radar signal. Table 2.1 gives the specifications of the UP/DOWN converter.
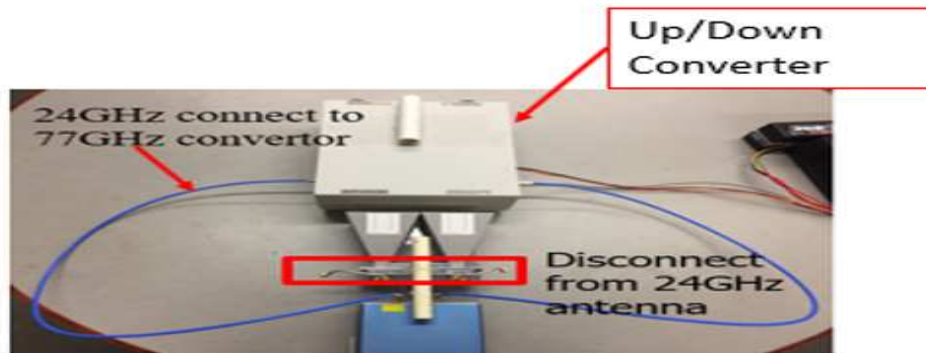
Fig. 2.4. 77 GHz Radar: 24 GHz Module + Up/down converter

Table 2.1.: UP/DOWN Converter Specifications

Parameter	Specifications
RF Frequency	76-78 GHz
LO Frequency	52 GHz, Internal
Tx RF Output Power	+20 dBm
IF Frquency	24-66 GHZ
Rx Conversion Loss	8 dB
Tx IF Input Power	+16 dB
Low Side Band Rejection	40 db
DC Bias	+12V (420mA), +8V (990mA)

SDR-RF 2400AD is configurable with the GUI software on a PC, which incites the SDR-RF 2400AD through a USB interface. As shown in Figure 2.5, the operating mode of the radar is FMCW. The module operates on the maximum bandwidth of 2GHz. The frequency of the radar wave changes from 24 GHz to 26 GHz within one sweep. Sweep time and samples per sweep jointly determine the amount of data generated within recording time.
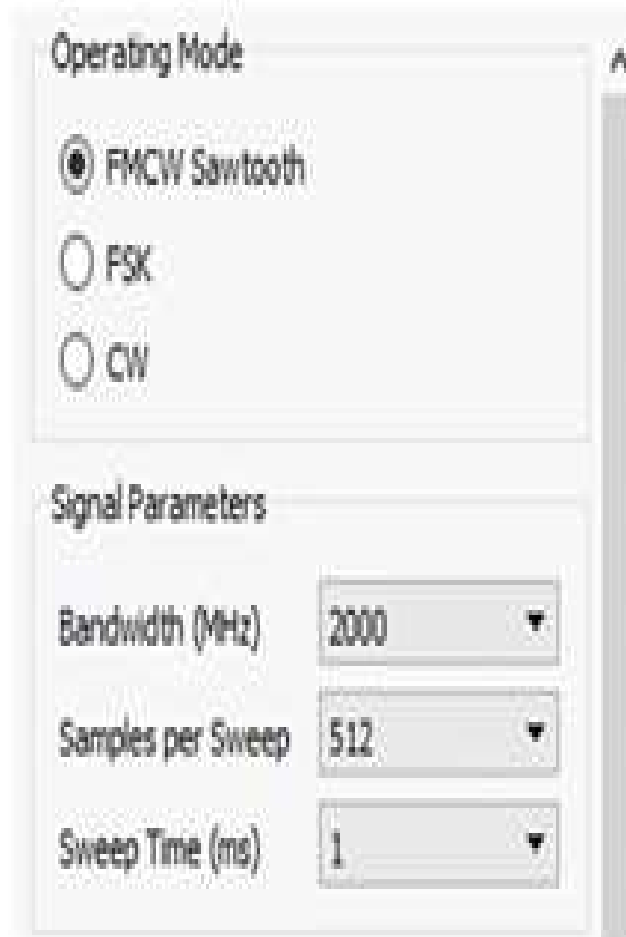
Fig. 2.5. Radar GUI Parameter Settings

It is necessary to consider the polarization of radar waves in any radar measurements since polarization affects the measurement result [13, 39]. The radar wave is an electromagnetic (EM) wave, which consists of an electric field and a magnetic field. Two fields are perpendicular to each other. The direction of the electric field is the polarization of the wave. There are two basic polarization directions: vertical polarization and horizontal polarization. The measurement result measured under these two polarizations can be used to derive results under any other degree of polarization. For vertical radar polarization, the antenna filament is kept perpendicular to the ground (Figure 2.6). For horizontal radar polarization, the antenna filament is kept in parallel with the ground. Different polarization measurements give the same result when the target object is symmetric about the origin, such as a sphere.
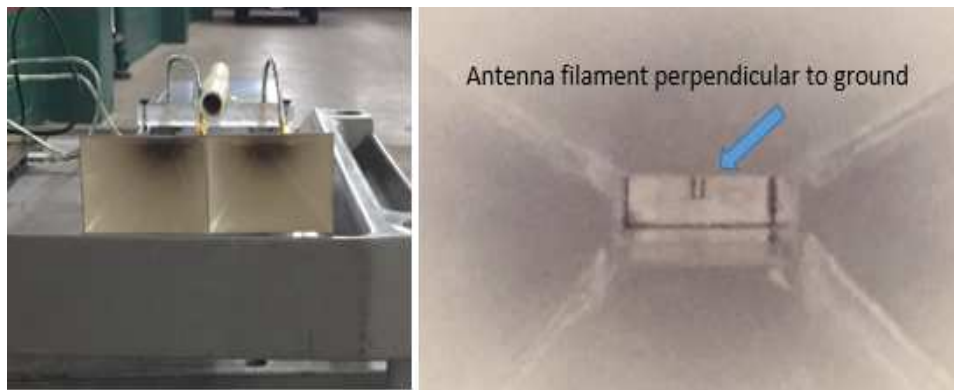
Fig. 2.6. Radar Vertical Polarization (Specific to TASI Antenna)

Before performing any measurements, one should do calibration of radar instrument. Calibration ensures that the radar is working correctly, and the measurement is accurate. If the difference between the measured RCS value of a reference object matches its ideal RCS within 1 dBsm, then the radar is considered to be working fine for our purpose. For RCS measurements, the reference object could be a metal spherical ball, a metal trihedral cone, or a flat metallic plate, whereas, for reflectivity measurements, a metallic plate is used as a reference. The type of calibration and calibration reference objects depends on what to be measured and the shape of the

object. The RCS calibration is performed for non-flat cross sectional objects. For targets like concrete dividers and curbs, whose cross sections are almost flat, for the maximum part of the structure, reflectivity measurement calibration serves the purpose. Figure 2.7 shows one such illustration. Radar measurement is hugely affected by the viewing angles. A viewing angle is an angle that the radar center beam makes with the normal to the surface. As the center beam of the radar is the strongest beam, therefore the strongest response is recorded if the center beam falls perpendicularly to the surface. Also, if the object is outside the beamwidth of radar, then the radar cannot measure that object. As seen in Figure 2.7, the center beam (red line) is not falling perpendicular to the surface, therefore this setup is not providing accurate measurements. The yellow side beam is reflected back to the radar, but it is not the strongest response. RCS is related to the Radar frequency and the radar-viewing angle and is affected by the shape and material of objects. For the same material types, the larger sized object will have a higher RCS. For the same sized objects, the object made of higher conductive material will have a higher RCS value. Furthermore, for objects which are not flat and do not have uniform curvature, measurement of the object from different angles provides different RCS values unless the object (such as the spheres) exhibits the same shape when viewed from different angles. As the curbs have maximum flat surface, in this study, for correct measurement, we kept the radar center beam perpendicular to the surface (Figure 2.8).
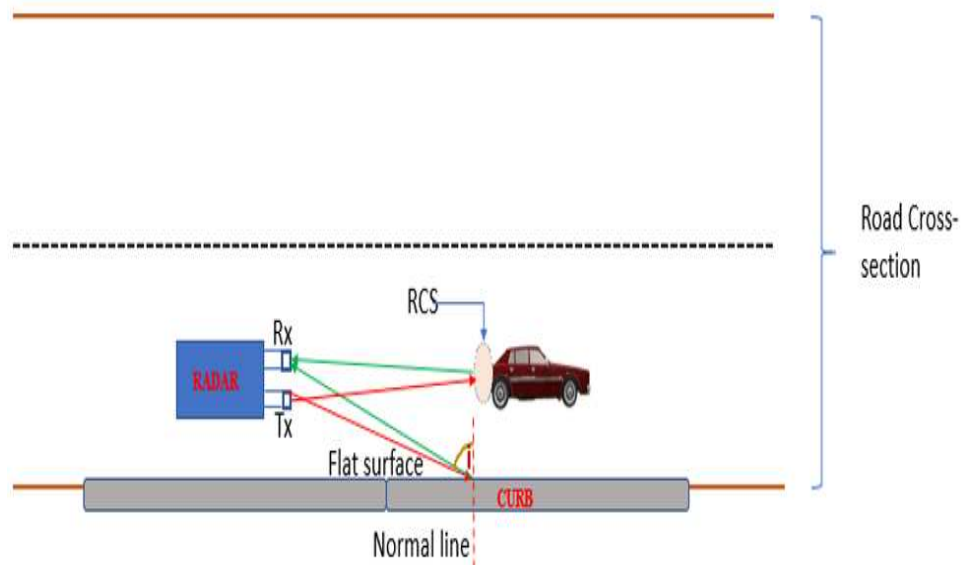
Fig. 2.7. Radar Reflectivity of Flat and Non-Flat Surface
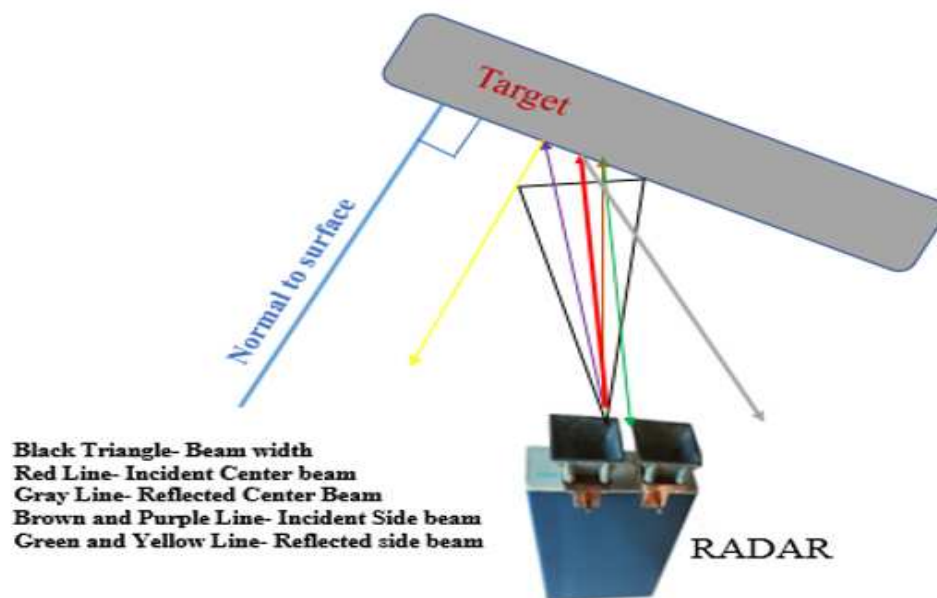
Fig. 2.8. Impact of Viewing Angle on Radar Measurement

2.8 Calibration for RCS Measurement

The reference data is used to convert raw target data to RCS value. Since the raw target data collected by a radar relate to the radar type, antenna pattern, distance, the same object measured by different radars can give different raw data. However, after calibration, their RCS value should be the same. The key point of RCS calibration is to measure some reference objects with known theoretical RCS values. These reference objects are known as reflectors. There are many types of reflectors, such as a trihedral reflector, sphere reflector, and cylinder reflector. In previous research work, the trihedral corner reflectors (Figure 2.9 left image) and sphere reflectors (Figure 2.9 right image) were used to do the calibration. The theoretical RCS value of this trihedral corner reflector (dBsm) is:

$$\sigma = \frac{10\log_{10}(4\pi L^4)}{3\lambda^2}$$

Where L is the inner dimension (red line in the left image of Figure 2.10) value (meters), and λ is the wavelength (meters).

The theoretical RCS value of sphere reflector (dBsm) is:

$$\sigma = 10\log_{10}(\pi r^2)$$

Where r is the radius of the sphere (meters). The RCS value of the sphere does is not related to wavelength. By calculation, the RCS value of this sphere reflector is -12.95 dBsm for any frequency wave.
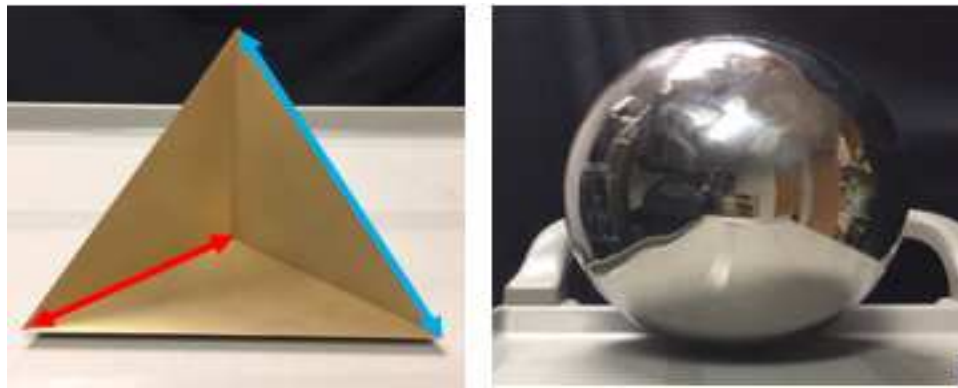
Fig. 2.9. Trihedral Corner Reflector (Left) and Sphere Reflector (Right)

This thesis is about the design and development of curb surrogates. Since the curb is short and close to the ground, the RCS measurement is profoundly affected by the road and roadside material. Since the shape of the curb is simple, knowing its surface radar reflectivity is suffice to for the radar specifications of the curb surrogate design, so we do not have to get the RCS of the curb.

2.9   Calibration for Radar Reflectivity Measurement

Reflectivity Calibration means using known reference reflectivity (received power intensity from reference) to calibrate the unknown reflectivity of a target object (received power intensity from the target) at the same measurement condition. The received power intensity from a reference metal plate is measured first and used as the reference data. This reference data is used to calculate the radar reflectivity of the surface of other targets. The radar reflectivity calibration follows five steps (the reflectivity measurement of the 24GHz Radar is described below. The reflectivity measurement of the 77GHz Radar follows the same process.

1. Set the reference object: Place the big flat metal (aluminum or stainless steel) plate on the flat surface of the target. For measuring the radar reflectivity of the concrete block, the reference metal plate is placed on the surface of the concrete block (Figure 2.10).
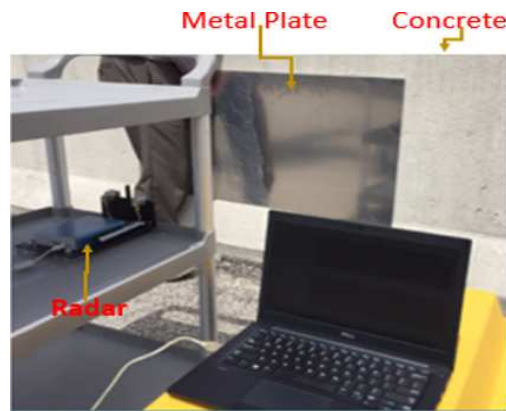
Fig. 2.10. Reflectivity Calibration using Metal plate

2. Set radar height: Set the radar to the same height as the height of the center of the metal plate (Figure 2.10).

3. Adjust the distance between the Radar and the metal plate: Adjust the distance between the radar and the reference metal plate in the following steps until Radar can only see the metal plate. (i) Put an absorber foam on the right side of the metal plate. Slowly move the absorber from right to left until the Radar peak response dropping down. Mark there as the right boundary of the Radar-viewing area. (ii) Using the same way to find the left boundary, top boundary, bottom boundary. These four boundaries will define the Radar-view area of the Radar-viewing area. If the Radar-viewing area is only on a metal plate, then the distance is correct. If the distance is too long, the radar-viewing area contains the area outside of the metal plate so the data will be incorrect. If the distance is too short, the target signal will be too close to the coupling signal, so it will be difficult or impossible to distinguish these two signals.

4. Adjust the Radar-aiming angle: Making the radar beam perpendicular to the object is essential for the radar to receive the maximum power response, which means the correct reflectivity measurement. The viewing angle is the angle that the radar center beam makes with the normal to the surface. It is shown in Figure 2.2, if the radar beam is perpendicular to the surface then we receive maximum radar response. The following steps are the procedure for setting the radar beam perpendicular to the surface of the metal plate. Initially, rotate the radar left and right horizontally to find the maximum power response, and lock at the horizontal aiming angle of the radar. Then rotate radar up and down to find the maximum power response and lock the radar vertical aiming angle to that position. Now record radar response data of the metal plate for 2 seconds.

5. Plot the recorded data: In the plot (Figure 2.11), the highest peak is the antenna coupling. The second highest peak is the signal response of the metal plate. In this measurement, the signal response of the metal plate (P_r ^{metalplate}) is 88.4 dB for 24GHz and 78.52 dB for 77 GHz.
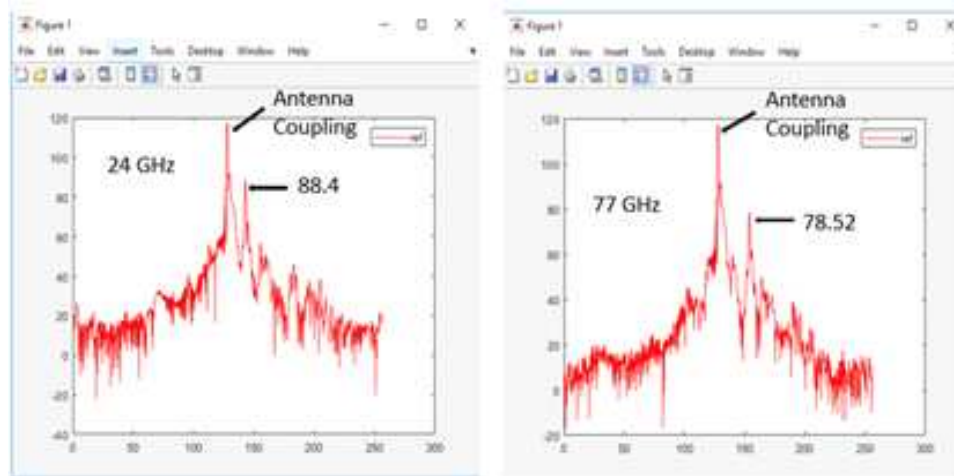
Fig. 2.11. Radar Reflectivity of Metal Plate. Left- 24GHz, Right- 77GHz

2.10 Radar Reflectivity Range of Curbs

TASI's already obtained the radar reflectivity bound of the concrete curb in previous work. It was shown that the radar reflectivity is not dependent on the color. Based on the measurement of many concrete samples, the reflectivity of 24GHz and 77GHz radar for dry and smooth concrete blocks are in the range of -7.3 $\pm$ 1 db. It was also shown that the radar reflectivity does not depend upon the shape and coating of the concrete dividers. The surrogate curbs must follow the reflectivity range of -7.3 $\pm$ 1 db.

3. LIDAR CHARACTERISTICS OF CURBS

Since LiDAR is commonly used for object detection in automated driving, understanding of LiDAR characteristics of the curb is necessary for developing a surrogate curb. The following section lists LiDAR working principles, instruments used for LiDAR reflectivity measurement, and the LiDAR (near-infrared) reflectivity satisfaction criterion.

Light detection and ranging (LiDAR) and imaging is a sensing method that detects objects and maps their distances from the LiDAR. LiDAR can provide a 3D characterization of objects without much back-end processing. This technology works by illuminating a target with an infrared light pulse and measuring the characteristics/information of the reflected return signal. The width/time-period of the optical pulse can range from a few nanoseconds to several microseconds. LiDAR works on a single wavelength and different LiDAR makers may use different wavelengths for LiDAR operations. Initially, LiDAR in wavelength range 800-1000nm was chosen for LiDAR operations because pulsed diode laser emitters were readily available and were relatively inexpensive. As the high power 800-1000nm waves can be harmful to human eyes, a new 1550nm operating wavelength was proposed for LiDAR. At 1550nm, human eyes are less at risk.

According to the LiDAR beam steering mechanism, there are two types of LiDAR systems; Mechanical steering and Solid-state steering systems. In a Mechanical LiDAR, a very high-quality optics and a rotating assembly are used, which creates a wide (normally 360-degree) Field-of-View (FOV). The mechanical facet does provide a high Signal to Noise Ratio (SNR) over a wide FOV, but it makes the implementation cumbersome. On the other hand, a Solid-state LiDAR is devoid of any spinning mechanical components and has a reduced FOV. Solid-state LiDAR has higher resolution, is smaller in size, more robust, and less expensive than conventional mechanical

LiDAR systems. Unlike mechanical radars, which requires precise and accurate arrangements of mechanical parts, Solid-state LiDAR sensors are based on a silicon chip and do not require mechanical moving parts.

3.1 Theory and Operations of LiDAR

LiDAR intensity is a measure of the power of reflected laser pulse, which is dependent on the transmitted power, viewing geometry, atmospheric and target characteristics, and other parameters specific to the system. The received power of LiDAR is generally specified by the LiDAR range formula:

$$PR = \frac{PT*\eta}{\pi^2 r^4} \frac{A_{rec}}{Div_{trans}} \frac{\rho A_{target}}{Div_{ref}}$$

Here, P_R is received power, P_T is transmitted power, η is quantum efficiency of the receiver, R represents the range to the target, A_{rec} is the area of the receiver, A_{target} is the area of the target, Div_{trans} is the laser beam divergence before reflection, Div_{ref} is the laser beam divergence after reflection, and finally, ρ is the target reflectance. The range of the target is calculated by formula:

$$R_{target} = \frac{C*(T_{st}+T_{tr})}{2}$$

Where R_{target} is the range of the target, C is the speed of light, T_{st} is the time the transmitted wave takes to travel from source to target, T_{tr} is the time taken by the reflected ray to travel from target to receiver.

This simplified equation ignores atmospheric effects and only takes sensor characteristics and target behavior into account. Other forms of the LiDAR range equation are also present in literature that considers environmental factors. One such form is given below:

$$P_R = \frac{P_T D_r^2 \eta_{atm} \eta_{sys} \rho \cos \alpha_i}{4R^2}$$

Here, η_{atm} is an atmospheric transmission factor, η_{sys} is system transmission factor, D_r is the receiver aperture diameter, and α_i is the angle of incidence.

This equation assumes that the target surface is purely Lambertian, i.e. the surface seems equally bright from every viewing direction. If the range is considered an independent variable and the other parameters are constant, then it is easy to notice that the received power is heavily dependent on the reflectance of the target surface. The target surface can be successfully detected by LiDAR if P_R has a sufficiently large signal-to-noise ratio. From above formula, it is apparent that if all other variables remain constant, P_R depends on the target reflectance ρ. Therefore, to make surrogate objects mimic real roadside objects, the surrogate objects must match the reflectance properties of real objects.

3.2 Reflectance and BRDF

In general terms, reflectance at a given optical wavelength is defined as the ratio of the radiance of surface to the irradiance of the surface. Reflectance is a directional property and is highly dependent on surface characteristics and viewing geometry. The dependence of the surface reflectance on the viewing angle is described by comparing the radiance of the target surface to the radiance of an ideal Lambertian surface illuminated and viewed in the same conditions as the surface. The ratio is called a reflectance factor. In general, the reflectance factor depends on the viewing angle and the incident angle (to be defined later). Since two light directions are involved, the term bidirectional reflectance factor (BRDF) is used.

Reflectance of a surface is fully described by Bidirectional Reflectance Distribution Factor (BRDF). The term Bi-directional emphasizes that it depends upon directions of both incident and reflected light. BRDF can be described by:

$$BRDF : f(\theta i, \phi i; \theta i, \phi i) = \frac{Lsurface(\theta r, \phi r)}{Esurface(\theta i, \phi i)}$$

The surface reflection depends both upon the viewing and illumination angle. Figure 3.1 shows the basic layout of surface reflection.
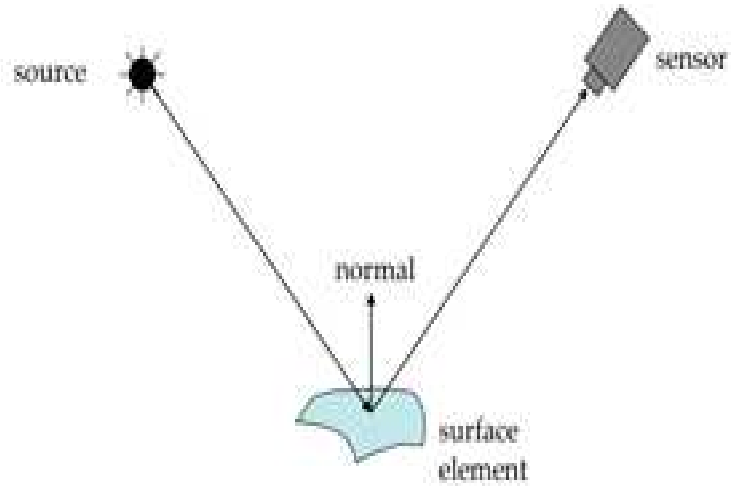
Fig. 3.1. The Surface Reflection

The definitions of the two directions and BRDF are shown in below Figure 3.2. The light direction and the vertical plane of the probe direction (i.e., 0° phase angle indicates probe and light source are in the same vertical plane). The phase angle is equal to the difference between the incidence azimuth angle ϕi and viewing azimuth angle ϕr [30].
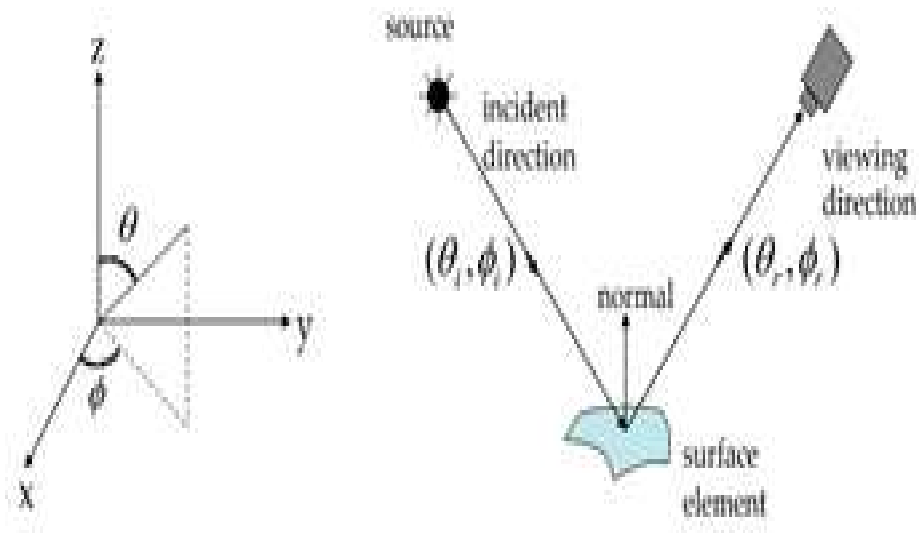
Fig. 3.2. Geometry of Bidirectional Reflectance Distribution Factor

$E^{surface}(\theta i, \phi i)$ Irradiance at surface in direction $(\theta i, \phi i)$

$L^{surface}(\theta r, \phi r)$Radiance of Surface in direction$(\theta r, \phi r)$

$BRDF : f(\theta i, \phi i; \theta r, \phi r) = \frac{L^{surface}(\theta r, \phi r)}{E^{surface}(\theta i, \phi i)}$

θr is the viewing zenith angle, ϕr is the viewing azimuth angle, λ is the wavelength of incident light, θi is the incident zenith angle, ϕi is the incident azimuth angle, $\mathrm{L}^{surface}$ is the radiance of the surface in the direction of viewing, and $\mathrm{E}^{surface}$ is the irradiance at the surface in the direction of incident light. Some terms relevant to the reflectance measurement setup are described below [37];

Normal line: Normal line is a line that is perpendicular to the surface plane. (Figure 3.3). The orange dashed line in the left figure denotes a normal line. When measuring a horizontal surface, the normal line is vertical. On the other hand, when measuring a vertical surface, the normal line is horizontal (right figure).

Fig. 3.3. Normal Line

Measurement angle: Measurement angle (or probe angle) is the angle between the normal line and probe direction is defined as a measurement angle (Figure 3.4). Measurement angle is also called the viewing zenith angle. 0 degree measurement angle means that the probe direction is perpendicular to the surface, and a 90 degree measurement angle means that the probe direction is parallel to the surface plane. When the probe is nearly horizontal (0 degree-20 degree measurement angles), we define such angles as near-horizontal measurement angles.
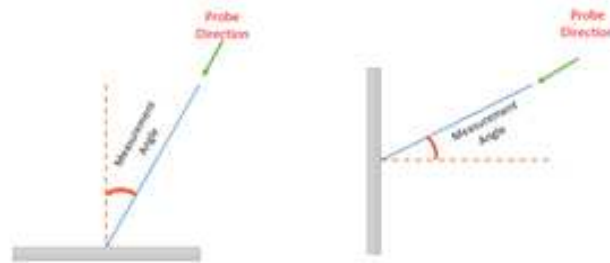
Fig. 3.4. Measurement Angle

Illumination angle: Illumination angle is the angle between the normal line and the light direction (Figure 3.5). Illumination angle is also known as the incidence zenith angle. 0 degree illumination angle means that light falls perpendicularly on the surface, and a 90 degrees illumination angle means that light emitted by the source is parallel to the surface plane. In the case of outdoor measurements where the sun is the light source, if the surface is vertical (Right figure), then the normal line is horizontal. Therefore, the illumination angle is equal to the sun elevation angle (i.e., the angle between sunlight direction and horizontal plane). If the surface is horizontal (Left figure), then the normal line is vertical. Therefore, in this case, sun illumination angle = 90 degrees - sun elevation angle.
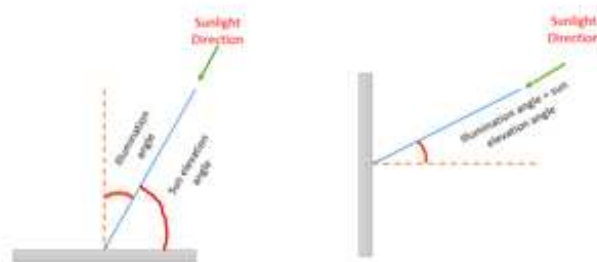
Fig. 3.5. Illumination Angle

Phase angle: Phase angle is the angle between the vertical plane of light direction and the vertical plane of probe direction (i.e., 0 degree phase angle = probe and light source are in the same vertical plane). This angle is equivalent to the difference between the incidence azimuth angle and the viewing azimuth angle. The geometry of the phase angle is understandable from Figure 3.6.
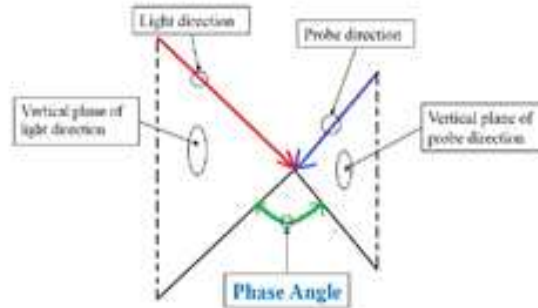
Fig. 3.6. Phase Angle

Reflection can be of two types- specular and diffuse. The light reflects off surfaces as per the law of reflection. The laws of reflection of light are valid for the reflection of light from a whole lot of different kinds of surfaces; flat surfaces, vertical surfaces, angled surfaces, and even curved surfaces. If we can draw a normal line at the point of incidence of the ray, then we can measure the angle of incidence and can determine the direction of the reflected ray. Different types of incident light and their corresponding reflected light are shown in Figure 3.7 Each ray incident on a surface at a different orientation, and yet each ray reflects as per the law of reflection.
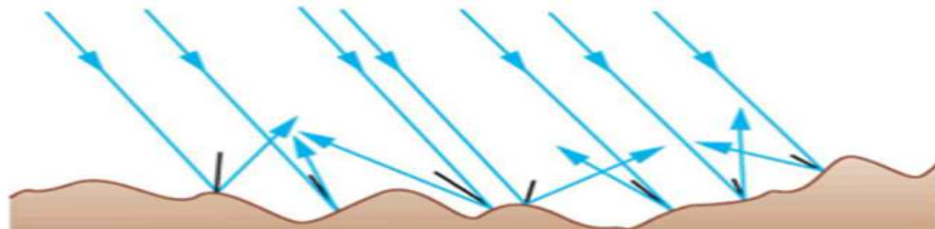
Fig. 3.7. The Laws of Reflection Always Holds

Mirrors are typically an example of smooth surfaces, even at the microscopic levels. Such that they can offer each ray of light the same surface orientation. However, most objects, which reflect light, are not smooth at the microscopic level. The clothes, the concrete curbs, the grass, the sands, the forests, and even paper are all rough when viewed at the microscopic level (mm scale). Figure 3.8 depicts a close view of the surface of one such concrete surface.

Fig. 3.8. The Surface of the Concrete Curb

Reflection from the smooth surfaces such as mirrors are known as **specular reflection**. Reflection of rough surfaces such as concrete curb, forest and asphalt roadway is called **diffuse reflection**. Whether the surface is microscopically rough or smooth has a tremendous impact upon the reflection of light or laser beam. Figure 3.9 depicts two beams of light incident upon a rough and a smooth surface.
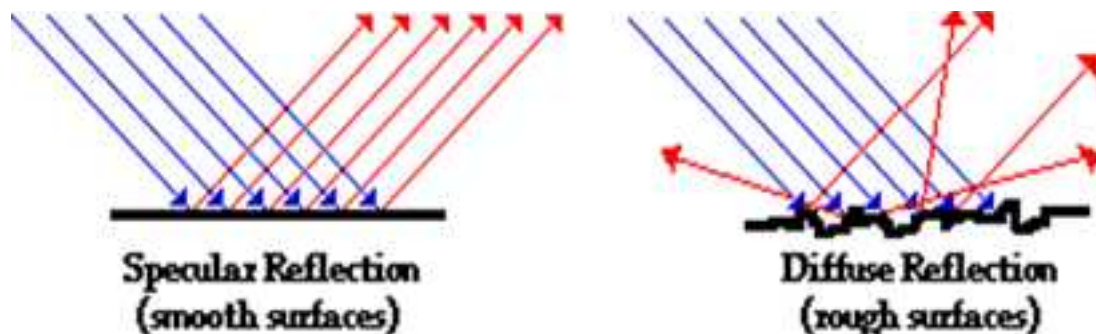
Fig. 3.9. Specular and Diffuse Reflection

Specular reflection: In the case of specular reflection, light energy is completely reflected in one direction. For example, mirrors and shiny metals exhibit mostly specular reflection because most of the light reflected by them follows the angle of reflection (BRDF is high if viewed from that direction), and a tiny amount of energy is reflected towards other directions (very low BRDF in those directions). The more a surface is specular, the more shiny or glossy it is. Figure 3.10 shows a few such examples.

Diffuse reflection: In case of diffuse reflection, light is uniformly reflected in every direction (i.e., BRDF is uniform for all viewing directions). Matte surfaces exhibit mostly diffuse reflection. Pure diffuse reflectors (i.e., reflectors which reflect all incident light in a diffuse manner) are called Lambertian reflectors. Figure 3.10 shows a few such examples.
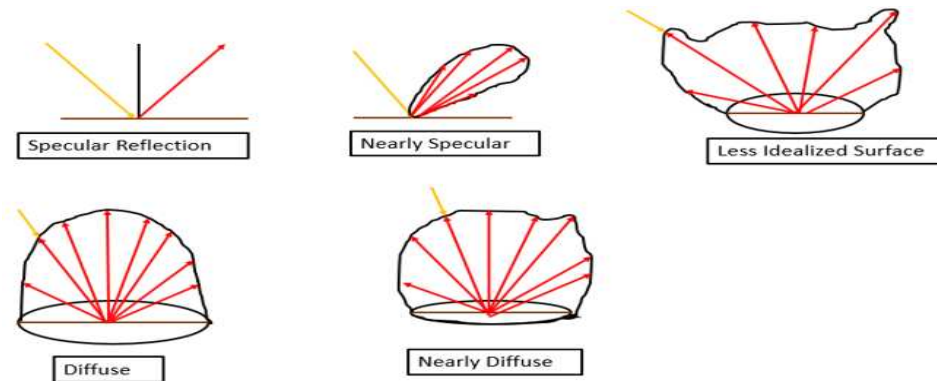
Fig. 3.10. Examples of Specular and Diffuse Reflection

As this study deals with concrete curbs and as stated, concrete curbs are Lambertian surfaces. The question is why does a rough surface diffuse a beam of light?

For each type of reflection, each individual ray abides the law of reflection. However, due to the roughness of the material each individual ray meets a surface, which has a different orientation at different places. The normal line at the point of incidence is different for different rays. Therefore, when the individual rays reflect off the rough surface according to the law of reflection, they scatter in different directions.

The result is that the rays of light are incident upon the surface are diffused upon reflection. Figure 3.11 shows the idea. The incident rays **A, B, C, D, E** are incident on a surface. The normal line at each point of incidence is shown in black and labeled with an **N**. For each case, reflected **A', B', C', D', E'** are also shown.
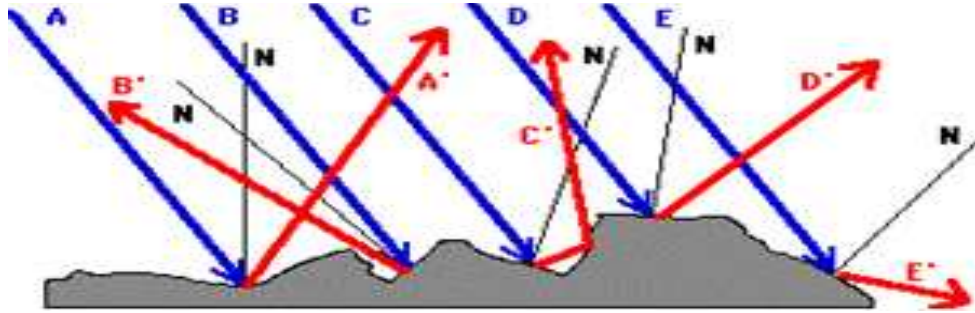
Fig. 3.11. The Idea Behind the Diffuse Reflection

3.3   Description of LiDAR used in this study (LiDAR OS-1)

Below is the description of one of the LiDAR being used in the automobile industry. The OS-1 is a 64-beam high-resolution imaging LiDAR, which has a laser wavelength of 850nm. It has a long lifetime and is an all-weather device for both indoor and outdoor setups. The 64 beams are in different elevation and depression angles. The LiDAR can rotate horizontally 360 degrees for measurements. The laser beams of LiDAR is shown in Figure 3.12.
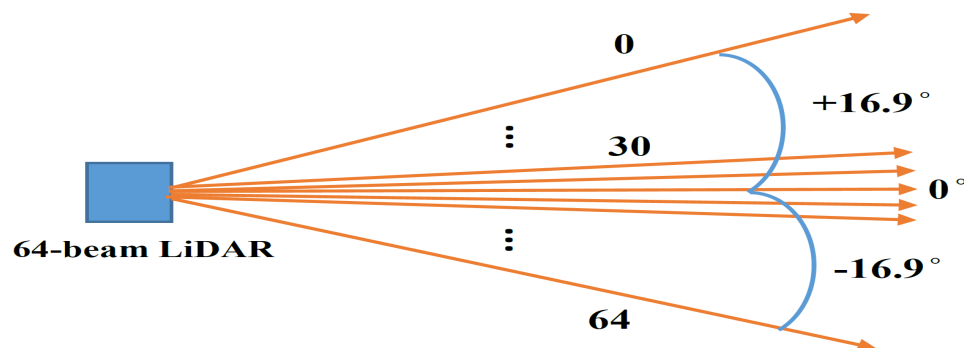
Fig. 3.12. LiDAR Beam Numbers and Distribution in the Vertical
Direction

The highlights of LiDAR OS-1 are:

- Fixed resolution per frame operating mode.

- Provides images of similar intensity and from a similar range as of the camera.

- Simultaneous and co-calibrated 2D and 3D output.

- Multi-sensor cross-talk immunity.

3.4   Instruments for IR Reflectance Measurements

Although the purpose of this thesis is to design a surrogate curb that can mimic LIDAR measurements of the real roadside curb, it is not suitable to use LIDARs for reflectance measurement. We used a spectrometer in place of LiDAR for IR measurements. The foremost reason is that each LIDAR sensor has its parameters and configurations that are often propriety of the manufacturer. Besides, there are atmospheric parameters such as the sun angle that are often hard to model. Without the knowledge of such parameters, it is often impossible to accurately measure the reflectance. Next, each LIDAR only uses a laser of a single wavelength. Since we are interested in covering a relatively broad wavelength range (800-1100 nm), the use of a LIDAR for our measurement is not suitable.

Spectrometer and Related Accessories: Spectroradiometers or spectrometers are commercially available instruments suited for IR measurement in a range of wavelengths. The spectrometer used for this thesis (ASD FieldSpec Pro), has a range of 350-2500 nm [38]. Spectrometers measure the reflectance of a surface relative to a reference panel with known reflectance characteristics. Spectrometers are often portable, making them well-suited for both outdoor and indoor measurements. For outdoor measurements, the sun acts as a light source. However, it is challenging to achieve the desired light direction because (i) the movement of the sun cannot be controlled and is time-dependent, and (ii) depending on the season and geographic

location of the experiment, some sun angles are not achievable at all. Indoor measurement can take care of this limitation. In this case, a standard indoor light source is used. Both the illumination direction and measurement direction can be customized to suit the requirements. Therefore, a combination of controllable light source and spectrometer helps to keep the source and the receiver at the same place, and thereby we can mimic the LiDAR.

1. ASD fieldSpec Pro Spectroradiometer made by Analytical Spectral Devices, Inc. (Model: FSP 350-2500P).

2. 99% Spectralon White Reference Panel by LabSphere Inc.

3. ASD fieldSpec Pro Spectroradiometers.

ASD FieldSpec Pro Spectroradiometers: The ASD FieldSpec Pro full range Spectroradiometers (spectrometer in short) is a field spectrometer that allows spectral measuring and viewing in real-time, enabling the user to measure radiance and reflectance spectra of materials readily. Analytical Spectral Devices, Inc. (ASD) manufactures this spectrometer. This spectrometer operates in the 350-2500 nm spectral region and consists of three separate detectors that perform reflectance measurement in VNIR (350-1050 nm), SWIR1 (900-1850 nm), and SWIR2 (1700-2500 nm) regions respectively. The VNIR detector has a sampling interval of 1.4 nm and a spectral resolution of 3 nm, while each of the 11 SWIR detectors has a sampling interval of 2 nm and spectral resolution of 10-12 nm depending on the scanning angle. Figure 3.13 shows the ASD FieldSpec Pro spectrometer and the optical fiber probe through which it collects light information.

Fig. 3.13. ASD FieldSpec Pro Spectrometer (Left), Optical Fiber Probe (Middle), and 1° Field-of-View Reducer Accessory (Right)

FieldSpec Pro makes use of a probe made of a fiber optics bundle to collect light information. The bare optical fiber has a 25 degree field of view (FOV), but an FOV reducer was used to bring down the field of view to 1 degree. Light is collected by the fiber optics and then fed to a holographic diffraction grating. The grating separates the wavelength components of the light and feeds it to the detectors for measurement. Incident photons are converted to electrons, and during readout, a 16-bit analog to digital converter converts the photoelectric current from each detector to a voltage and digitizes the voltage. Data acquisition and examination are done using proprietary software provided by ASD named 'RS3' and 'ViewSpec Pro.' By using the RS3 software, it is possible to see and record real-time measurement data. The recorded data can later be seen and exported in suitable formats using the ViewSpec Pro software.

White Reference Panel: The measurement taken from a reference surface with known characteristics helps to ensure that the spectrometer functions correctly. After ensuring the proper functioning of the spectrometer, if the light source is stable and the illumination geometry of the unknown object is kept identical to the reference object, then the measured reflectance value of the unknown object is accurate. That is, during measurement, both the unknown material and the reference material must be in a similar orientation relative to the light source and probe, and lighting should stay similar throughout. In summary, the reflectance is computed using measurements from both the sample material and reference material with known reflectance properties. A reference panel with nearly 100% reflectance throughout the whole wavelength range is called a white reference standard or white reference panel. The reference panel used for this work is a 99% Spectralon white reference panel manufactured by LabSphere Inc. (shown in Figure 3.14), which exhibits near-perfect reflectance properties to ensure reflectance data collection with high accuracy.

Fig. 3.14. The White Reference Panel (99% Spectralon)

ASD ProLamp Light Source: The ASD ProLamp (shown in Figure 3.15) is a controllable 14.5V-50W Lamp. It is mountable on a tripod and provides light over a 350 - 2500 nm wavelength range. Thus it feasible to make indoor reflectance measurements for various viewing angles.
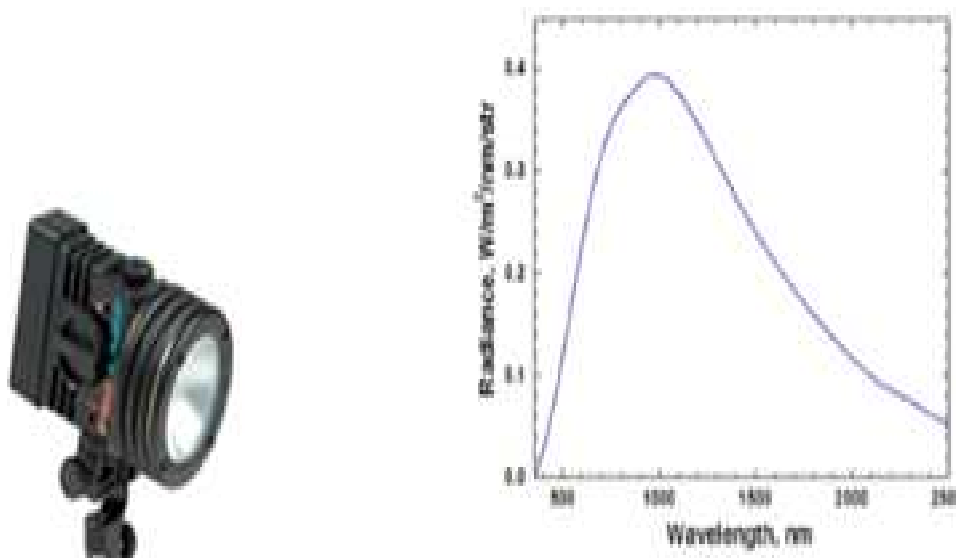
Fig. 3.15. ASD Pro-Lamp Light Source (Left) and the Radiance of the Lamp Measured Using 99% Spectralon White Reference Panel (Right)

Procedure for IR Reflectance Measurement

1. Turn on the laptop and the spectrometer at the test site and warm up the spectrometer for at least 30 minutes before use.

2. Launch the 'RS3' software.

3. Choose a suitable sample site for taking the measurement (for example, a fixed portion of the road). For the movable samples, the sample is fixed in the desired angle using an angle calculator.

4. Keep the white reference plate on top of the chosen site and fix the probe at the desired angle. In the case of indoor measurement, the light source is also fixed at a desired angle and distance.

5. Optimize the instrument by selecting "Control ⇒ Optimize instrument settings" in the software.

6. Use the ruler and an angle calculator for determining the desired distance and angle between the optical fiber probe and the sample. The probe must point at the white reference panel.

7. Select the following option in the software: "Control ⇒ Take white reference measurement." After this measurement, the subsequent measurements would return reflectance values.

8. Remove the white reference plate from the site. The optical fiber probe points towards the target material at the same geometric orientation used in the case of the white reference panel. We can now see the real-time reflectance spectrum of the material on the software interface.

Also, note that a LiDAR sends and receives light in the same direction. Therefore, to mimic LiDAR conditions during reflectance measurement, the illumination angle should be equal to the measurement angle for all measurements, and the phase angle should ideally be 0 degree. However, due to equipment limitations, keeping the phase angle exactly 0 degree results in uneven illumination or severe shadowing on the surface being measured. Therefore, for most measurements, a small 10 degrees-20 degrees phase angle was kept.

Reflectivity Bounds of Curbs: In the previous work [46], the IR reflectance bound of Portland concretes was established. These bound is used as the requirement for making surrogate concrete curbs However, the bounds were established using the old curbs and not the new curbs. The reflectance of the newly painted concrete was much higher than that of the older curbs and the proposed bonds (Figure 3.16).
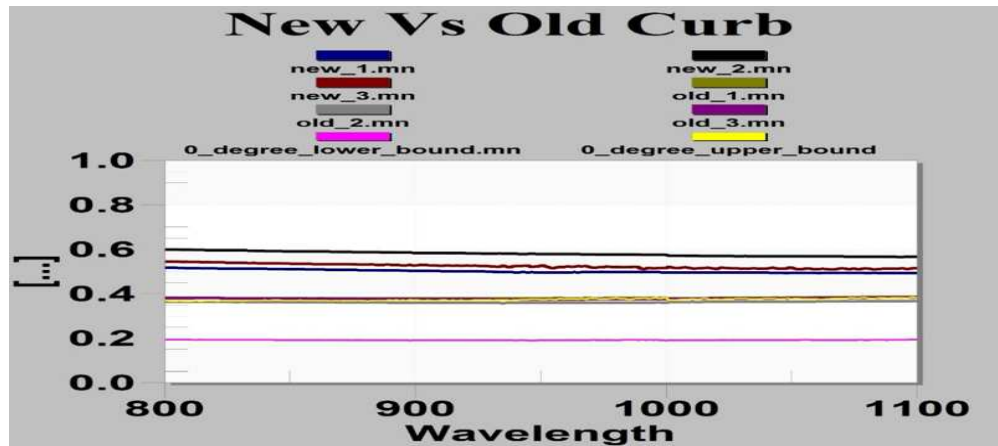
Fig. 3.16. IR values of New and Old Curb-Two Year Back

- IR values for new curbs (new_1, new_2, and new_3) are higher than the required IR bounds (pink and yellow line).

- IR values of old curbs (old_1, old_2, old_3) are within the bounds.

The curing compound coating creates a reflective membrane on the concrete surface, resulting in a higher reflectance of the new concrete samples. [41] hypothesized that the curing compounds coating applied to the new concrete cause the IR reflectance values to be high, and the coating would fade down in a year or so. Thus, the new curb should behave like an old curb after a year or so. However, we are not sure if the above-mentioned assumption is valid. Therefore, we need to verify the hypothesis that the coating on the new curbs fades down, and ultimately it would follow the IR reflectance bounds of old curbs. If the hypothesis stands, then we can use the previously defined bounds, or else, we need to redefine new bounds. For this purpose, we tested the same new curb beside the IUPUI SL building at the N Blackford St, which was tested before by TASI. The setup is explained below and shown in Figure 3.17. The images shown below are for measurement angles 10, 20, 40, and 60 degrees.
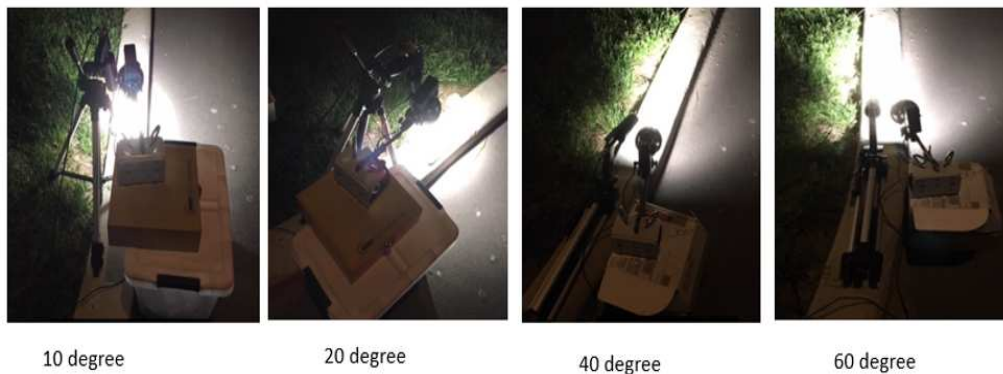
Fig. 3.17. Test Setup for IR Bound Verification

Results of Verification Measurement: After performing the test, we compared the new IR reflectance value of the curb to its value one-year-old. The new value was significantly lower than the older value (Figure 3.18).
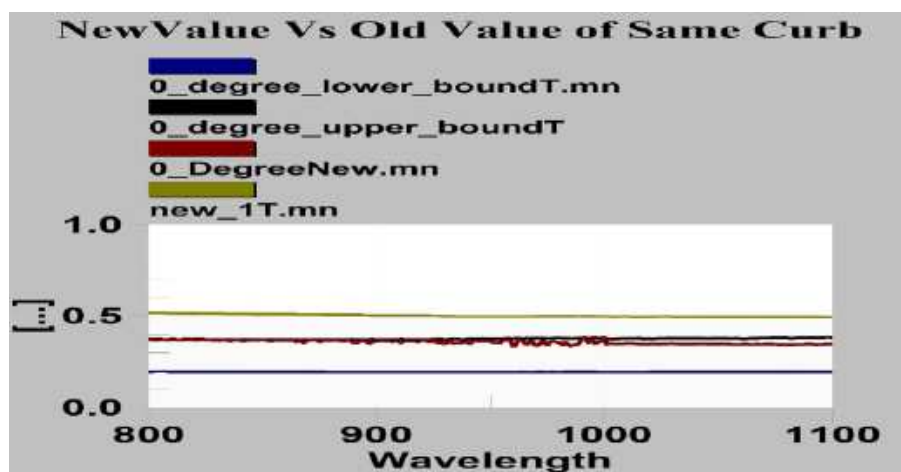
Fig. 3.18. New IR Value vs. Old IR Value of the Same Curb

- The brown line in Figure 3.18 is the new IR value, and the yellow line is the old IR values.

Next, we plotted the new IR values for viewing angles 0 to 70 degrees. Figure 3.19 to 3.26 shows the plot from 0 to 70 degrees measurement angles.
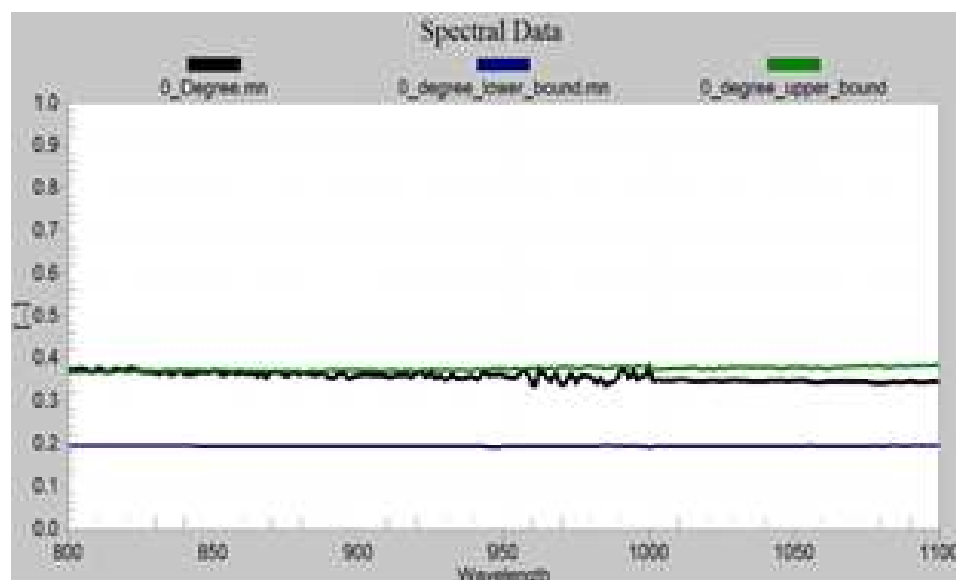
Fig. 3.19. 0 Degree Measurement Angle
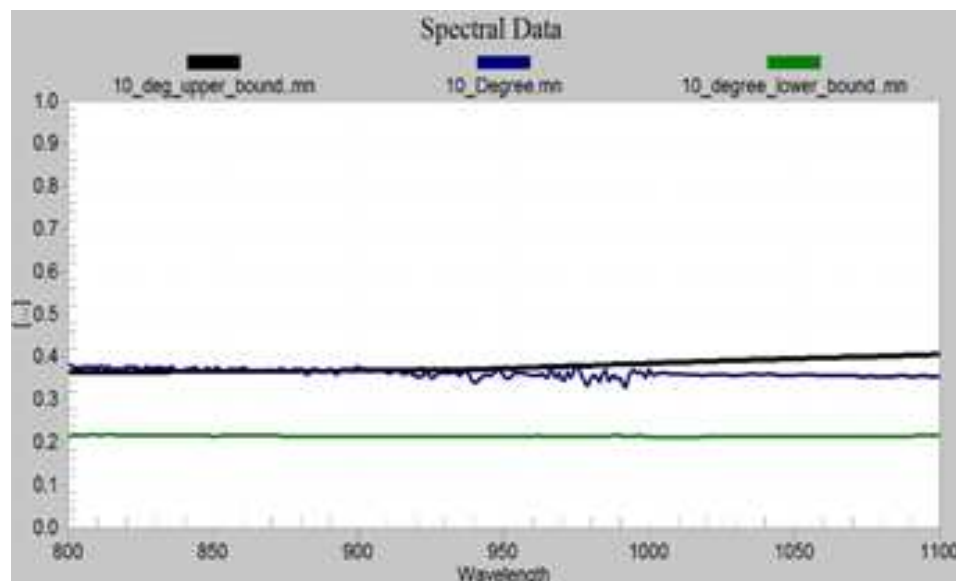
Fig. 3.20. 10 Degree Measurement Angle
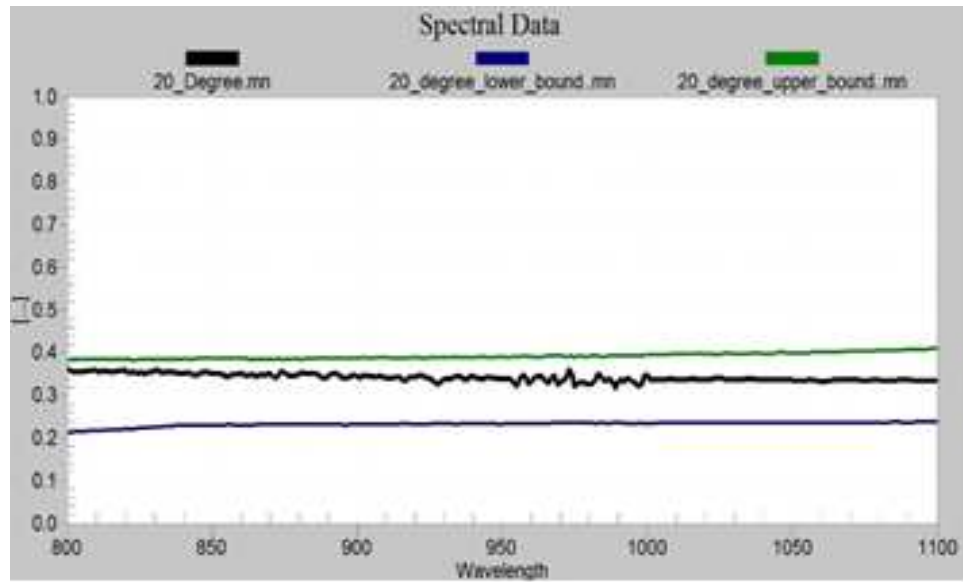
Fig. 3.21. 20 Degree Measurement Angle
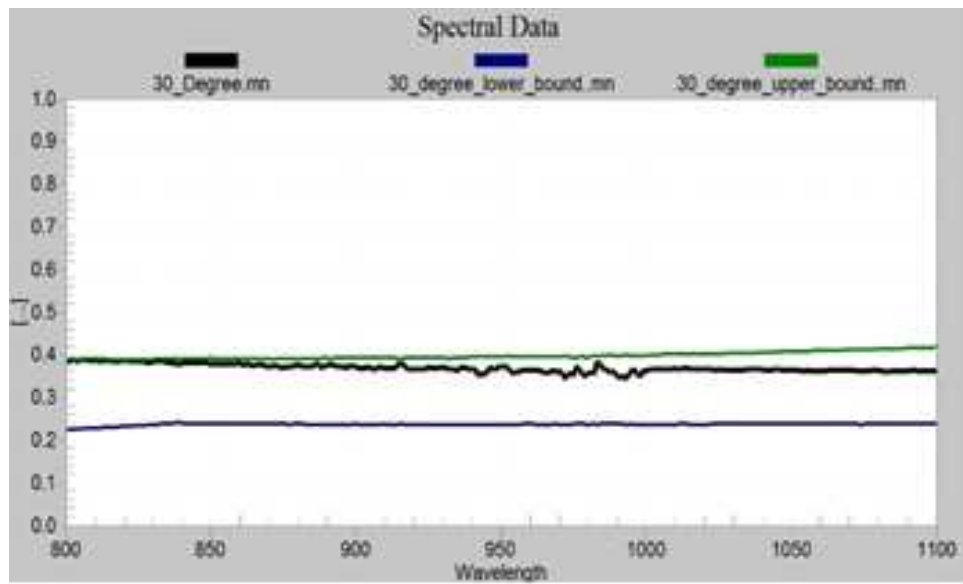
Fig. 3.22. 30 Degree Measurement Angle
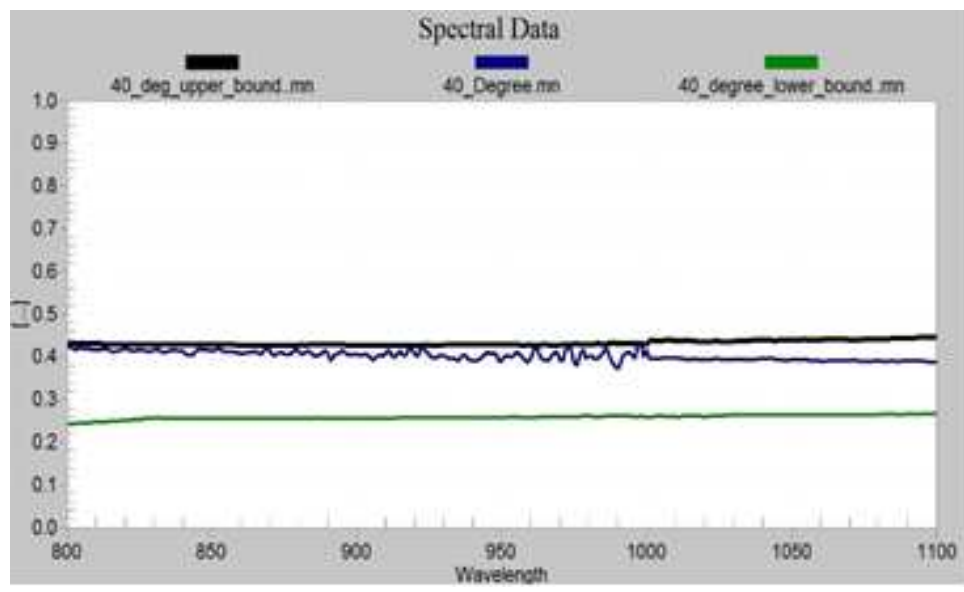
Fig. 3.23. 40 Degree Measurement Angle
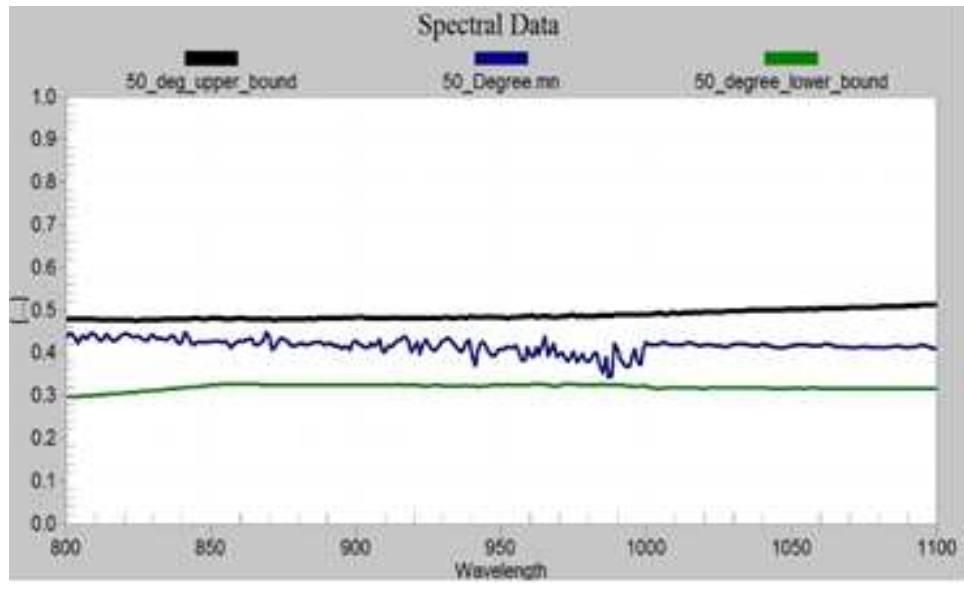
Fig. 3.24. 50 Degree Measurement Angle
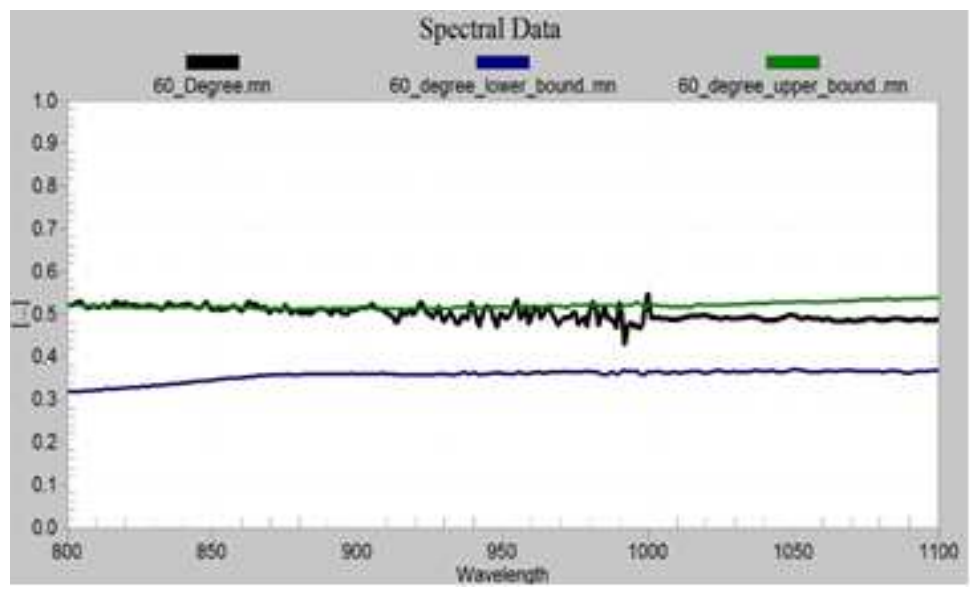
Fig. 3.25. 60 Degree Measurement Angle
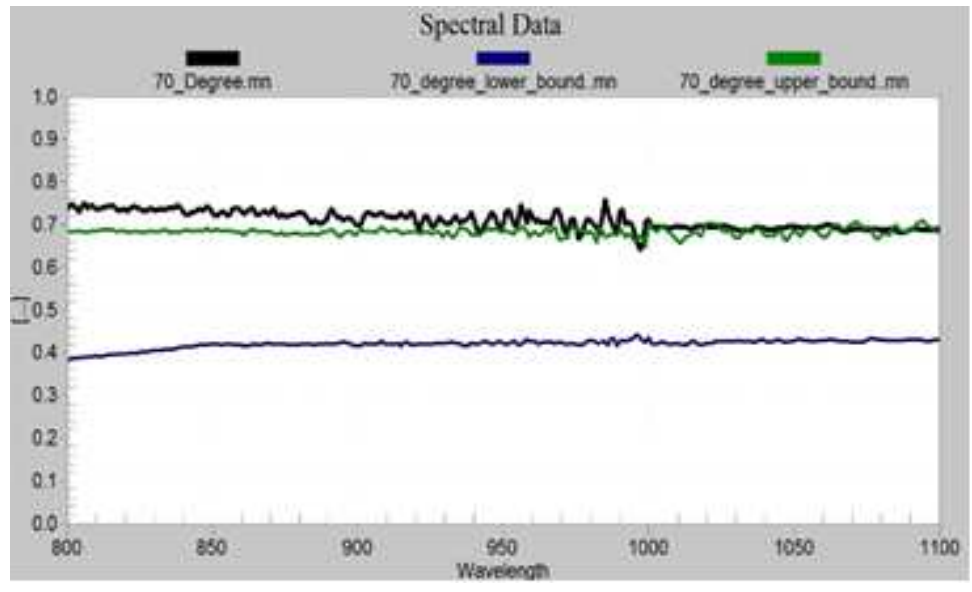
Fig. 3.26. 70 Degree Measurement Angle

The post-test results are:

1. New IR values are lower than the older IR values.

2. IR values for 0 to 70 degrees viewing angles are within or on the border of bounds.

Hence, we can conclude that the assumption holds. The IR reflectance value of a one-year-old curb has decreased significantly. The values were on or below the upper bounds. In a half year or so, it would behave exactly like an old curb. Therefore, we can use the already setup IR reflectance bounds as the IR reflectance requirement for surrogate curb development.

4. CAMERA CHARACTERISTICS OF CURBS

TASI developed curb surrogates previously. The surrogate satisfied the radar and LiDAR requirements. However, the color of that curb surrogate is uniform and looked like a very new curb. Since a high percentage of US roadside curbs look old, we need to make realistic looking curb surrogates that can represent commonly seen curbs on US roads. Therefore, it is imperative to conduct a comprehensive study of all types of curbs found on the US roadside. Specifically, it is essential to identify the colors and color patterns of the representative curbs on US roadsides. This section describes the method for obtaining camera characteristics of curbs. The clustering technique is used for grouping similar colored curbs and lay down the representative color and color patterns, which will serve as part of the requirements for making realistic surrogate curbs.

Color Spaces: RGB (red, green, and blue) is the most common color space for color description. However, similar colors are more clustered together in RGB color space and more challenging to distinguish the color groups. Distinguishing the color groups is less problematic in CIELAB or LAB color spaces. Therefore, we try to group (or cluster) the colors on the curb in LAB color space. The RGB color models are useful to visualize color on monitors and cameras. The database of this study has images from google street view. Hence, we needed to verify the color displayed on the screen. Therefore, we need to conceptualize both the RGB and LAB color models.

RGB (red, green, and blue) is the most common color space for color description. The RGB color models are useful for visualizing colors. The database of this study has a large number of roadside object images captured from Google street view. Hence, we used the RGB model to analyze those images. However, colors in RGB color space are not evenly distributed and some similar colors are more clustered together, so it

is challenging to distinguish the color using the clustering method. Distinguishing the color groups is less problematic in CIELAB or LAB color spaces. Therefore, we try to group (or cluster) the colors on the curb in LAB color space.

RGB Color Space: RGB is a commonly used color representation. Variations in proportions of Red, green, and blue can provide any color in the visible spectrum [15]. The percentage mix of all R, G, and B can range from 0 to 100 of full intensity. Using an 8-bit resolution, the level of presence is representable by the decimal numbers ranging from 0 to 255 (Total, 256 levels for each color), or hexadecimal numbers from 00 to ff. By mathematics, the total number of available colors is 256 by 256 by 256, which is equal to 16,777,216 possible colors.

In the Hypertext Markup Language (HTML) format, the RGB values are expressed in hexadecimal format. In hexadecimal format, six digits are used, where the first and second digits characterize red, the third and fourth digits characterize green, and the fifth and sixth digits characterize blue. The digits also represent the level (percentage mix) of these colors. For example, the color white is represented as #ffffff, where each of R, G, B is on the highest level (ff, ff, ff). The color black is represented as #000000, where each of R, G, B is on the lowest level (00, 00, 00). Yellow is represented as #ffff00, where each of R and G has the highest level (ff, ff), and B is at its lowest level (00). This format has the maximum suitability as no two colors can have the same hex codes, and thus variations of the same shades of color are distinguishable. Table 4.1 shows a few colors and their hex values. Figure 4.1 lists hex values of different variations in RED and BLUE colors.

Table 4.1.: RGB Hex Value of a Few Standard Colors

Color	Hex Values
Red	#ff0000
Green	#008000
Blue	#0000ff
Magenta	#ff00ff
Black	#000000
White	#ffffff
Yellow	#ffff00
Cyan	#00ffff

Fig. 4.1. RGB Hex Values of Variations of Red and Blue Color

CIELAB Color Space: CIELAB was designed to fulfill the requirement that the same amount of numerical change in LAB values would correspond to roughly the same amount of visually perceived change by humans [16]. The International Commission on Illumination defines CIELAB color space. It is abbreviated as L* a* b* or LAB color space. For simplicity, now onwards in this document L means L*, A means a*, and B means b*. It expresses a color as a three-tuple: L is used for specifying for the brightness or luminous. L ranges from black (0) to white (100), A from green ($-$)

to red (+) (green-red axis), and B from blue (−) to yellow (+) (blue-yellow axis). The 0 value for both A and B represent neutral gray. How much to scale or limit the values of the A and B axes depend on the specific implementation, but they often run in the range of negative 100 to positive 100 or negative 128 to positive 127. Figure 4.2 shows the CIELAB space and the ranges of all three L, A, B axis.
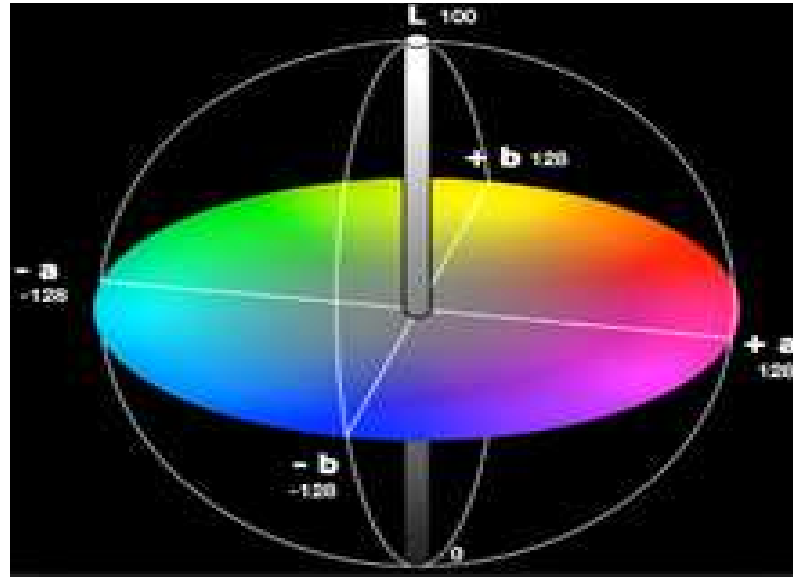
Fig. 4.2. The CIELAB Color Axis

Purpose of CIELAB in this study: The study uses image segmentation for the separation of curbs from the original image. In RGB space, it sometimes becomes difficult to separate the images. The CIELAB space is comparatively much easy to segment the images since using Euclidean distance in CIELAB space for image segmentation presents no limitations. If we denote d as the Euclidean distance between two colors and d1 as the 'perceived' difference between the two colors, then, in RGB space, d may be the same for two pairs of colors, but in reality, the d1(perceived color) may be different.

d((R1,G1,B1),(R2,G2,B2)) = d((R1,G1,B1),(R3,G3,B3)) and,

d1((R1,G1,B1),(R2,G2,B2)) ≠ d1((R1,G1,B1),(R3,G3,B3))

The difference is because the human eye is more sensitive to certain colors than the other colors, and the RGB color space does not have such broad gamut to match the range of colors perceived by the human eyes. The CIELAB color space is designed to include all colors perceivable by human eyes. The range of colors in the LAB space is much larger than the range of colors of RGB space. Moreover, CIELAB space is perceptually uniform than the RGB space, and hence, it effectively solves the problem that affects the RGB color space when using the Euclidean distance.

Conversion from RGB to CIELAB: The CIELAB color space was developed from the parent CIE 1931 XYZ color space. CIE XYZ predicts which spectral power distributions are perceived as the same color, but colors in XYZ is not particularly perceptually uniform. The CIELAB was created as a color space of which values can be computed with the help of simple formulae from the CIEXYZ space. Color described in CIELAB is perceptually more even than that in CIEXYZ. Below are the steps to convert RGB values to LAB values:

(A) Conversion from RGB to XYZ: The International Commission on Illumination (CIE) built the CIE XYZ color space in 1931. They are the results of experiments done in the late 1920s by William David Wright and John Guild. The experimental results were concatenated to the specification of the CIE RGB color space, from which the CIE XYZ color space was derived. RGB values are a set of primaries, which can be transformed to and from CIE XYZ via a 3 by 3 matrix transform. These transforms involve tristimulus values, which is a set of three linear-light components that conform to the CIE color-matching functions. In CIE XYZ color space, any color is represented as a set of positive values.

Tristimulus values: The human eye in normal vision has three kinds of cone cells and one type of rod cells. Rod cells are monochromatic black and white "night vision" receptors. The cone cells can sense colors and have peaks of spectral sensitivity in short wavelength range (420 nm – 440 nm), middle wavelength

range (530 nm – 540 nm), and long long-wavelength range (560 nm – 580 nm). These cone cells trigger human color perception in conditions of medium and high brightness. In the very dim light, the color vision ability of eyes diminishes, and the rod cells become effective. The International Commission on Illumination (CIE) developed XYZ tristimulus values, where Y represents the radiance/luminance, Z represents mostly blue wavelengths, and X represents the remaining wavelengths. The XYZ tristimulus values correspond to the responses of the human eye. The corresponding XYZ values against the RGB primaries can be calculated by performing the below conversion:

$$\begin{bmatrix} X \\ Y \\ Z \end{bmatrix} = \begin{bmatrix} R \\ G \\ B \end{bmatrix}$$

Where N is a 3*3 matrix and has values depending on the chosen reference white. For example, if color space is RGB, and the chosen reference white is E, then, N[17] is:

$$\begin{bmatrix} 0.4887180 & 0.3106803 & 0.2006017 \\ 0.1762044 & 0.8129847 & 0.0108109 \\ 0.0000000 & 0.0102048 & 0.9897952 \end{bmatrix}$$

A reference white point is a set of tristimulus values that define the color white in image capture, encoding, or reproduction [47]. Depending on the application, one can use different definitions of white, such as D50, D65, E, or C, and can achieve suitable results. D65 is also called the daylight illuminant. This study uses D65 as the reference white point because: (i) the study uses Google Street View images, and the collected images are of daytime (ii) D65 is a widespread standard used for monitor and display calibration. That is when a monitor displays a white point (RGB values of ([255 255 255]) the color of the display match the D65 color point, (iii) D65 is mathematically standardized by CIE and thus can be easily used for conversion between color spaces.

(B) Conversion from XYZ to CIELAB: A white point or the target white is a set of tristimulus values or chromaticity coordinates that defines the color white in image capture, encoding, or reproduction. The white point used by us is called D65. This white point normalizes the XYZ values. CIE 1976 LAB is based directly on CIE XYZ and is developed to model and present the perceptibility of color differences in a linear way. The non-linear equations for L, A, and B are designed to imitate the logarithmic responses of the eyes. The color information is referred to the color of the white point of the system, subscript as "n."

$$\text{If} \frac{Y}{Y_n} > 0.008856:$$

$$L = 116 * \left(\frac{Y}{Y_n}\right)^{1/3} - 16$$

$$\text{Else}:$$

$$L = 903.3 * \left(\frac{Y}{Y_n}\right)$$

$$A = 500 * \left(f\left(\frac{X}{X_n}\right) - f\left(\frac{Y}{Y_n}\right)\right)$$

$$B = 200 * f\left(\frac{Y}{Y_n}\right) - f\left(\frac{Z}{Z_n}\right))$$

$$\text{Where}$$

$$f(t) = t^{1/3} \text{ for t} > 0.008856$$

$$f(t) = 7.787 * t + \frac{16}{116} \text{otherwise}$$

Here Xn, Yn, and Zn are the tristimulus values of the reference white, and t is a variable corresponding to X/Xn or Y/Yn in the corresponding formula.

The MATLAB has functions to do all the above conversions. It uses functions makecform(), applycform() and rgb2lab() which does RGB to LAB conversions. The makecform() function supports conversions between members of the family of device-independent color spaces. Before conversion from one color space to another color space, a color transformation structure needs to made and applied. The structure is made by makecform(), and this structure is passed as an argument to applycform() function. Color transformation structure means,

application of formulae mentioned in the above sections. The applycform() function takes argument from makecform() function and apply device-independent color space transformation. That is, the structure formed by makecform() is being applied. If the MATLAB version is >2014, then instead of using makecform() and applycform(), one can use the rgb2lab() function. This function directly perform the color conversion from RGB space to CIELAB space. This study used rgb2lab() function.

Conversion from CIELAB to RGB: The study uses CIELAB color space for accurate color pattern determination of curbs. But, unlike the other color models, there is no output from the CIELAB color model. Depending on the application, it would need to be changed into a different color model for output – such as RGB, if it was to be displayed, CMYK-if it were was to be print. This conversion also has two steps. In the first step, conversion from LAB to XYZ and in the second step, conversion from CIE XYZ to RGB space [17].

(A) Conversion from CIELAB to XYZ:

$$\text{If}(\frac{Y}{Y_n} > 0.008856):$$

$$X = X_n * (P + \frac{A}{500}) * 3$$

$$Y = Y_n * P^3$$

$$Z = Z_n * (P - \frac{B}{200}) * 3$$

$$\text{Else:}$$

$$X = X_n * P$$

$$Y = Y_n * P$$

$$Z = Zn * P$$

$$\text{Where}$$

$$P = \frac{(L+16)}{116}$$

(B) Conversion from XYZ to RGB:

$$r = X * 3.2406 + Y * (-1.5372) + Z * (-0.4986)$$

$$g = X * (-0.9689) + Y * 1.8758 + Z * 0.0415$$

$$b = X * 0.0557 + Y * (-0.2040) + Z * 1.0570$$

If $(r > 0.0031308)$:

$$R_n = 1.055 * (r^{\frac{1}{2.4}}) - 0.055$$

Else:

$$R_n = 12.92 * r$$

If $g > 0.0031308)$

$$G_n = 1.055 * (g^{\frac{1}{2.4}}) - 0.055$$

Else:

$$Gn = 12.92 * g$$

If $b > 0.0031308$

$$B_n = 1.055 * (b^{\frac{1}{2.4}}) - 0.055$$

Else:

$$Bn = 12.92 * b$$

$$R = R_n * 255$$

$$G = Gn * 255$$

$$B = B_n * 255$$

Where r, g, b, Rn, Gn, Bn are arbitrary intermediate variables for easing calculations.

The MATLAB has functions to do all the above conversions. It uses functions lab2rgb() which does CIELAB to RGB conversions. This function directly performs the color conversion from CIELAB space to RGB space. The values obtained are the

normalized value in the range [0, 1]. Multiply each value by 255 to achieve RGB values in the range [0, 255]. Alternatively, mention output type as uint8 as a parameter in lab2rgb() to directly achieve RGB values in range [0, 255] (example: lab2rgb([L A B], 'OutputType', 'uint8') [19].

K-mean clustering: For finding the representative colors of all curb samples, we used the "K-Means" clustering scheme [20, 21, 22] that is a common method to separate groups of objects. K-means algorithm is an iterative procedure that tries to partition the dataset into pre-defined K distinct and non-overlapping clusters. Each data point of the dataset belongs to only one cluster. The K-means scheme makes the inter-cluster data points as similar as possible and keeps the clusters as different as possible. Each data points are assigned to a cluster in a way that the sum of the squared Euclidean distance between the data points and the cluster's centroid is minimum. The less variation we have within clusters, the more homogeneous (similar) the data points are within the same cluster. In 2-D space, Euclidean distance is the same as Pythagorean distance. The Euclidean distance between point A(X1, Y1) and a point B(X2, Y2) is:

$$D(E) = \sqrt{((X2 - X1)^2 + (Y2 - Y1)^2}$$

The pixels of the images acted as those points. Since colors are more evenly distributed in LAB color space than RGB color space, the conversion is done from RGB color space to LAB space, and then clustering is performed in LAB color space. K-means clustering requires specifying the number of clusters in advance to find the color patterns of the representative curb. K-means clustering with various cluster numbers need to be tried, and the best clustering are is selected based on Silhouette-Plot.

The algorithm for K-means is as follows:

1. Choose the number of clusters.

2. Determine the centroid of each cluster.

3. Assign the data points to the cluster based on minimum Euclidean distance.

4. Repeat step 2 and 3 until no change.

Silhouette-Plot: Silhouette is one of the best available techniques for the interpretation and validation of the consistency of data values within a cluster [23, 24]. The method provides a graphical representation of Silhouette-value that describes how well each object has been classified. Silhouette-value determines how similar an object is to its cluster (called cohesion) when compared to other clusters (called a separation). The silhouette axis ranges from negative 1 to positive 1, where a higher value (more towards positive 1) indicates that the element is better matched to the cluster into which it is placed and is poorly matched to other neighboring clusters. If most object elements have a high value (more towards +1), then the clustering configuration is right. If many points have negative values or even low values (more towards negative 1 or 0), then the clustering configuration is poor that is an indication that more clusters or fewer clusters may be used to do clustering. The silhouette values can be computed with any distance metric, such as the Euclidean distance or the Manhattan distance. More the silhouette average value is near to 1; better is the K-value associated with it. For running the K-means clustering, the silhouette-averaging method is most advantageous. Appendix 3 lists a small python function for calculating silhouette values.

4.1 Find Representative Color Patterns

Now, as we have determined the concepts and tools required for finding the representative colors of curbs, we must now find out the representative color patterns for making surrogate curb. This section deals with finding out (1) the area coverage of the dataset, (2) the validity of color values extracted from the Google Street images (3) colors that could represent almost 90% of US roadside curbs, (4) color patterns of curbs based on color composition.

Curb Image Dataset: TASI (Transportation Active Safety Institute) at IUPUI (Indiana University Purdue University, Indianapolis) has collected over 24,735 Google Street View images of road edges in all states of the US. Out of these 24,735 images, 924 concrete curb specimens that looked to have some curb road edges are selected for this study. Out of 924 images, 641 images show the distinct and clear road curb edges. Figure 4.3 shows the distribution of our specimens all across the US on a Google map. As seen in Figure 4.3, the data set covers the whole US geographical area, which practically means the study is covering all types of curbs on US roads. The geotags of few pictures are displayed in Figure 4.4.

Fig. 4.3. Mapping of Curb Image Locations Across the US Including
Hawaii and Alaska

ID	StreetImage	Long	Lat
3000301	003-Location000301D090.jpg	ActualGPS_Long_W: 34.21083048	ActualGPS_Lat_N: -92.00491671
3000443	003-Location000443D000.jpg	ActualGPS_Long_W: 32.76709470	ActualGPS_Lat_N: -89.10611737
3000451	003-Location000451D045.jpg	ActualGPS_Long_W: 31.56990325	ActualGPS_Lat_N: -90.07096568
3000500	003-Location000500D315.jpg	ActualGPS_Long_W: 35.90318486	ActualGPS_Lat_N: -80.09396886
3000732	003-Location000732D045.jpg	ActualGPS_Long_W: 40.85301033	ActualGPS_Lat_N: -73.87099922
3000788	003-Location000788D315.jpg	ActualGPS_Long_W: 35.49573000	ActualGPS_Lat_N: -97.50162414
3000981	003-Location000981D135.jpg	ActualGPS_Long_W: 36.10983913	ActualGPS_Lat_N: -86.70704700
3001325	003-Location001325D270.jpg	ActualGPS_Long_W: 33.63001358	ActualGPS_Lat_N: -84.45298022
3003153	003-Location003153D180.jpg	ActualGPS_Long_W: 36.75584032	ActualGPS_Lat_N: -108.15661210
3003354	003-Location003354D045.jpg	ActualGPS_Long_W: 34.91402679	ActualGPS_Lat_N: -80.98378896
3003463	003-Location003463D270.jpg	ActualGPS_Long_W: 32.83731323	ActualGPS_Lat_N: -97.14004286
3003479	003-Location003479D225.jpg	ActualGPS_Long_W: 40.03181650	ActualGPS_Lat_N: -111.73543550
3004824	003-Location004824D270.jpg	ActualGPS_Long_W: 38.89478849	ActualGPS_Lat_N: -77.00522518
3004978	003-Location004978D000.jpg	ActualGPS_Long_W: 38.51443263	ActualGPS_Lat_N: -89.98022675
3005105	003-Location005105D045.jpg	ActualGPS_Long_W: 38.98975031	ActualGPS_Lat_N: -77.06988577
3005118	003-Location005118D270.jpg	ActualGPS_Long_W: 38.95567471	ActualGPS_Lat_N: -76.81249215
3005141	003-Location005141D090.jpg	ActualGPS_Long_W: 36.18490143	ActualGPS_Lat_N: -94.12196910
3005418	003-Location005418D180.jpg	ActualGPS_Long_W: 35.10866752	ActualGPS_Lat_N: -106.53311170
3005517	003-Location005517D045.jpg	ActualGPS_Long_W: 35.56973999	ActualGPS_Lat_N: -97.44933519
3005522	003-Location005522D000.jpg	ActualGPS_Long_W: 35.20198249	ActualGPS_Lat_N: -97.40022649
3005548	003-Location005548D090.jpg	ActualGPS_Long_W: 42.18661791	ActualGPS_Lat_N: -122.67531990

Fig. 4.4. Example of Geotags of Sample Curb Pictures

Check the Reliability of the Colors Seen on these Images: The image dataset was collected from Google Street View. It is a well-known fact that for the same curb sample, the color looks quite different from different computer and cellphone screens. Therefore, two crucial questions need to be answered.

1. Google images may have been taken from different cameras. Does the camera affect the color of images captured?

2. Does the distance between the camera and curb affect the color of the captured image?

To answer these questions, an experiment was conducted. An arbitrary location was chosen in Indianapolis that has Google Street View images, and then we took pictures of several objects of different colors in that location but at several distances by different cameras. Figure 4.5 shows the images of the same arbitrary location by

two different cameras but from different distances. That is, for an exact same location A, the images were captured from each different camera for distance X1, X2, and so on and then compared.

iPhone image at 3m   Samsung phone image at 3m   iPhone image at 2m   Samsung phone image at 2m

Fig. 4.5. Images from Two Different Cameras for the Same Location at Different Distances

Experiment Result: Table 4.2 lists the average RGB values of the images from a different camera and for different distances.

Table 4.2.: RGB Values for Different Distance

Distance	iPhone Images RGB Values			Samsung Images RGB Values		
2 M	235	235	235	229	229	229
3 M	204	204	204	203	203	203

It can be inferred from Table 4.2, the difference between RGB values of the same phone for different distance is significant. However, the difference between the RGB values from different phones for the same distance is almost negligible. That is, the difference in the appearance of the colors of the same object on the picture taken at different distances is significant, but the difference in the appearance of the colors of

the same object taken by different cameras at the same distance are not as significant. As the distance from the camera to the object affects the amount of light captured from that object in the image (the brightness of the object), the brightness of light reflected from an object significantly affects the color of the object on the image.

Therefore, we conclude that the color captured in the Google Street View is the color in a range of colors affected by the brightness of the light. Thus, the representative color of the curb is described in a range with $\pm 10\%$ brightness of the measured RGB color. Now, in applying $\pm$ 10% margin to measured RGB values for iPhone and Samsung phone images, they all fall under one group with range [197, 197, 197] to [240 240 240] with an average value of [218, 218, 218]. After verifying the Google image with pictures taken from different distances, it is concluded that the curb color obtained from Google image can be used as a reference to generate the color requirement of surrogate curbs.

Color Determination of Curbs: The procedure for finding the representative colors of curbs has the following steps:

1. Raw image segmentation to find curb in each sample image.

2. Cluster all curb samples into a small number of representative color groups.

3. Identifying the color pattern of each curb sample and find 10 to 20 representative colors from the color patterns of all curb samples combined.

4. Find the representative pattern(s) for each cluster.

Raw image segmentation to find curb in each sample image: This step is to find the curb area in the image. The raw image is segmented to find the curb area using the K-mean clustering method. The optimal value of K is determined from silhouette indexing (code in Appendix-1). K =4 is the best choice found for the most common curb samples. The mean RGB value of the final curb cluster in an image sample is the color of the curb in that image. Figure 4.6 illustrates the segmentation process. The top left is the original image. It has sections with pictures of curb,

road, and grass. Top right is the result of K-mean clustering with X marks denoting the centroid of each cluster. The x-axis and y-axis are the A and B planes in LAB space, respectively. The best K-values for this example is 3. The bottom left shows the images of three clusters in LAB space. "Object in cluster 1" (Yellow rectangle) is the curb. The bottom right is the bar plots of the average RGB value of the curb cluster. In the bar plot, the y-axis is the numeral values from 0 to 255 in RGB space. Thus, the curb, as shown in cluster 1, has average RGB values [202, 190, 167] (as shown in a yellow rectangle). This RGB value corresponds to Grayish Orange Color (Sisal color).
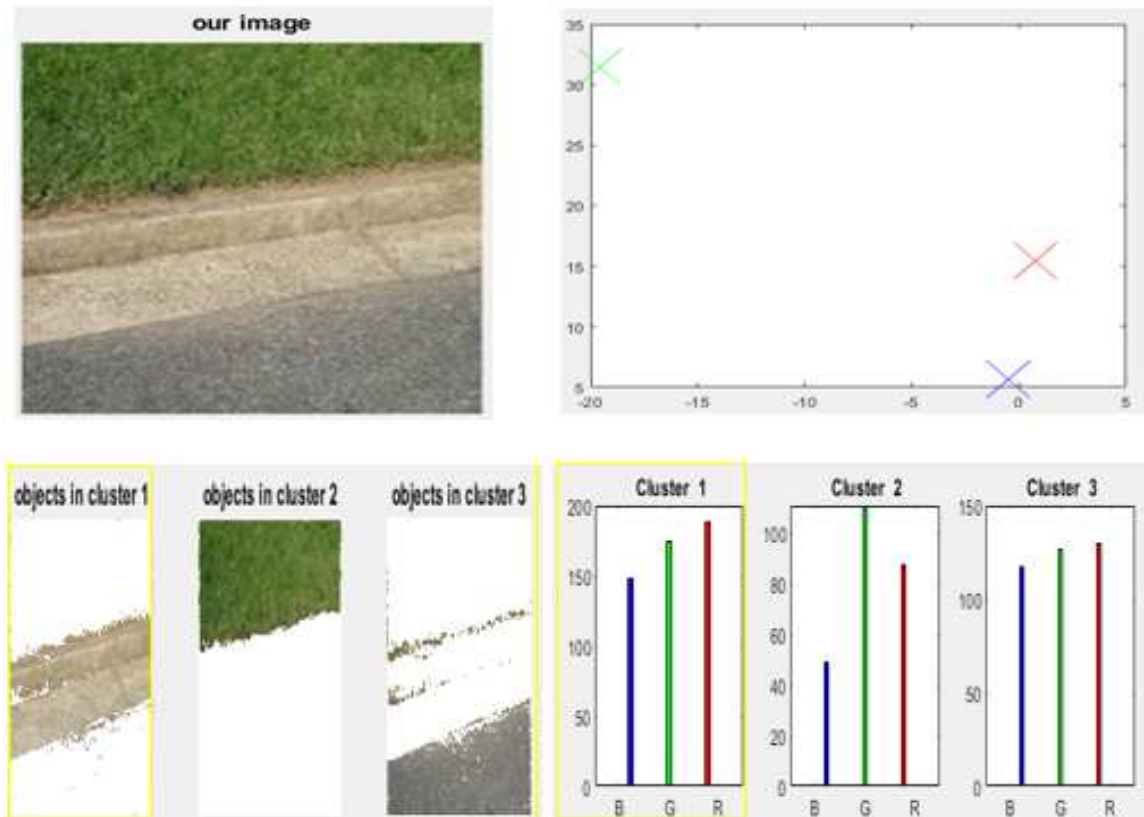
Fig. 4.6. Curb Separation

In Figure 4.6, top left is the original image; top right is the center of each segment and Image segments in LAB space (The x-axis and y-axis are the A and B plane in LAB space, respectively); bottom left is the image of segmented clusters; bottom right is the RGB bar plot of each cluster in RGB space.

Cluster all curb samples into a small number of representative color groups: This step clusters all curb samples into a small number of representative color groups based on the average color of each curb sample. For doing this, the following steps are performed:

1. Gather all curb segments of all samples with the average LAB value of all pixels in the curb area of each sample image.

2. Use K-means clustering with various K-values (2 to 15) and the metric of the minimum Euclidean distance to find color groups among all curb samples. K=4 generates the best Silhouette value. Hence, all curb samples are represented in four groups based on their general color.

Figure 4.7 shows the average silhouette values for the corresponding K-values from 2 to 15. K=4 has the maximum average silhouette value (0.859). Figure 4.8 shows the silhouette value distribution for K=4. Table 4.3 gives the details of these four groups. The group number is the same as the cluster number. According to the table, group1 has the highest percentage on the US roads (36%), and group 2 has the lowest (3%). Together groups 1, 3, and 4 represent 97% of all curbs across the US roads.
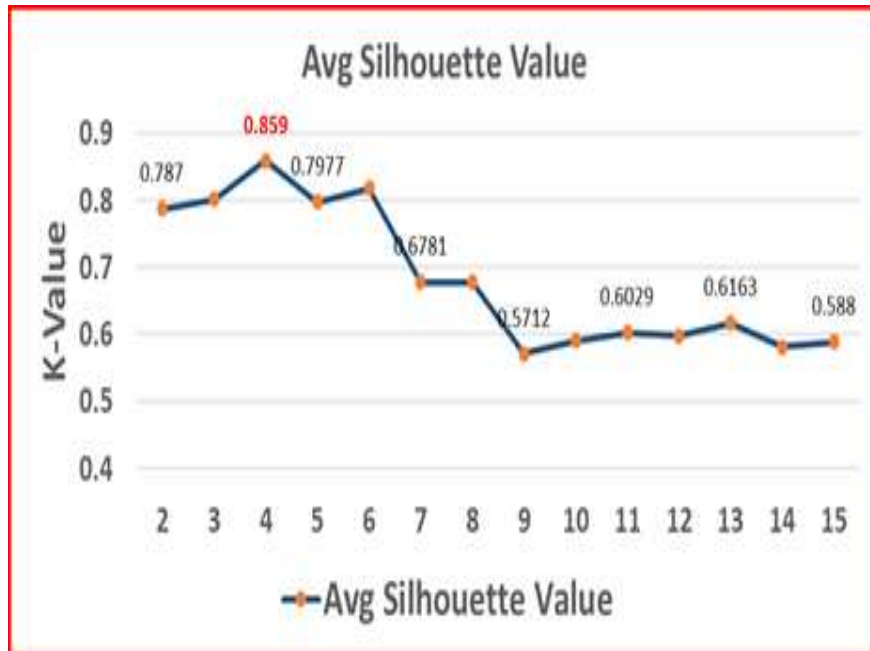
Fig. 4.7. K-values vs. Silhouette Values for RGB Values of all Curbs
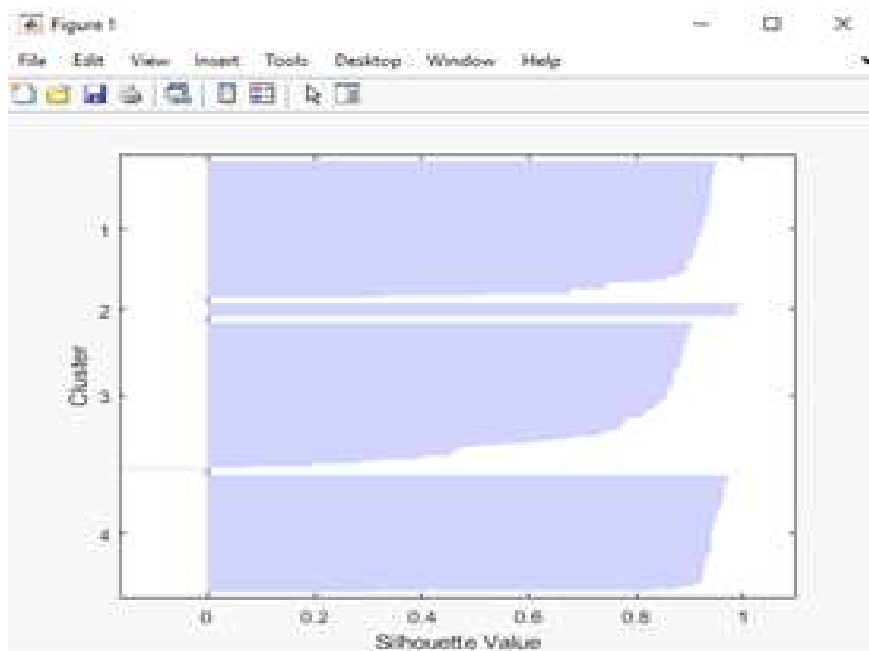
Fig. 4.8. Silhouette Value Distribution for K= 4

Table 4.3.: Curb Groups

Curb Cluster Number	Cluster Centroid RGB Color	RGB	Number of Curbs	% on US Roads	LAB Values
1		[228 226 225]	212	33	[8.4909, 0.0424, 0.0618]
2		[215 173 68]	17	3	[7.1144, 0.7943, 4.9860]
3		[192 183 167]	231	36	[7.1886, 0.0391, 0.7927]
4		[178 179 178]	181	28	[7.0260, -0.0460, 0.0329]
Total			*641*	*100*	

Identifying the color pattern of each curb sample: This step identifies a set of 10 to 20 representative colors shown in all curb samples. The purpose is to use these colors to describe the representative color patterns of each curb group (described in the next step).

The process for identifying a set of 10 to 20 representative colors is as follows:

(1) The foremost step is to identify the size of a region of interest (ROI) so all patterns generated can be in the same physical scale. A common curb section is 6 inches wide by 72 inches long, which implies that the curb width to length ratio is 1:12. Choosing ROI in the same ratio enables easy and precise mapping of the curb between the image space and the physical space. The convenient curb sample descriptions can be 3 by 36 pixels, 6 by 72 pixels, 12 by 144 pixels, or many others. Choosing 3 by 36 pixels would require scaling the ROI by 2 to cover 6 inches by 72 inches physical area so effectively each square pixel means a 2 inches by 2 inches "physical area. Choosing 12 by 144 pixels make

each square pixel a 0.5 inch by 0.5 inch area. Choosing a representative curb image size equal to 6 by 72 pixels allows one-to-one mapping of 1 pixel to 1 square inch area. One can perform ROI selection by using the Matlab code in Appendix 4. In the appendix, the command line 1, where S = [X1, Y1, 72, 6] helps to locate the ROI position and choose the ROI size. X1, Y1 indicates the starting pixel positions. Then the code draws the 72 by 6 pixels ROI. Double click on the ROI for receiving the ROI image. Now, as the ROI is fixed with 72 by 6 pixels, scaling of ROI image does not change the x and y resolution. Also, while scaling, maintaining width : length ratio as 1:12 maintains the one-to-one mapping In Figure 4.9, the left-side image shows the curb and the selected 72 by 6 pixels ROI, and the right-side shows the scaled ROI image.
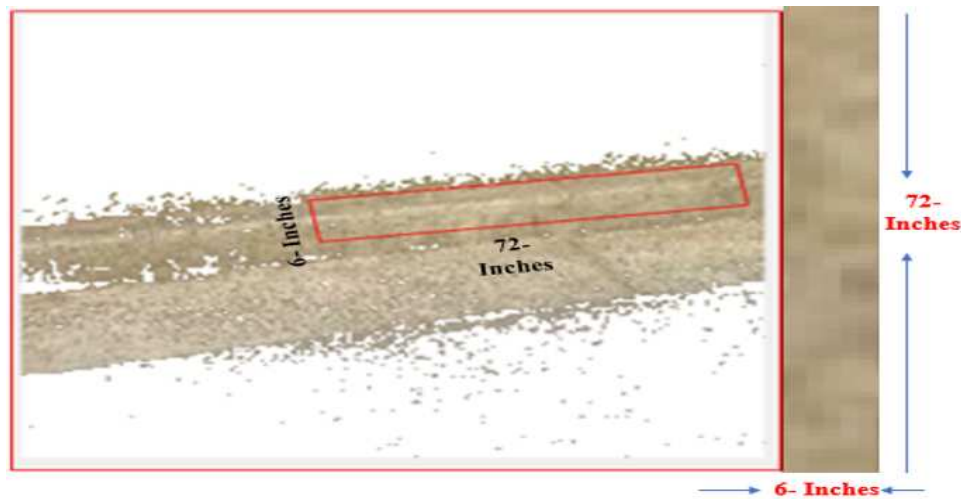
Fig. 4.9. ROI Selection

(2) Dividing the 6 inches wide by 72 inches long ROI into 3 by 36 (108 blocks) of 2 inches by 2 inches, and thus there are total 641 by 108 (69228 blocks for all curb samples. The MATLAB blockproc() function [25] is used for this division. Figure 4.10 shows the blocks. The top image is the ROI image, and the bottom image is the division of ROI into 108 blocks.

6 pixel

72 pixel
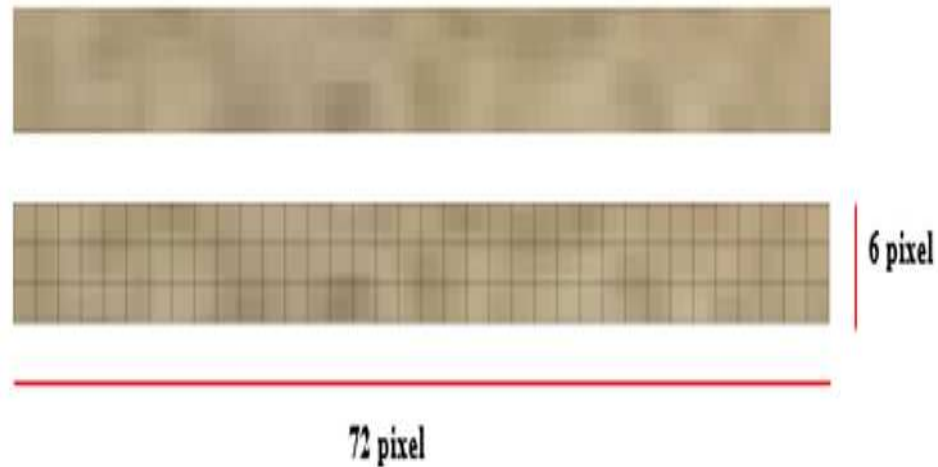
Fig. 4.10. Division of ROI into 108 Blocks

(3) The average LAB values of all 69228 blocks were determined based on the average color of each block. The bottom image of Figure 4.10 shows the ROI and its division into blocks.

(4) Apply K-means clustering, with K= 2 to 15, to extract the representative block colors in these 69228 blocks. Figure 4.11 shows the average Silhouette value vs. K-values. As seen. In Figure 4.11, clustering with K=10 has the best Silhouette value, which means that ten colors are enough to distinguish the representative colors in all blocks. Figure 4.12 shows the Silhouette value distribution for K=10.
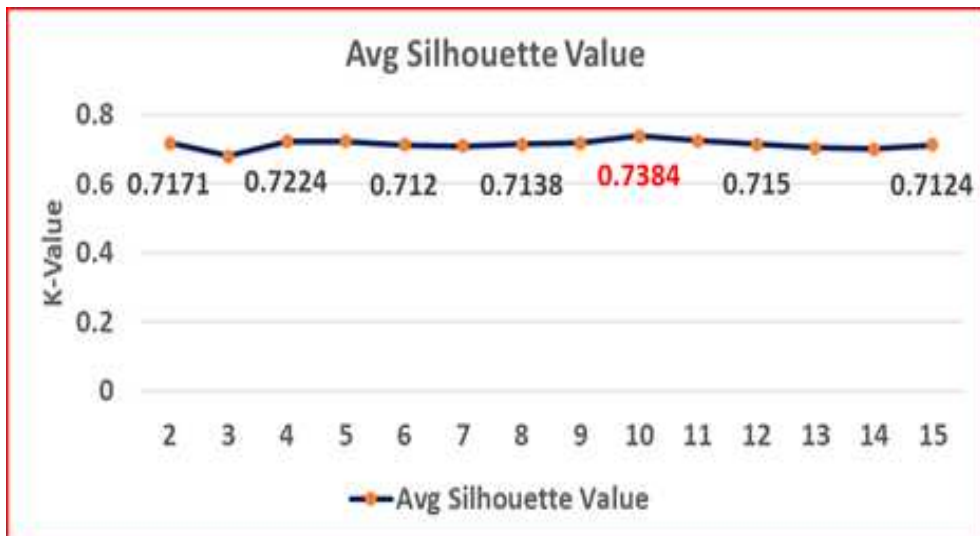
Fig. 4.11. K-values vs. Silhouette Values for Color Templates
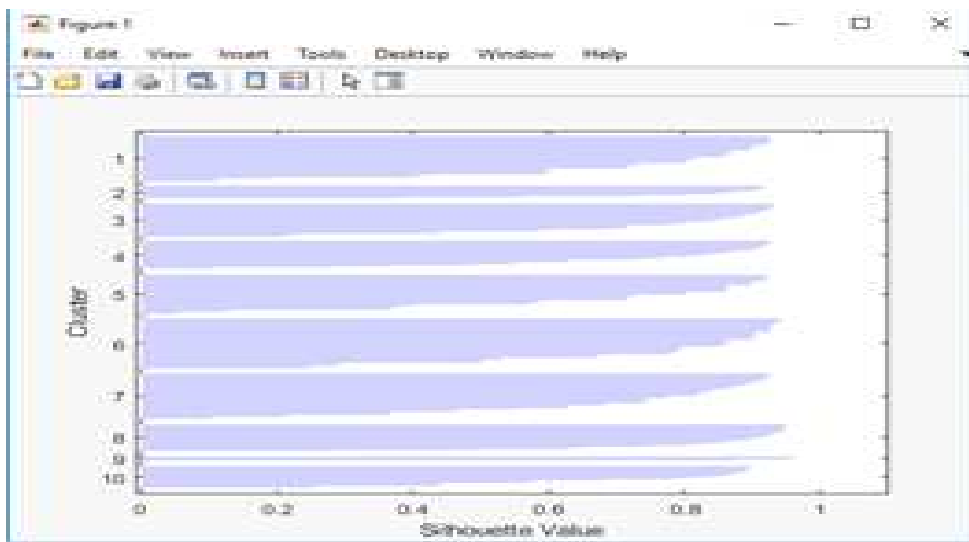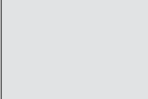
Fig. 4.12. Silhouette Value Distribution of ROI Pixels for K=10

Table 4.4 shows the ten color clusters representing the 69228 blocks. It lists the names and RGB values of all clusters. In this table, column 2 lists the number of blocks in each of 10 color clusters; column 6 shows the centroid color for each of 10 block color clusters.

Table 4.4.: Template Colors Name and RGB Value

Color Template for 69,228 Blocks						
Cluster Number	Block count (69228)	Image Count (641)	RGB	LAB Values	Color Repre- sentation	Color Name
6	11263	104	[172 172 172]	[6.8135 0 0]		Gray
7	10427	97	[141 140 135	[5.7723 -0.0503 0.2400]		Mild Dark Gray
1	10232	95	[187 178 152]	[7.0126 -0.0939 1.2361]		Grayish Orange
5	8728	81	[160 110 85]	[5.1659 1.4654 1.8989]		Dark Grayish Orange
4	6407	59	[206 206 206]	[7.8734 0 0]		Mild Light Gray
8	6072	56	[225 227 228]	[8.4998 -0.0418 -0.0616]		Light Grayish Blue
9	771	7	[245 245 245]	[9.0469 0 0]		Very light Gray
3	7391	68	[123 123 123]	[5.2072 0 0]		Dark Gray
10	5246	49	[103 103 103]	[4.5162 0 0]		Dark Gray
2	2693	25	[216 173 64]	[7.0324 0.4493 5.0102]		Moderate Orange

Recolor all curb samples using the ten representative block colors: In steps B, four curb groups based on the average color of each curb sample were determined. From step C, ten color groups based on the central color of each 2"x2" block were determined. In this step, we recolor all curb samples using the ten representative block colors, i.e., replacing the color of each of 69,228 blocks by the nearest ten template colors. The block recoloring is done in the LAB color space as follows

- Calculate Euclidean distance between CIELAB values of each of the 10 template colors and the centroid LAB values of each and all 69,228 blocks. Thus, for each block, there are 10 Euclidean distances.

- Out of 10 Euclidean distances for each block found above, find the template color that has the minimum Euclidean distances and recolor that block with that template color.

- Next, find the percentage of colors of all recolored 2"x2" blocks in each of the 4 curb groups. Table 4.5 gives details about the percentage of each color in each of the 4 curb groups.

Table 4.5.: Percentage of Each Color in a Curb Group

	Block Color Clusters			Block Color in Each Curb Color Groups (each column is a color group)			
Color Cluster Number	[R G B]	LAB Values	% in all groups	% block color in group 1	% block color in group 2	% block color in group 3	% block color in group 4
8	[225 227 228]	[8.4998 -0.0418 -0.0616]	30.94	66			
6	[172 172 172]	[6.8135 0 0]			25	29 76	
1	[187 178 152]	[7.0126 -0.0939 1.2361]	16.13 912	12.50	91253		
5	[160 110 85]	[5.1659 1.4654 1.8989]	11.44		6.25	18	2
7	[141 140 135]	[5.7723 -0.0503 0.2400]	8.75				17.75
9	[245 245 245]	[9.0469 0 0]	3.00	21			4.25
4	[206 206 206]	[7.8734 0 0]	2.05	12			
2	[216 173 64]	[7.0324 0.4493 5.0102]	1.69		56.25		
10	[103 103 103]	[4.5162 0 0]	0.50	1			
3	[123 123 123]	[5.2072 0 0]	0.50				

Since curb group 2 only represents 3% of all curb samples, it is not worthwhile to make surrogate curb for this group. So, we ignore curb group 2 and only work for defining color and color patterns for curb groups 1, 3, and 4.

With 72-pixels by 6-pixels ROI, we were able to achieve one-to-one mapping with the real 72-inches by 6-inches curb, and finally achieved the template's colors that could color all the curbs on the US roads. Most curbs are 6-inches wide and 6-inches high, and during the making of surrogate curb skin, we try to generate a 1:1 color pattern on a 12-inch x 24-inch area to support the making of the surrogate curb. That is 3 pieces of 12-inches x 24-inches material for covering the 6-inches by 6-inches by 72-inches (width, height, length) curb. As each piece is of a 1:2 ratio, the selected area of the pattern should also be of a size ratio of 1:2.

The pictures in the images may be inclined and not straight. Therefore, as per the alignment of the real curb image, find the width to length ratio. Whichever provides a larger area to mimic, fix the length/width and enlarge/reduce the length/width to make the ratio as 1:2. The listed step ensures the real image of ratio 1:2 can be one-to-one mimic into surrogate skin of size 1:2 ratio. For generating the color pattern on the curb surface, a 1-1 pattern is desirable. For example, in Figure 4.13, the viewing angle of the curb section is about 45°. So, the actual width should be $\sqrt{2}$ times the width seen on the image. The top image is the original image in which the curb surface is inclined at 45 degrees. The bottom image is the flattened curb surface.
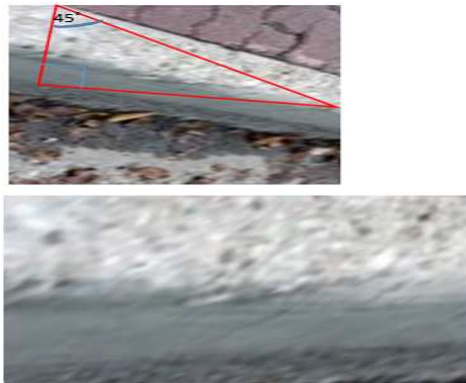
Fig. 4.13. Geometric Illustration for 1-1 Mapping

4.2 Distinguish Color Patterns in Each Color Group

In the preceding section, curbs were classified in 4 general color groups, and the colors of each of the all 2"x2" area curb are recolored by one of 10 representative colors. Then the percentage of each color type of recolored 2"x2" curb block in each of the 4 general groups was determined. The primary goal of this section in the study is to determine the representative color pattern in each group. Since group 2 only represents 3% of all curb samples, it is not worthwhile to make surrogate curb in this group. Working for making curbs for groups 1, 3, and 4 is below.

As shown in Table 4.3, group1 has 212 curbs samples, group3 has 231 curbs samples, and group4 has 181 curbs samples. The RGB and CIELAB values of all recolored 2"x2" blocks in each sample curb has already been obtained.

Process for Finding Representative Colors: The percentage of each of 10 representative colors in each of the 4 recolored curb group is already shown in Table 4.5. For Example: recolored curb group1 has 4 colors: Color8 (66%), color9 (21%), color10 (12%), and color4 (1%). There are 0% of the other 6 representative colors in recolored curb group 1. Table 4.6 shows the percentage of curb samples with various mix of colors in recolored curb group1. Table 4.7 shows the percentage of curb samples with various mix of colors in recolored curb group3. Table 4.8 shows the percentage of curb samples with various mixes of colors in recolored curb group4.

Table 4.6.: Color Combination in Recolored Group1

%of recolored curb samples have a mix of four colors	% of recolored curb samples have a mix of three colors				% of recolored curb samples have a mix of two colors						% of recolored curb samples have only one color			
Mix of colors 8, 9, 10 ,4	Mix of colors 8, 9, 10	Mix of colors 8, 9, 4	Mix of colors 8, 10, 4	Mix of colors 9, 10, 4	Mix of colors 8, 9	Mix of colors 8, 10	Mix of colors 8, 4	Mix of colors 9, 10	Mix of colors 9, 4	Mix of colors 10, 4	only Color 8	only Color 9	only Color 10	only Color 4
100%	0	0	0	0	0	0	0	0	0	0	0	0	0	0

Table 4.7.: Color Combination in Recolored Group3

% of recolored curb samples have a mix of three colors	% of recolored curb samples have a mix of two colors			% of recolored curb samples have only one color		
Mix of colors 1, 5, 6	Mix of colors 1, 5	Mix of colors 1, 6	Mix of colors 5, 6	only Color 1	only Color 5	only Color 6
100%	0	0	0	0	0	0

Table 4.8.: Color Combination in Recolored Group4

% of recolored curb samples have a mix of four colors	% of recolored curb samples have a mix of three colors				% of recolored curb samples have a mix of two colors						% of recolored curb samples have only one color			
Mix of colors 5,6,7,9	Mix of colors 5,6,7	Mix of colors 5,6,9	Mix of colors 6,7,9	Mix of colors 5,7,9	Mix of colors 6,9	Mix of colors 5,6	Mix of colors 5,7	Mix of colors 5,9	Mix of colors 6,7	Mix of colors 7,9	only Color 5	only Color 6	only Color 7	only Color 8
76.79%	0	0	0	0	0	0	0	0	0	0	0	23.21%	0	0

Up to now, we know the percentage of different colors in each of the four curb groups. Next, we describe how to find the representative color patterns in each of the four curb groups.

Definition of high presence: If a color in an image covers over x% area of the image, it is defined as have a high presence in the image. Otherwise, it is considered as having a small presence in the image.

If a curb has a high presence color distributed all over its area, and other colors have patches/spots over it, we call the high presence color as the 'base color,' and we would develop a pattern for each base color. But x could be anything between 0 to 100. Also, x should be selected as that, if x is the base color, the other color's

patches or spots must not overshadow the base color. For finding the optimal x, we tried different x values. In fact, choosing x value determines the number of curb color patterns we will make.

x = 10: The choice of x as 10 made almost every color in each of the groups as a base color. For group1 colors 8, 9, 10, and 4 as a base color, for group3, colors 6, 1, and 5 as a base color and for group4, colors 5, 6, 9, and 7 as a base color. Thus effectively, we had 11 patterns of curbs: 4 types each for group1 and group4 and 3 types for group3. But the maximum patterns in each group look quite similar because the other color's patches overshadowed the base color. In group1, the base colors 4, 10, and 9 were overshadowed by the color8. Thus, all patterns in group1 look liked patterns of color8 as a base color. In group3, all patterns looked like patterns of color1, and in group4, patterns looked like those of color6. The choice of x = 15 behaved the same as x=10.

x = 20: For the choice of x =20, group1 has now color colors 8, 9, and 4 as a base color, group3 has colors 6, 1, and 5 as a base color, and group4 has colors 5, 6, 9, and 7 as a base color. Although the patterns for x =20 look distinct for all colors, the percentage of such patterns were meager for maximum colors. For example, in group3, color1 has a high presence on 69% curbs, color5 has a high presence on 9% curbs, and color6 has a high presence on 18% curbs.

x = 25: The choice of x =25, behaved same as x =20 for group1 and 3. But, for group4, the patterns were quite monotonic. Many dissimilar curbs looked similar. As from Table 4.8, group4 has two types of color mix curbs. One type of curbs which has a mix of colors 5, 6, 7, and 9, and another type of curbs which has only color6. The choice of x = 25 makes both types of curbs quite similar in look.

Similarly, the choice of x = 30, 40 have the same behavior as x = 20 for group1 and group3, but it does not work for group4. Hence, it was not worth trying another x values, and we decided on sticking on x = 20. Therefore, x = 20 was the best choice to decide for a high presence. We want to make minimum patterns of curbs that could represent at least 80% of the US road curbs. As discussed for x = 20, % of patterns

for many colors as a base color is low. We chose to develop representative patterns for those colors, which has at least 20% of curbs on which it has a high presence. The choice of 20% enables us to represent more than 80% of US roadside curbs in minimum (optimal) number of patterns.

Table 4.9 provides % of curbs on which each color of group1 has a 20% (high) presence; Table 4.10 provides % of curbs on which each color of group3 has a 20% (high) presence. Table 4.11 provides % of curbs on which each color of group4 has a 20% (high) presence.

Table 4.9.: Curbs of Group1 Having a High Presence

Group1. Curb Count-212			
% of curbs with a high presence of color 8	% of curbs with a high presence of color 9	% of curbs with a high presence of color 4	% of curbs with a high presence of color 10
97%	16%	11%	0%

Table 4.10.: Curbs of Group3 Having a High Presence

Group3. Curb Count-231		
% of curbs with a high presence of color 1	% of curbs with a high presence of color 5	% of curbs with a high presence of color 6
69%	9%	18%

Table 4.11.: Curbs of Group4 Having a High Presence

Group4. Curb Count-181			
% of curbs with a high presence of color 6	% of curbs with a high presence of color 5	% of curbs with a high presence of color 7	% of curbs with a high presence of color 9
100%	0%	0%	0%

Until now, we have achieved the base colors for each group (and for their types, if any). Now, it is required to find the distribution types of other colors (non-base colors) in the representative patterns. The other colors can have the following types of presence:

- Type 1- non-base colors present as spots.

- Type 2- non-base colors present as random shaped patches.

- Type 3- non-base colors present as both spots and random shape patches on the curbs.

- Type 4- no presence of non-base colors. That is, the curb is made of base color only.

By visual examination, all recolored curb samples in the groups1 and 3 are of type 3. In group4, recolored curb samples are of both type 3, and type 4. Therefore, group 4 has two types of curbs; we call them group4-TypeA for spots distribution type 3 and group4-TypeB for spots distribution type 4. But spots could be dense and sparse too. Therefore, the found type(s) is further grouped into dense and sparse spot patterns. If the dense or the sparse type has more than 20% curbs, then the already

perceived pattern would divide into more patterns. Here also, 20% choice act as an enabler for making the minimum number of patterns that could achieve at least 80% representational curbs. Table 4.12 shows the non-base color distribution of group1, Table 4.13 shows the non-base color distribution of group3, and Table 4.14 shows the non-base color distribution of group4-TypeA. Curbs of group4-TypeB are of type 4, therefore no need to find the distribution for non-base colors.

Table 4.12.: Non-base Color Distribution of Group1

	Block 9-Dense Spots	Block 9-Sparse Spots	Block 4-Dense Spots	Block 4-Sparse Spots	Block 10-Dense Spots	Block 10-Sparse Spots
	Very Light Gray	Very Light Gray	Mild Gray	Mild Gray	Dark Gray	Dark Gray
Count of curb	212	0	116	96	0	212
% Curbs	100	0	55	45	0	100

Table 4.13.: Non-base Color Distribution of Group3

	Block 5-Dense Spots	Block 5-sparse Spots	Block 6-Dense Spots	Block 6-sparse Spots
Count of curb	195	36	231	0
% Curbs	84%	16%	100%	0%

Table 4.14.: Non-base Color Distribution of TypeA

Group4-Color Distribution Pattern- Color Blocks 6, 7, 5 and 9 present (Total Curbs-139)						
	Block 7- Dense Spots	Block 7- Sparse Spots	Block 5- Dense Spots	Block 5- sparse Spots	Block 9- Dense Spots	Block 9- sparse Spots
Count of curb	115	24	122	17	3	136
% Curbs	83	17	88	1 2	2	98

Group1: From Table 4.12, in group1, only color4 has distribution disparity. Therefore, the color 4 distribution type divides the already perceived pattern is into two patterns. We call them Pattern1 and Pattern2.

- **Pattern 1**: Color 8 as a base color, color 9 as dense spots, color 10 as sparse spots and color 4 as "dense" spots (116 curbs).

- **Pattern 2**: Color 8 as a base color, color 9 as dense spots, color 10 as sparse spots and color 4 as "sparse" spots (96 curbs).

Figure 4.14 shows a few samples of pattern 1 curbs, and Figure 4.15 shows a few examples of pattern 2 curbs. Examples are shown in pairs, with the left image being the real curb, and the right image is the separated curb only.
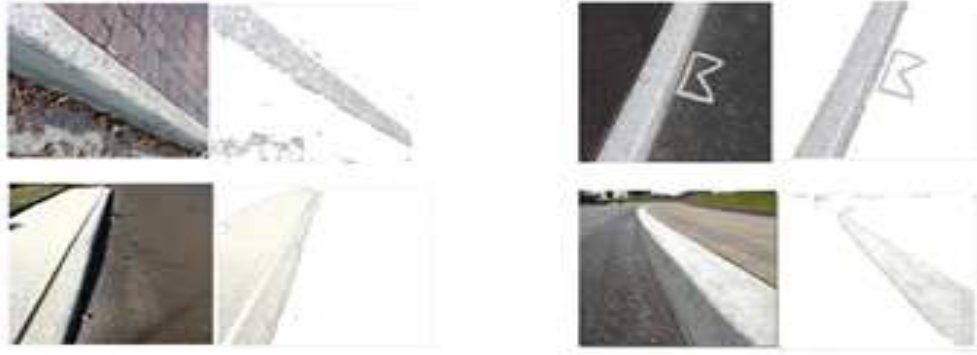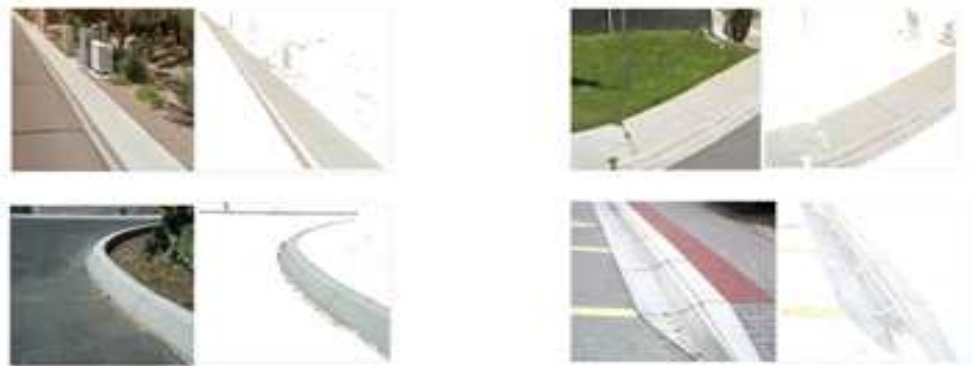
Fig. 4.14. Sample Pair of Curbs for Pattern 1

Fig. 4.15. Sample Pair of Curbs for Pattern 2

Curbs in group1 with the proper ratio of color compositions as that of pattern 1 and pattern 2 are selected as representative curb patterns 1 and 2, respectively. Figure 4.16 shows one representative curb of 6 inches wide, 6 inches tall and 24 inches long for pattern 1, and Figure 4.17 shows one representative curb for pattern 2. The representative curb patterns 1 and 2 are used as the required color pattern for the surrogate curb.

Fig. 4.16. Pattern 1. Real curb (Left), Example Pattern of 6 inches
Wide, 6 inches Tall and 24 inches Long (Right).

Fig. 4.17. Pattern 2. Real curb (Left), Example Pattern of 6 inches
Wide, 6 inches Tall and 24 inches Long (Right).

Group3: From Table 4.7, each template color have an over 20% presence in either dense or in and sparse spots. That is, no non-base color has distribution disparity Hence, group3 has only a one color pattern. We call it pattern3.

- **Pattern 3**: Block color 1 as the base, color 6 as dense spots, and color 5 as dense spots.

Figure 4.18 shows a few samples of pattern 3 curbs. Examples are shown in pairs, with the left image being the real curb in the original image and the right image being the separated curb only.
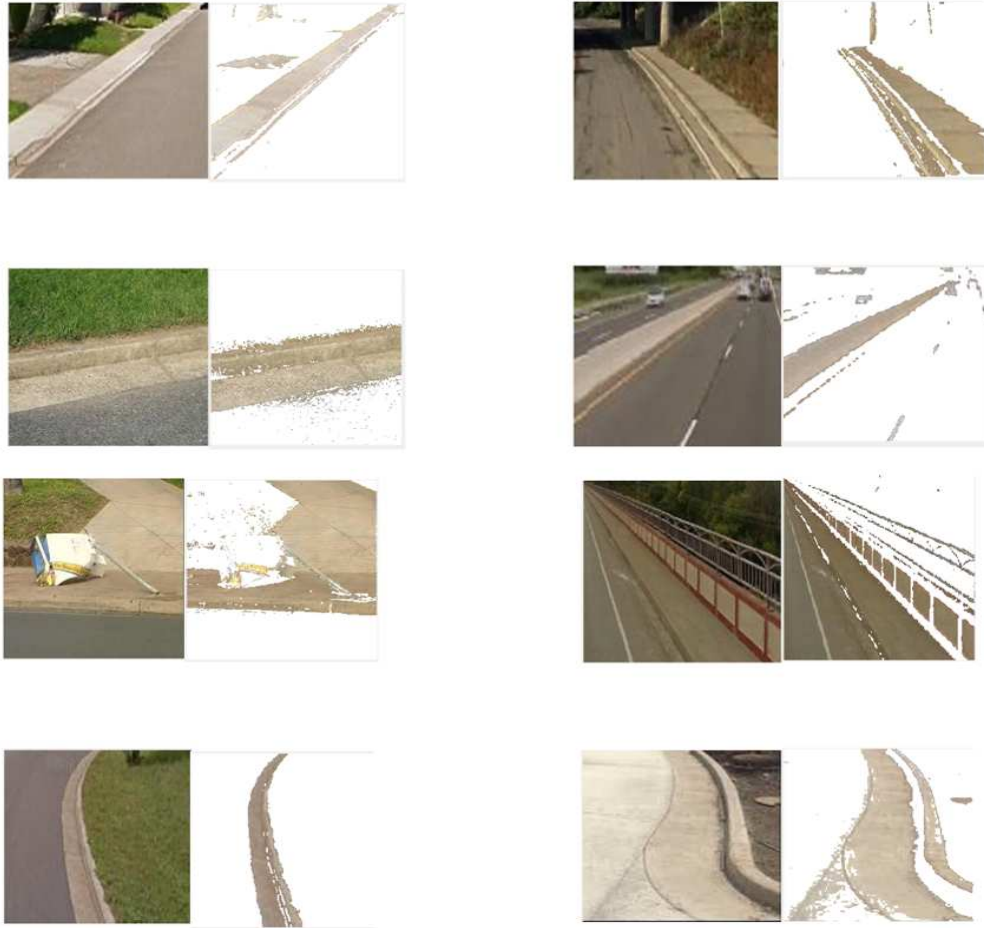
Fig. 4.18. Sample Pair of Curbs of Group3

Figure 4.19 shows one representative curb of 6 inches wide, 6 inches tall and 24 inches long for pattern 3. The representative curb pattern is used as the required color pattern for the surrogate skin. We interpret this group representing old curbs.

Fig. 4.19. Pattern 3. Real curb (Left), Example Pattern of 6 inches
Wide, 6 inches Tall and 24 inches Long (Right)

Group4:

1. **Group4-TypeA:** From Table 4.8, each non-base color has more than 20%
   presence either in dense or in sparse type. That is, no non-base color has
   distribution disparity. Hence, group4-TypeA has an only one color pattern. We
   call it pattern 4.

   - **Pattern 4**: Color 6 as a base color, color 7 and 5 in dense spots, color 9 in
     sparse spots, dense patches of spots of colors 7 and 5, and isolated patches
     of those of color 9.

   Figure 4.20 shows a few samples of pattern 4 curbs. Examples are shown
   in pairs, with the left image being the real curb, and the right image is the
   separated curb only.

Fig. 4.20. Sample Pair of Curbs for Pattern 4

2. **Group4-TypeB:** TypeB has curbs that are made of only one color. We call this type as pattern5.

- **Pattern 5**: Having only Color 6.

Figure 4.21 displays few samples of pattern 5. Samples are shown in pairs, with the left image being the real curb, and the right image is the separated curb only.

Fig. 4.21. Sample Pair of Curbs for Pattern 5

Figure 4.22 shows one representative curb for pattern 4. The representative curb
pattern is used as the required color pattern for the surrogate skin.

Fig. 4.22. Pattern 4. Real curb (Left), Example Pattern of 6 inches
Wide, 6 inches Tall and 24 inches Long (Right)

Figure 4.23 shows one representative curb for pattern 5. The representative curb
pattern is used as the required color pattern for the surrogate skin.
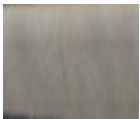
Fig. 4.23. Pattern 5. Real curb (Left), Example Pattern of 6 inches
Wide, 6 inches Tall and 24 inches Long (Right)

5. SURROGATE CURB DEVELOPMENT

Table 5.1 summarizes all types of patterns developed in Chapter 4. This chapter describes the development of the curb surrogate according to the requirements set in Chapters 3, 4, and 5.

Table 5.1.: Summary of all Type of Curb Patterns

Pattern Name	Total Curbs	% of Total Curbs	Color Distribution	Example Curb	Pattern Figure
Group1_Pattern1	120	23.51	Color8 as base. Color 9(21%) as dense spots, color4(12%) as dense spots and color10(1%) as sparse spots		
Group1_Pattern2	92	10.63	Color8 as base. Color9(21%) as dense spots, color4(12%) and color10(1%) as sparse spots		
Group3_Pattern 3	231	37.2	Color1 as base. Color5(18%) and 6(29%) as dense spots		
Group4_Pattern 4	139	22.38	Color6 as base. Color7(17.75%) and color5(2%) as dense spots. Color9(4.15%) as sparse spots		
Group4_Pattern 5	39	6.28	Uniform color 6		

Curb Structure: For lightweight and durability in vehicle testing, the surrogate concrete curb is made of foam and covered by a specially designed skin. According to the curb construction standards from various states in the U.S., most curbs are 6-inch tall and 6-inch wide with a round corner of the various radius (1 to 3 inches) on the top. We used the configuration of a 6-inch tall, 6-inch wide, and 1.5-inch radius, as the dimension of the surrogate curb (Figure 5.1). The concrete curb was made of polyethylene foam with a skin satisfying the color, IR reflection, and RCS requirements.
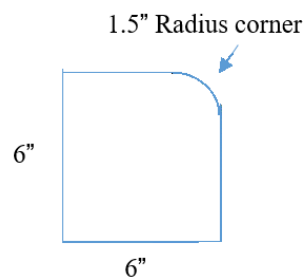
Fig. 5.1. The Suggested Cross Section Shape of the Concrete Curb

The Skin Material: It is required that the skin material should be durable and lightweight. A semi-transparent polycarbonate film is used for the skin. Few other properties also make polycarbonate sheets an optimal choice for skin preparation. They can be easily thermoformed and molded; they are easy to cut and have excellent ink and paint adhesion. The skin design: Is a three-layer structure (Figure 5.2):

- The top layer (visible by the vehicle) is for satisfying the IR and color requirements.

- The middle layer provides the strength of the skin and contributes mainly to the 24GHzs radar reflectivity.

- The bottom layer fine-tunes the 77GHz radar reflectivity.
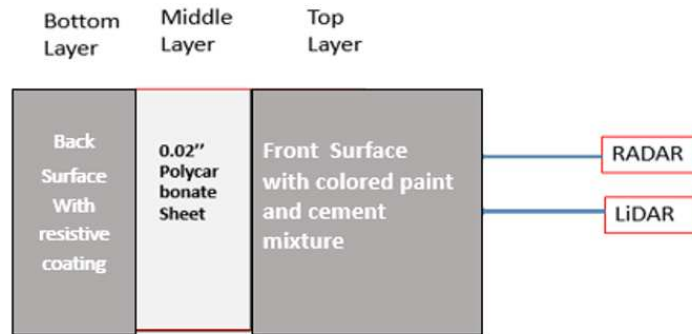
Fig. 5.2. Three-Layer Skin Structure

For satisfying the IR reflectivity requirement, the desired color paint was mixed with cement. The back layer is resistive paint, which makes the skin satisfy the required 7.3 ± 1 dB for both 24GHz and 77GHz radar reflectivity. The IR and radar requirements were met, but the color of the surrogate curb was a single color that made it looked too new and not like a commonly seen curb. In this redesign, a comprehensive study was conducted to create a more realistic looking curbs. The new color requirement is described in Section 4, and the implementation is described here. The following process is used in Surrogate curb development:

1. Making foam curb frame.

2. Make the surrogate curb skin according to the specified color and color patterns.

3. Make the surrogate curb skin that satisfies the IR requirements.

4. Make the surrogate curb skin that meets the radar reflectivity requirements.

5. Attaching the skin to the curb shaped foam.

For surrogate skin making, we used the three-layer skin design. The skins were to be made as per requirements set up in Chapters 2, 3, and 4. The color requirement is easy to meet since any paint shop can produce the paint with our required colors. We have re-shown the required colors in Table 5.2. In this section, we show the developed surrogate skins alongside the real curb and the representative patterns. Table 5.3 shows the color distribution for all five patterns.

Table 5.2.: Template Colors

Color Cluster Number	[R G B]	Brand Model	Brand Number	% in all groups	% block color in group1	% block color in group3	% block color in group4
8	[225 227 228]	Valspar/Storm Coat	4005-1C	30.94	66.00		
6	[172 172 172]	Valspar/Dura Max	4006-2A	25.00			76.00
1	[187 178 152]	Valspar/Storm Coat	3002-10A	16.13		53	
5	[160 110 85]	Valspar/Storm Coat	2008-9A	11.44		18	4.25
7	[141 140 135]	Valspar/Dura Max	4006-2B	8.75			17.75
9	[245 245 245]	Valspar/Storm Coat	7004-2A	3.00	21		2.00
4	[206 206 206]	Valspar/Storm Coat	4006-1C	2.05	12.00		
2	[216 173 64]	Valspar/Storm Coat	3008-7A	1.69			
10	[103 103 103]	Valspar/Dura Max	4009-1A	0.50	1		
3	[123 123 123]	Valspar/Dura Max	4006-2B	0.50			

Table 5.3.: Color Distribution for all Five Patterns

Color Distribution of All Patterns			
Pattern	Base Color (Color No.)	Minor Colors (color Number)	Minor Colors Distribution
1	Light Gray (8)	Very Light Gray (9), Mild Light Gray (4), Dark Gray (10)	Very Light Gray-Dense, Mild Light Gray-Dense, Dark Gray-Sparse
2	Light Gray (8)	Very Light Gray (9), Mild Light Gray (4), Dark (10)	Very Light Gray-Dense, Mild Light Gray-Sparse, Dark Gray-Sparse
3	Grayish Orange (1)	Dark Grayish Orange/Brown (5), Gray (6)	Dark Grayish Orange/Brown-Dense, Gray-Dense
4	Gray (6)	Dark Grayish Orange/Brown (5), Dark Gray (10)	Dark Grayish Orange/Brown-Dense, Dark Gray-Dense
5	Gray (6)	None	None

Select Paint: For paint mixing experiments, 12 inches by 24 inches polycarbonate sheet is painted for each group with the representative paints. As established in Section 4, there are three base paint colors needed to make surrogate curb (color 8 (light gray), 1 (grayish orange), and 6 (gray)). Color 8 is the base color of group 1, so it is denoted as G1 (i.e., group1), and similarly, color 1 as G3 (i.e., group 3) and color 6 as G4 (i.e., group 4). Acrylic paints were used for colors. By adding the proper amount of cement, the coating satisfies the IR and color requirements.

IR Satisfaction: Figures 5.3 to 5.5 show the IR satisfaction of skin for groups 1, 3, and 4. Figure 5.3 shows that the surrogate skin satisfies the IR requirements for group1. Figure 5.4 shows that the surrogate skin satisfies the IR requirements for group3, and Figure 5.5 shows that the surrogate skin satisfies the IR requirements for group4.
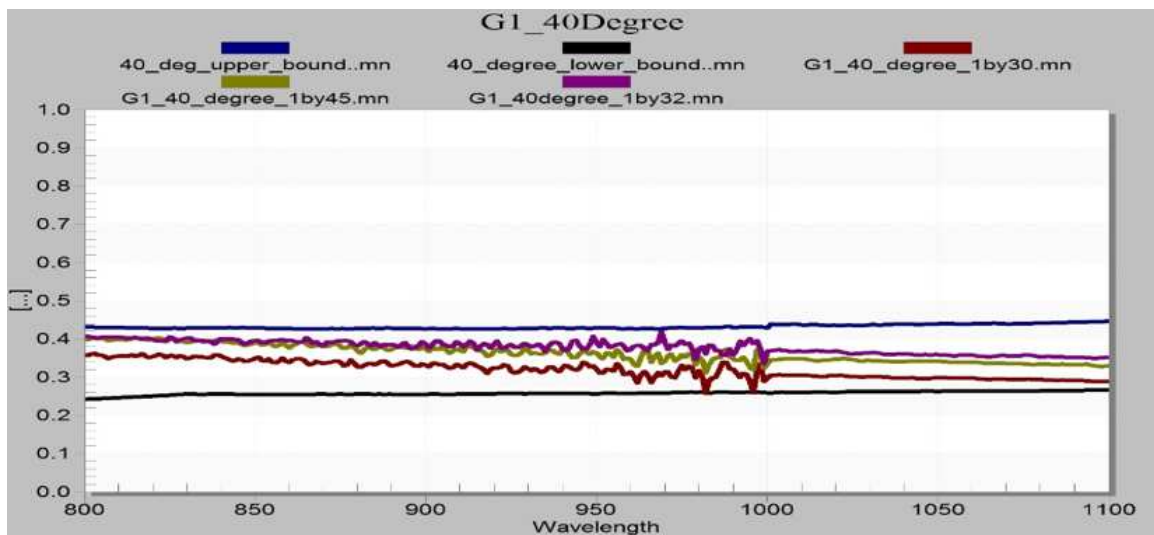
Fig. 5.3. IR Satisfaction Group1
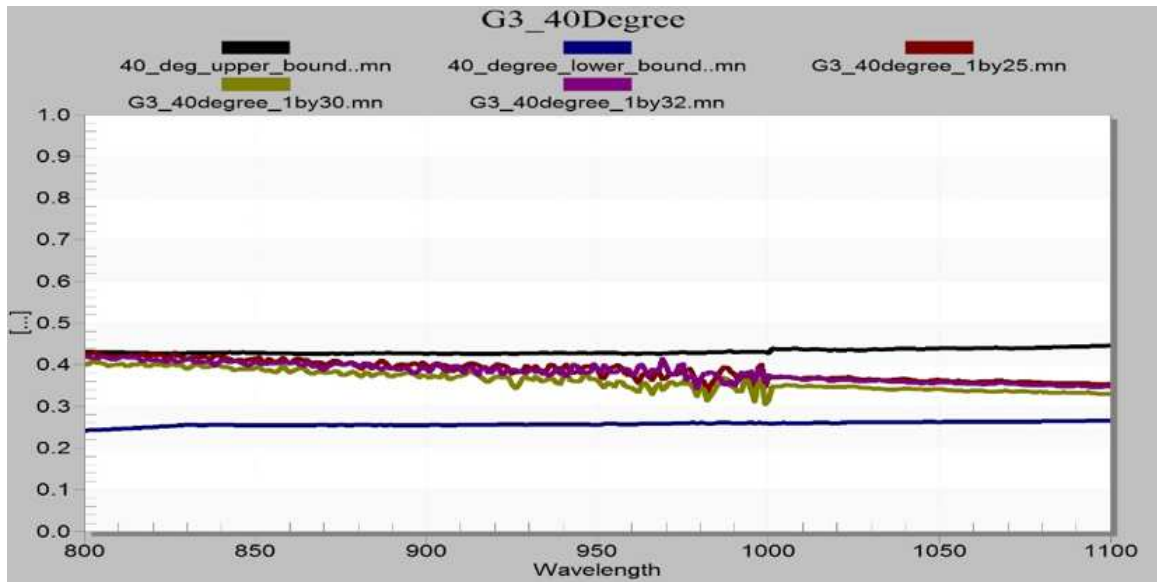
Fig. 5.4. IR Satisfaction Group3
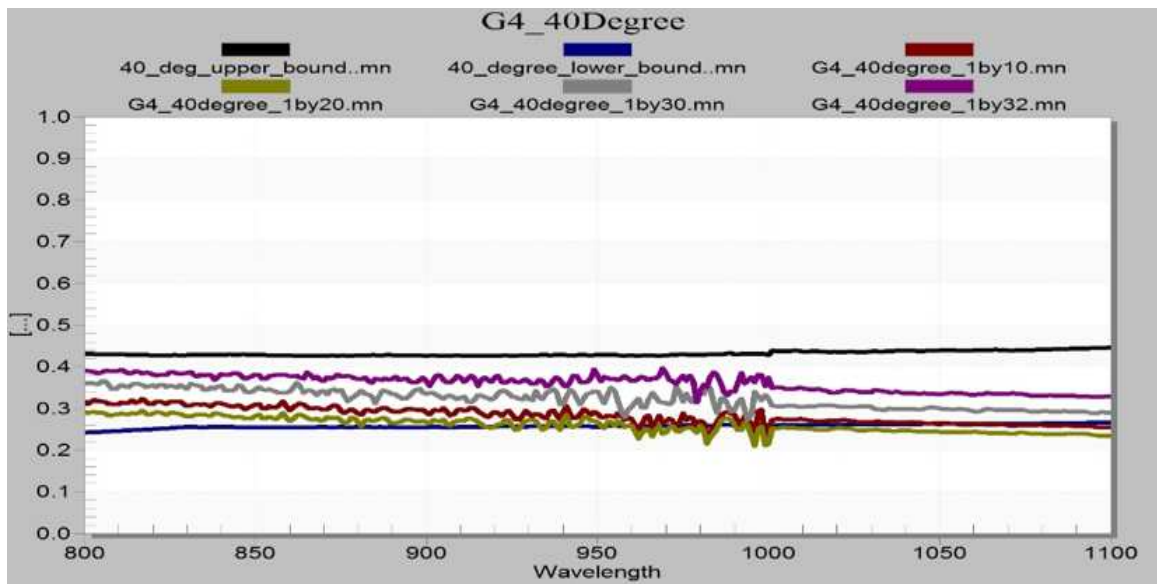
Fig. 5.5. IR Satisfaction Group4

Radar Reflectivity Satisfaction: In the previous section, we selected the paints for satisfying the color and IR requirements. Now we must also ensure the 24 GHz and 77GHz radar reflectivity requirements are met. The 24 GHz and 77GHz radar reflectivity requirement is in range 7.3 ± 1 dB. A resistive coating was put on the polycarbonate film. Then the radar reflective of the surrogate curb skin was measured. Figure 5.6 shows the plots of reflectivity for reference (metal plate) and the target (Skin) for 24 GHz, and Figure 5.7 shows the plots of reflectivity for reference (metal plate) and the target (Skin) for 77 GHz. The bottom picture of both images shows the reflectivity values.
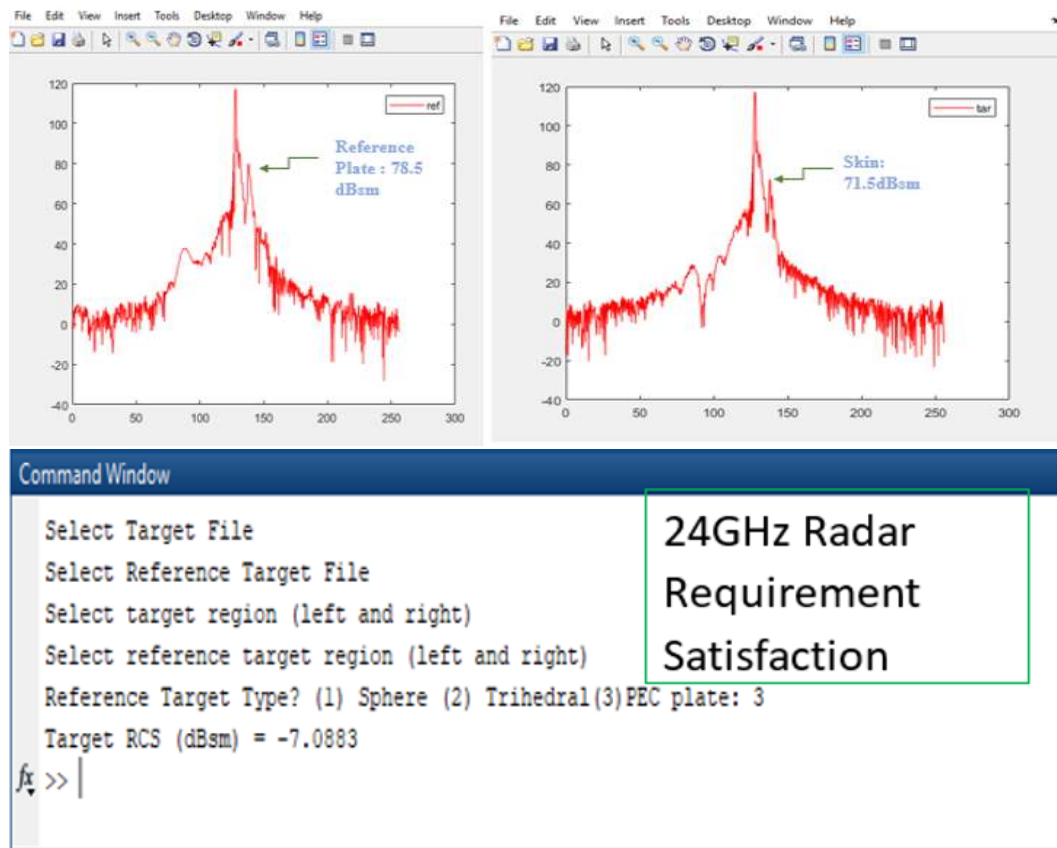
Fig. 5.6. 24 GHz Reflectivity Plot-Reference (Left) and Target (Right)
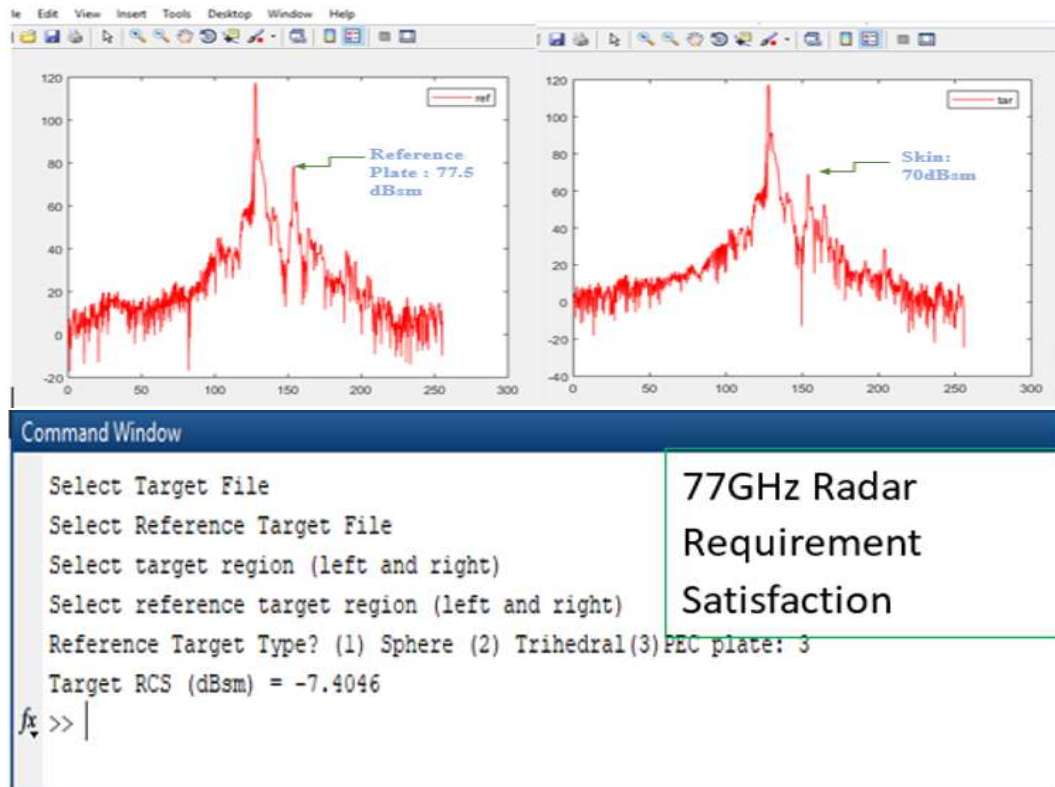
Fig. 5.7. 77 GHz Reflectivity Plot-Reference (Left) and Target (Right)

Having satisfied all the three requirements (color, Radar, and IR), we can make the color pattern for the curb surrogates.

Pattern 1: As shown in Table 5.2, pattern 1 is painted with colors 8 (light gray, base), 9 (very light gray, dense), 4 (mild dark gray, dense), and 10 (dark gray, sparse). In Figure 5.8, the left image shows the real curb, the second left image shows the cropped curb image, the second right image is the developed skin, and the right image is the generated surrogate.

Fig. 5.8. Pattern1 Surrogate

Pattern 2: Pattern 2 is painted with colors 8 (light gray, base), 9 (very light gray, dense), 4 (mild dark gray, sparse), and 10 (dark gray, sparse). In Figure 5.9, the left image shows the real curb; the second left image shows the cropped curb. The second right image is the developed skin, and the right image is the surrogate of pattern 2.

Fig. 5.9. Pattern2 Surrogate

Pattern 3: Pattern 3 is painted with colors 1 (grayish orange, base), 5 (dark grayish orange/brown, dense), and 6 (gray, dense). In Figure 5.10, the left image shows the real curb; the second left image shows the cropped curb. The second right image is the developed skin, and the right image is the surrogate of pattern 3.
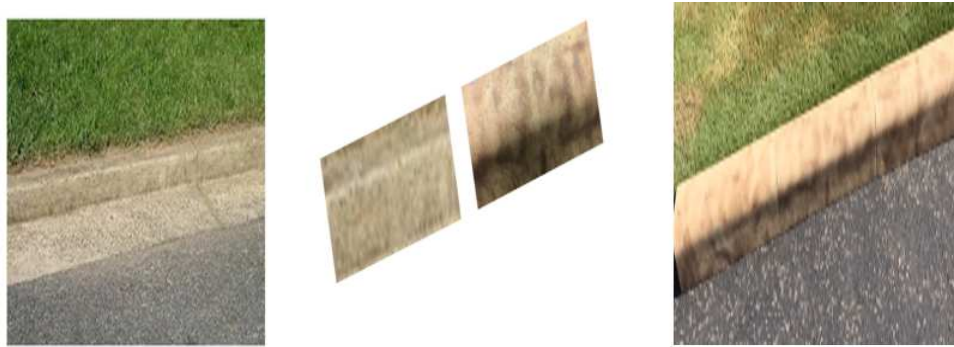
Fig. 5.10. Pattern3 Surrogate

Pattern 4: Pattern 4 is painted with colors 6 (gray, base), 7 (dense), 5 (dark grayish orange/brown, sparse), and 9 (very light gray, sparse). In Figure 5.11, the left image shows the real curb; the second left image shows the cropped curb. The second right image is the developed skin, and the right image is the surrogate of pattern 4.

Fig. 5.11. Pattern4 Curb

Pattern 5: Pattern 5 is painted with color 6 (uniform color 6). In Figure 5.12, the left image shows a real curb, and the second left image shows the cropped curb. The second right image is the developed skin, and at the right, the surrogate skin. The lower image is the surrogate curb skin in actual shape.


Fig. 5.12. Pattern5 Curb

6. SURROGATE ROAD CRASH TEST

The curb surrogate of all color patterns was constructed. As shown in Figure 6.1, these surrogate curbs were placed aside from each other.

Fig. 6.1. Surrogate Curb of 5 Color Patterns

Some crash tests of the curb surrogate were also conducted. One section of the surrogate curb was used. A 2008 Toyota Prius was driven at 10 mph in the test. In all tests, the vehicle ran over the curb surrogate. Since the clearance between the vehicle bottom and ground is about 6". The curb surrogate was stuck under the vehicle and dragged by the vehicle after the crash. It took some effort to take the surrogate curb out from the bottom of the vehicle (do not need to lift the vehicle). Figure 6.2 shows the pictures of a pre-crash surrogate curb, curb surrogate stuck below the car, and post-crash curb surrogate. The skin and the foam were intact, but there were wear and tear on the skin due to a car run over the curb surrogate.
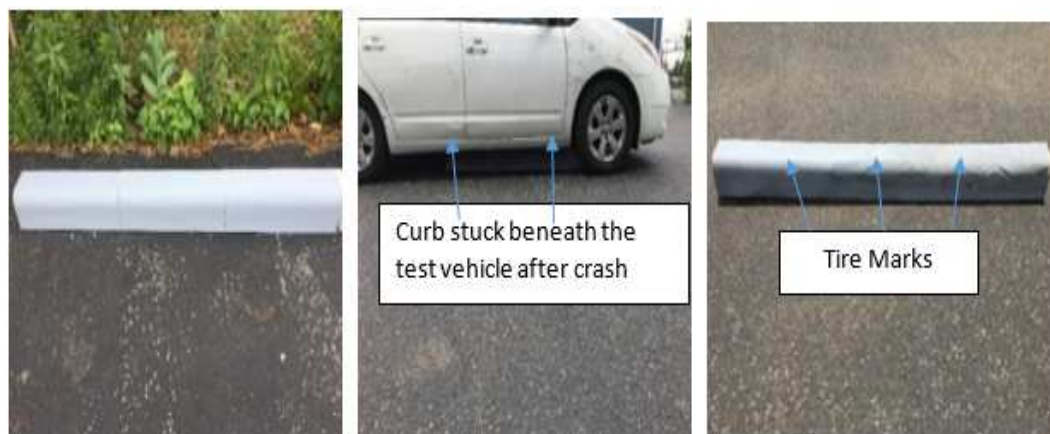
Fig. 6.2. Surrogate Crash Test

7. CONCLUSION AND FUTURE WORK

7.1 Conclusion

The purpose of the study was to determine the sensor characteristics for developing a surrogate for curbs found on US roadsides that could be used for RDMS testing. The study defines the requirement for surrogate curb as to be lightweight, reliable, durable, and, most importantly, have similar sensor characteristics as the real roadside curbs. The color and pattern determination was one of the significant work done in this thesis. Out of the discovered four groups of curbs, three group covers more than 90% of US roadsides curbs. The study verified the old IR bonds established by TASI in previous works. The flurry of IR measurement iterations helped to find the suitable color types that could achieve the required IR values in range 800-1100 nm. It was determined that seven colors could paint almost 90% of these four groups. The type of paint used, and the painting technique affects the measurement values significantly. Similarly, for the RCS, the painting technique and measurement setup affect the output values. Lastly, the developed surrogates were crashed tested, and results were found satisfactory.

7.2 Future Work

The study found suitable paint types and appropriate paint: cement mix that could achieve the desired IR values in range 800-1100 nm range. Now automotive LiDARs of wavelength 1500nm were introduced. The further surrogate curb study is required to achieve IR reflectivity for the 1500nm LiDARs.

APPENDICES

APPENDIX 1: IMAGE SEGMENTATION CODE

```
SegmentationCode
import numpy as np

import cv2

import matplotlib.pyplot as plt

original_image = cv2.imread("image path")

image=cv2.cvtColor(original_image,cv2.COLOR_BGR2Lab)

image_reshape = img.reshape((-1,3))

image_reshape = np.float32(image_reshape)

measure = (cv2.TERM_CRITERIA_EPS +

cv2.TERM_CRITERIA_MAX_ITER,

10, 1.0)

K = optimal number of clusters determined by

silhouette plotting attempts = 10

ret,label,center=cv2.kmeans(image_reshape,

K,None,measure,attempts, cv2.KME_CENTERS)

center = np.uint8(center)

result = center[label.flatten()]

result_image = result.reshape((img.shape))

figuresize = 15

plt.figure(figsize=(figuresize,figuresize))

plt.subplot(1,2,1),plt.imshow(img)

plt.title('Original Image'), plt.xticks([]), plt.yticks([])

plt.subplot(1,2,2),plt.imshow(result_image)
```

```
    plt.title('Segmented Image when K = %i, % K),
plt.xticks([]), plt.yticks([])
    plt.show()
    plt.figure()
    edges = cv2.Canny(img,150,200)
    plt.figure(figsize=(figuresize,figuresize))
    plt.subplot(1,2,1),plt.imshow(img)
    plt.title('Original Image'), plt.xticks([]), plt.yticks([])
    plt.subplot(1,2,2),plt.imshow(edges,cmap = 'gray')
    plt.title('Edge Image'), plt.xticks([]), plt.yticks([])
    plt.show()
```

APPENDIX 2: CURB CLUSTERING CODE

$\boxed{KMeansCode}$

```
import c1
import numpy as np
import cplot
import matplotlib.pyplot as plt
from sklearn.cluster import KMeans import statistics as s
file = open("csv file path having color values")
csv = c1.file_read(file)
data = csv.file_operation()
dat1 = np.array(data)
dat2 = dat1.astype(np.float64)
ColorDict = { }
ColorDict[0] = dat2[:,columnnumber]
ColorDict[1] = dat2[:,columnnumber]
ColorDict[2] = dat2[:,columnnumber]
ColorDict[3] = dat2[:,columnnumber]
colormap =[]
for k in range(0,len(ColorDict[1])):
        colormap.append([int(ColorDict[0][k]), int(ColorDict[1][k]),
int(ColorDict[2][k])])
        ColorDict[4] = np.array(colormap)
class stats():
        def_ _ init_ _ (self):
```

```
        self.x =0
    def statoperations(self, data):
        m = s.mean(data)
        SD = s.stdev(data)
        Var = s.variance(data)
        gauss =[]
        j =0
        norm =[]
    k =0
    for i in data:
        j = (i-m)/(SD)
        gauss.append(j)
    for n in data:
        k = (n-min(data))/(max(data))
        norm.append(k)
    return gauss, norm
def Kmeansample(self,x,x1,x2,title,xlabel,ylabel):
    plt.figure(figsize = (8,8))
    kmeans=KMeans(nclusters=obtained from silhouette plotting)
    kmeansoutput=kmeans.fit(x)
    kmeansoutput
    plt.figure(figsize=(12,12))
    plt.scatter(x[:,x1], x[:,x2], c=kmeansoutput.labels_)
    plt.scatter(kmeans.cluster_centers_[:, x1],
kmeans.cluster_centers_[:, x2],marker = '*', s=300, c='red')
    plt.xlabel(xlabel)
    plt.ylabel(ylabel)
    plt.title(title)
    plt.show()
```

```
    Kmeansample(dat2,xvalues,yvalues, 'Clustering KMeans',
'RG','B') st = stats()
    [RGS, RGN] = st.statoperations(ColorDict[3])
    [BS, BN ] = st.statoperations(ColorDict[2])
    dat2[:,11] = np.array(RGN)
    dat2[:,3] = np.array(BN)
    plots.Kmeansample(dat2,xvalue,yvalue,
'Clustering KMeans','RG','B')
```

APPENDIX 3: SILHOUETTE PLOTTING CODE

$\boxed{SilhoutteFunction}$

```
import matplotlib.pyplot as plt

from sklearn.cluster import KMeans

from sklearn.metrics import silhouette_score

def sil(self,x,ncluster):

    Sscore =[]

    for j in range(2,ncluster):

        kmeans = KMeans(nclusters=j).fit(x)

        silhouetteavg = silhouette_score(x,kmeans.labels_)

        Sscore.append(silhouette_score(x,kmeans.labels_)

        print('Silhouette Score for %i Clusters: %0.4f' %
(j, silhouetteavg))
```

APPENDIX 4: ROI REGION SELECTION

S = [X1 Y1 72 6]; %the size of your ROI starts at point X1, Y1

I = imread('G31.png'); % your input image

  figure, imshow(I)

  h = imrect(gca, S)

  addNewPositionCallback(h,@(p) title(mat2str(p,3)))

fcn = makeConstrainToRectFcn('imrect',get(gca,'XLim'),

get(gca,'YLim'))

setPositionConstraintFcn(h,fcn)

  position = wait(h)

  I2 = imcrop(I,position)

  imshow(I2) % the output image of the ROI

REFERENCES

REFERENCES

[1] ANSI D16.1-2007, "Manual on Classification of Motor Vehicle Traffic Accidents," 2007, [Online]. Available: https://crashstats.nhtsa.dot.gov. [Accessed: December 28, 2019]

[2] Roadway Departure Safety, "U.S. Department of Transportation Federal Highway, 2019 Administration," [Online]. Available: https://safety.fhwa.dot.gov/roadway_dept/. [Accessed: February 11, 2020]

[3] NHTSA. (2014). "Traffic Safety Facts 2012: A compilation of motor vehicle crash data from the fatality analysis reporting system and the general estimates system," [Online]. Available: http://www-nrd.nhtsa.dot.gov/Pubs/812032.pdf. [Accessed: February 11, 2020].

[4] Hobbs, C. A, McDonough, P. J, "Development of the European new car assessment program Euro NCAP," Regulation, vol. 44, p. 3, 1998. [Online]. Available: https://www.nrd.nhtsa.dot.gov. [Accessed: February 11, 2020]

[5] Shaban, A, "Determination of concrete properties using hyperspectral imaging technology: A review," Science Journal of Civil Engineering and Architecture, pp. 1–11, 2003. [Online]. Available: http://www.sjpub.org/sjcea.html. [Accessed: February 27, 2020]

[6] Sorensen, T. C and Spudis, P. D, "The Clementine mission a 10-year perspective. *Journal of Earth System Science*, vol. 114, no. 6, pp. 645–668, 2005. [Online]. Available: https://link.springer.com/article/10.1007/BF02715950. [Accessed: February 11, 2020].

[7] Dennison, P.E, Gardner M.E, Herold, M and Roberts, D. A, "Spectrometry for urban area remote sensing - development and analysis of a spectral library from 350 to 2400 nm," *Remote Sensing of Environment*, vol. 91, no. 3-4, pp. 304–319, 2004. [Online]. Available: http://www.citeseerx.ist.psu.edu/viewdoc/download. [Accessed: February 11, 2020]

[8] Kerekes, J.P, Salvaggio, C and Strackerjan, K, "Spectral reflectance and emissivity of man-made surfaces contaminated with environmental effects," *Optical Engineering*, vol. 47, issue 10, pp. 2-10, 2008. [Online]. Available: http://www.cis.rit.edu/people/faculty/kerekes/pubs.html. [Accessed: February 11, 2020]

[9] Akamatsu, Y, Kato, S, T. Iwata, Minami, Y and Mori, M.M, "Spectral analysis of building materials used in japan: The international archives of the photogrammetry," *Remote Sensing and Spatial Information Sciences*, vol. XXXVII Part B8, pp 50-53, 2008. [Online]. Available: https://www.isprs.org/XXXVII/congress/8_pdf/1_WG-VIII-1. [Accessed: February 13, 2020]

[10] Ahokas, E, Hakala, T, Honkavaara, E, Marklin, L, Peltoniemi, J and Suomalainen, J. "Analysis of properties of reflectance reference targets for permanent radiometric test sites of high-resolution airborne imaging systems," *Remote Sens*, vol. 2, pp. 1892–1917, 2010. [Online]. Available: https://www.mdpi.com/2072-4292/2/8/1892. [Accessed: February 13, 2020]

[11] Daimler Chrysler, A.G, Wegner, and Schneider, J, "High resolution radar for automobile applications," *Research & Technology, REM/CR, Wilhelm-Runge-Str. 11, D-89081 Ulm, Germany*, pp. 105-111, 2003. [Online]. Available: https://www.pdfs.semanticscholar.org. [Accessed: February 15, 2020]

[12] Kim, S, Lee, D, Jung-Young Son, and Yeom, S, "Automatic image segmentation for concealed object detection using the expectation maximization algorithm," pp.2-7, 2010. [Online]. Available: https://www.osapublishing.org/oe/abstract.cfm?uri=oe-18-10-10659. [Accessed: February 27, 2020]

[13] Griffiths, P, "Vehicle Dynamics Lab, Sensor-Friendly Vehicle and Roadway Systems," *IMTC 2001. Proceedings of the 18th IEEE Instrumentation and Measurement Technology Conference, Budapest, Hungary*, May 21, 2001.

[14] Ono, D, "Stationary object detection method for use with scanning radar," US Patent 765,523B2, June 20, 2004.

[15] "Color spaces with RGB Primaries". Wikipedia. [Online] Available: https://en.wikipedia.org/wiki/RGB_color_space. [Accessed: February 13, 2020]

[16] "CIELAB Color Space." Wikipedia. [Online]. Available: https://en.wikipedia.org/wiki/CIELAB_color_space. [Accessed: February 13, 2020]

[17] Lindbloom, B.J, "Color Spaces, RGB to CIELAB and CIELAB to RGB," [Online]. Available: http://www.brucelindbloom.com. [Accessed: February 13, 2020]

[18] "Color Spaces, RGB to CIELAB," MathWorks. [Online]. Available: https://www.mathworks.com. [Accessed: July 17, 2019]

[19] "Color Spaces, CIELAB to RGB," MathWorks. [Online]. Available: https://www.mathworks.com. [Accessed: July 17, 2019]

[20] Oyelade, O. J, "Application of k-Means Clustering algorithm for prediction of Students," *(IJCSIS) International Journal of Computer Science and Information Security*, Vol. 7, 0. 1, pp. 292-295, 2010. [Online]. Available: https://arxiv.org/abs/1002.2425. [Accessed: February 15, 2020]

[21] "k-Means Clustering." Wikipedia. [Online]. Available: https://en.wikipedia.org/wiki/K-means_clustering. [Accessed: February 17, 2020]

[22] "kmeans." MathWorks. [Online]. Available: https://www.mathworks.com/support/search.html?q=kmeans&page=1. [Accessed: February 27, 2020]

[23] "Silhouette_(clustering)." Wikipedia. [Online]. Available:https://en.wikipedia.org/wiki/Silhouette_(clustering). [Accessed: February 17, 2020]

[24] "Silhouette." MathWorks. [Online]. Available: https://www.mathworks.com/help/stats/silhouette.html. [Accessed: February 17, 2020]

[25] "blockproc." MathWorks. [Online]. Available: https://www.mathworks.com/help/images/ref/blockproc.html. [Accessed: February 17, 2020]

[26] Skolnik, M.I, *Introduction to radar, Radar handbook*, vol. 2, 1990. McGraw-Hill.

[27] Ishimaru, A, *Electromagnetic wave propagation, radiation, and scattering: from fundamentals to applications*, 2017. Wiley-Blackwell.

[28] Wenger, J, "Automotive radar-status and perspectives". *IEEE Compound Semiconductor Integrated Circuit. Symposium*, 2005. CSIC'05, Palm Springs, CA, USA, October 31, 2005.

[29] Klotz, M and Rohling, H, "A 24 GHz short-range radar network for automotive applications." *CIE International Conference on Radar Proceedings. IEEE, Beijing, China*, October 14, 2001.

[30] Donohoe, J.P and Ingels, F.M, "The ambiguity properties of FSK/PSK signals," *Radar, IEEE International Conference, Arlington, VA, USA, May 07, 1910.*

[31] Heo, S, Son, Y, and Sung, H, "Sensors, Automotive Frequency Modulated Continuous Wave Radar Interference Reduction Using Per-Vehicle Chirp Sequences." MDPI, 2001. [Online]. Available: https://www.mdpi.com/1424-8220/18/9/2831. [Accessed: February 19, 2020]

[32] NRCAN, "Polarization in radar systems." [Online]. Available: https://www.nrcan.gc.ca/node/9567. [Accessed: February 19, 2020]

[33] Currie, N.C, *Radar reflectivity measurement: techniques and applications*, 1989, Artech House.

[34] ITU. (2005), "Evaluating fields from terrestrial broadcasting transmitting systems operating in any frequency band for assessing exposure to non-ionizing radiation." [Online]. Available: http://emfguide.itu.int/pdfs/R-REC-BS.1698.pdf, [Accessed January 11, 2020]

[35] Khader, M and Cherian, S, "An introduction to automotive LIDAR and solutions to serve future autonomous driving systems." [Online], Available: http://www.ti.com/lit/wp/slyy150/slyy150.pdf. [Accessed: February 19, 2020]

[36] Haran, T and Chien, S, "Infrared reflectivity of pedestrian mannequin for autonomous emergency braking testing." *IEEE 19th International Conference on Intelligent Transportation Systems (ITSC), Rio de Janeiro, Brazil*, November 1, 2016.

[37] Glenn, N.F and Wang, C, "Integrating LIDAR intensity and elevation data for terrain characterization in a forested area". *IEEE Geoscience and Remote Sensing Letters*, vol. 6, no. 3, 2009. [Online]. Available: https://ieeexplore.ieee.org/abstract/document/4840427. [Accessed: February 27, 2020]

[38] "FieldSpec Pro User's Guide." (2002). [Online]. Available: https://www.snowserver.colorado.edu/fromDominik/fieldspec_pro_manual. [Accessed: February 02, 2020]

[39] Daughtry C. S.T, Irons J. R and Ranson, K. J, "Theory and Operations of LiDAR, BRDF, Surface albedo from bidirectional reflectance." *Remote Sens. Environment.* 35:201-211, 202-203, 1991. [Online]. Available: https://www.sciencedirect.com/science/article/abs/pii/003442579190012U?via%3Dihub. [Accessed: February 27, 2020]

[40] Akbari, H and Levinson, R, "Effects of composition and exposure on the solar reflectance of Portland cement concrete." [Online]. Available: https://digital.library.unt.edu/ark:/67531/metadc737346/. [Accessed: February 27, 2020]

[41] "Fresnel Equation." Wikipedia. [Online]. Available: https://en.wikipedia.org/wiki/Fresnel_equations. [Accessed: February 9, 2020]

[42] Lin, J. (2018), "Radar Characteristics Study For The Development Of Surrogate Roadside Objects," Masters Thesis, Dept. Electrical and Computer Engineering, Indiana University Purdue University, Indianapolis, IN, USA, 2018. [Online]. http://hdl.handle.net/1805/17772.

[43] "Ancortek 2400AD Radar." [Online]. Available: http://ancortek.com/wp-content/uploads/2019/04/SDR-2400AD-Datasheet.pdf. [Accessed: February 17, 2020]

[44] "Ancortek 2400AD Radar." [Online], Available: http://ancortek.com/wp-content/uploads/2017/02/DS-SDR-KIT-2400AD.pdf. [Accessed: February 17, 2020]

[45] "K-Band WR-42 Waveguide Standard Gain Horn Antenna." [Online]. Available: http://ancortek.com/sdr-kit-2400ad. [Accessed: February 27, 2020]

[46] Saha, A, "Development of infrared reflectance characteristics of surrogate road-side objects," Masters Thesis, Dept. Electrical and Computer Engineering, Indiana University Purdue University, Indianapolis, IN, USA, 2018. [Online]. http://hdl.handle.net/1805/16930.

[47] Kennel, G, *Color and Mastering for Digital Cinema. Focal Press*, 2013.